Cardiovascular Research Institute

Research Day 2023

June 09, 2023

Katz Lecture Theatre and Atrium

UNIVERSITY OF ALBERTA

Welcome

Director's Message

Welcome to Research Day 2023! Cardiovascular research is a notable strength here at the University of Alberta and our researchers are having impact here in the province, nationally and internationally. The Cardiovascular Research Institute is proud to be continuing the tradition of bringing the cardiovascular research community together to celebrate these accomplishments, learn about each other's work, share ideas, and build collaborations.

We have exciting day planned and are happy to welcome two visiting speakers. Dr. Kim Connelly from the University of Toronto kicks off the day with his presentation as the Dvorkin Lecturer at Medical Grand Rounds and Dr. Richard Whitlock from McMaster University, generously supported by the Faculty of Medicine's Walter Mackenzie Speaker Fund, jump starts our afternoon session. The rest of the day is focused on our trainees. We have selected several of the submitted abstracts to present their work from the podium, some in more traditional oral presentations and new this year are the 3-minute-thesis-style presentations, and many more in poster format. The agenda is jam packed and sure to be informative and inspiring.

I want to thank both the Royal Alexandra and University Hospital Foundations, and all of our industry sponsors for their generous support. Events like these are an important way to acknowledge all the hard work, dedication and team work that is required to make research a success, but cannot occur without their help. I also want to thank our Organizing Committee, Drs. Christi Andrin, Jennifer Conway, Debraj Das, Jason Dyck, Michelle Graham, Rod MacArthur, Sean McMurtry and Ms. Lisa Soulard, for all their time invested to make this event happen.

I sincerely hope you enjoy the day.

Justin A. Ezekowitz, MBBCh, MSc
Professor of Medicine
Director, Cardiovascular Research, University of Alberta
Co-Director, CVC
Cardiologist, Mazankowski Alberta Heart Institute
AHS Chair in Cardiac Sciences

Acknowledgements:

This event is generously sponsored and supported by:

Gold Sponsorship

- Novartis Canada

Silver Sponsorship

- AstraZeneca Canada
- Bayer Canada
- Bristol-Myers Squibb Canada Co.
- Pfizer Canada Inc.
- Servier Canada

Foundations

- Royal Alexandra Hospital Foundation
- University Hospital Foundation

Awards:

In addition to the sponsorships listed above, the trainee awards presented today are generously supported through the following:

Research Day Presentation Awards:

- Adarsh Gopal Education and Research Fund and University Hospital Foundation
- Royal Alexandra Hospital Foundation

Cardiology Awards:

- Henry Anton Deutsch Fund
- Jose Galante Chicurel Fund

Visiting Speakers:

Medical Grand Rounds & Dr. Joseph Dvorkin Memorial Lecture Presenter

"SGLT2 Inhibitors – Miracle drugs, but how do they work?"

presented by Dr. Kim Connelly

Dr. Kim Connelly MBBS, PhD, FSCMR, FCCS

Director, Keenan Research Centre for Biomedical Science, Unity Health

Division Head, Cardiology St. Michael's Hospital

Keenan Chair in Research Leadership

Associate Professor of Medicine
University of Toronto

Dr. Kim Connelly is a Cardiologist and Scientist who is both nationally recognized as an expert in echocardiography, cardiovascular MRI and the impact of diabetes upon cardiac function and ventricular remodeling. Dr. Connelly runs a basic research laboratory at the Keenan Research Centre at St. Michael's Hospital where he focuses upon basic mechanisms of disease – primarily around the role of pathological extracellular matrix accumulation with a focus upon translating discoveries into therapies in humans. His work is diverse covering clinical guidelines statements, clinical trials, and preclinical studies along the themes of ventricular remodeling, diabetes, magnetic resonance imaging and echocardiography.

Dr. Connelly has been recognised for his contributions to science by being awarded an HSF clinician scientist award, a CIHR New Investigator Award, an Early Researcher Award from the Ministry of Ontario, the SC Verma award and the Insulin 100 emerging leader award to celebrate 100 years since the discovery of insulin at University of Toronto, as well as Canadian Cardiovascular Congress YIA 2012. He is past chair of the Canadian Cardiovascular guideline and was chair of the macrovascular complication section for Diabetes Canada CPG 2018.

Visiting Speaker

"Arguing for large surgical trials: global collaboration is key"

Presented by Dr. Richard Whitlock

Dr. Richard Whitlock M.D., Ph.D., FRCSC
Professor, Surgery, Faculty of Health Sciences
David Braley Cardiac, Vascular and Stroke Research Institute
Hamilton General Hospital

Dr. Whitlock is a Professor of Surgery at McMaster University and a practicing cardiac surgeon at Hamilton Health Sciences. He is a lead investigator at the Population Health Research Institute and the principal investigator of the LAAOS III trial. Dr. Whitlock holds the Canada Research Chair in Cardiovascular Surgery and a career award from the Heart and Stroke Foundation of Canada. Through the multinational studies that he has led, which include SIRS, TRICS III, VISION Cardiac, and LAAOS III, he has established a network of over 200 collaborating cardiac surgical centres in 32 countries. He is now leading several industry-partnered trials including LeAAPS, LAAOS IV, and STAR T.

This visit has been funded, in part, by the Walter Mackenzie Visiting Speaker Fund.

Event Schedule

06:45 – 07:45	Registration & Poster Set-Up
07:45 – 08:00	Welcome & Introductions
08:00 – 09:00	Medical Grand Rounds & Dr. Joseph Dvorkin Memorial Lecture Presenter & Keynote Speaker **Dr. Kim Connelly, University of Toronto** ***"SGLT2 Inhibitors – Miracle drugs, but how do they work?"***
09:00 – 09:15	Coffee Break
09:15 – 09:20	Welcome from the Faculty of Medicine & Dentistry – Dr. Lawrence Richer
09:20 – 10:20	**Podium Abstract Session #1: Acute Care / Recovery / Rise of the Machines** **Co-Chairs: Drs. Carla Prado and Richard Whitlock** Presenter 1: **Hazal Babadagli** *"Pharmacist-led short term follow-up pilot program for acute coronary syndrome patients: a retrospective cohort study"* Presenter 2: **Stephen Foulkes** *"Myosteatosis is associated with disease burden and decreased aerobic endurance in adults recovered from COVID-19"* Presenter 3: **Anita Khalafbeigi** *"Machine Learning-based Approach for Predicting Post-treatment Survival for CAD Patients"* Presenter 4: **Marwa Ramsie** *"Development of novel vasopressor therapy during neonatal resuscitation"* Presenter 5: **Alexandra Saunders** *"Invasive and Noninvasive Measurements in the Diagnosis of Pulmonary Arterial Hypertension: A Quality Improvement Project"*

10:20 – 10:50 Coffee Break and Poster Session

10:50 – 11:50 **Podium Abstract Session 2: Women's and Children's Cardiovascular Health**
Co-Chairs: Drs. Kim Connelly and Sandra Davidge

Presenter 1: **Amanda Almeida de Oliveira**
"Toll-like receptor 4 activation contributes to systemic vascular dysfunction in pregnant rats fed a high cholesterol diet during pregnancy"

Presenter 2: **Shubham Soni**
"Maternal Ketone Supplementation during Pregnancy Protects Against Iron Deficiency Induced Cardiac Dysfunction in the Offspring"

Presenter 3: **Kai Yi Wu**
"The Impact of Early-Stage Breast Cancer on Cardiac Structure and Function"

Presenter 4: **Xiaoying Wu**
"Early Atherosclerotic CVD and Impaired Cardiac Function in High-Risk Young Women with and without Polycystic Ovary Syndrome"

Presenter 5: **Xiang Xiao**
"Sex-differences in 5 year Survival with Percutaneous Coronary Intervention Compared to Coronary Artery Bypass Graft surgery in patients with Diabetes and Multivessel Disease"

11:50 – 13:00 Lunch Break and Posters Session

13:00 – 14:00	Visiting Speaker **Dr. Richard Whitlock, McMaster University** **"Arguing for large surgical trials: global collaboration is key"** *This visit has been funded, in part, by the Walter Mackenzie Visiting Speaker Fund*

14:00 – 15:00	**Podium Abstract Session #3: Cells, Pathways & Pathogenesis** **Co-Chairs: Drs. Gopinath Sutendra and Donna Vine** Presenter 1: **Jordan Chan** *"The GLP-1 receptor agonist liraglutide alleviates type 2 diabetes-related diastolic dysfunction in a pyruvate dehydrogenase dependent manner"* Presenter 2: **Aleksandra Franczak** *"Effect of angiostatin and its neutralization on cell death and cellular infection by SARS-CoV and SARS-CoV-2"* Presenter 3: **Saymon Tejay** *"Tumor-Secreted Nucleosides Promote RbFox1 Degradation and Signalling Pathways Relevant to Dedifferentiation in Cardiomyocytes; A Two-Hit Hypothesis with Implications for Cardiotoxicity"* Presenter 4: **Lynn Lunsonga** *"Investigating SGLT2 inhibitors as a potential novel therapy for patients with congenital Long QT syndrome 3: A precision medicine approach."* Presenter 5: **Matthew Martens** *"Reactive Oxygen Species Modulator 1 (ROMO1) Plays an Obligate Role in Cardiomyocyte Hypertrophy"*
15:00 – 15:30	Coffee Break and Poster Session

15:30 – 16:30

3 Minute Thesis-style Presentations

Co-Chairs: Drs. Padma Kaul and John Ussher

Presenter 1: **Gala Araujo**

"Efficacy of novel production variants for an chimeric anti-atherosclerotic antibody, chp3r99, to produce an immune response."

Presenter 2: **Wesam Bassiouni**

"MMP-2 Inhibition Protects Against Mitofusin-2 Proteolysis and Mitochondrial Dysfunction During Myocardial Ischemia-Reperfusion Injury"

Presenter 3: **Pishoy Gouda**

"Feasibility of utilising quality of life adjusted days alive and out of hospital in heart failure clinical trials"

Presenter 4: **Bridgette Hartley**

"Proteomic and degradomic approaches to assess the implications of matrix metalloproteinase-2 in the heart"

Presenter 5: **Qutuba Karwi**

"Dissecting the role of branched-chain amino acids and branched-chain keto acids in modulating cardiac adverse remodelling in heart failure"

Presenter 6: **Scott Bennett**

"Impact of Socioeconomic Status and Remoteness of Residence on Fetal Outcomes in Major CHD"

Presenter 7: **Brittany Gruber**

"Ertugliflozin does not inhibit the late component of the cardiac voltage-gated sodium channel"

Presenter 8: **Noorossadat Seyyedi**

"Determining the effect and mechanism of action of SARS-CoV-2 spike protein on von Willebrand factor expression and/or release from endothelial cells"

	Presenter 9: **Weijie Sun** *"ECG for high-throughput screening of multiple diseases: Proof-of-concept using multi-diagnosis deep learning from population-based datasets"*
16:25 – 16:45	Networking (Q&A with Speakers) and Poster Take-Down
16:45 – 17:00	Awards & Closing Remarks
17:00	**Reception – Katz Atrium**

ABSTRACTS

All abstracts submitted in alphabetical order by submitter's last name

Cannflavin-C protects against angiotensin II-induced cellular hypertrophy through the inhibition of Cytochrome P450 1B1 (CYP1B1) in human ventricular cardiomyocyte cell line

Ahmad H. Alammari, Conor O'Croinin, Neal M. Davies, Ayman O. S. El-Kadi

BACKGROUND

Cannflavin-C is a prenylated flavonoid found in Cannabis sativa that has been shown to have anti-inflammatory and analgesic properties. Currently there is no evidence to suggest that Cannflavin-C has any significant effects on the heart or cardiac hypertrophy. Cytochrome P450 1B1 (CYP1B1)-mediated metabolism of arachidonic acid contribute to the development of cardiac hypertrophy, a condition characterized by an increase in the size of cardiac cells. Therefore, we aimed to investigate the potential role of Cannflavin-C in modulating CYPs and protection against cardiac hypertrophy.

METHODS/RESULTS

In this study, the effects of Cannflavin-C 100 nM in the presence and absence of angiotensin (Ang) II 10 µM on human ventricular cardiomyocyte cell line (AC16) were investigated using real-time PCR to determine mRNA expression of CYPs and cardiac hypertrophic markers, as well as Western blot analysis to determine CYPs protein levels. Confocal fluorescence microscopy was utilized to measure the total cell boundary of individual AC16 cells and quantify their cell surface area. Our results indicate that Cannflavin-C inhibits CYP1B1 mRNA and protein expression levels, and protects against Ang II-induced cardiac hypertrophy. The cardioprotection effect is evidence by inhibition of hypertrophic markers and a decrease in cell surface area induced by Ang II.

CONCLUSIONS

Our results suggest that Cannflavin-C, by inhibiting CYP1B1 enzyme, protects against Ang II-induced cardiac hypertrophy.

Aging is associated with organ-specific alterations in level and expression pattern of von Willebrand factor

Parnian Alavi, Douglas Brown, Jayan Nagendran, John Lewis, Stephane L. Bourque, Nadia Jahroudi

BACKGROUND
Aging is associated with a state of hypercoagulability due to increased concentrations of plasma coagulation proteins. As people get older a significant impairment of the endothelial cells' (monolayer of cells that cover the lumen of all blood vessels) function may also occur, leading to their increased procoagulant activity. Endothelial cells have distinct characters in different organs, different types of vasculatures, and different pathological states. A gap in the knowledge exists due to the heterogeneity of endothelial cells in their response to stimuli, including aging, which is a universal and nonmodifiable risk factor for thrombosis. Von Willebrand factor (VWF) is an endothelial specific pro-coagulant protein with a major role in thrombosis. Aging is associated with increased circulating levels of VWF, which presents a risk factor for thrombus formation.

METHODS/RESULTS
Circulating plasma, cellular protein, and mRNA levels of VWF were determined and compared in young and aged mice. Major organs were subjected to immunofluorescent analyses to determine the vascular pattern of VWF expression and presence of platelets aggregates. An in vitro model of aging, using extended culture time of endothelial cells, was used to explore the mechanism of age-associated increased VWF levels.
Increased circulating plasma levels of VWF were observed in aged rodents. VWF mRNA and protein levels were significantly increased in the brains, lungs, and livers, but not in kidneys and hearts of aged mice. Higher proportion of small vessels in brains, lungs and livers of aged mice exhibited VWF expression compared to young, and this was concomitant with increased platelets aggregate formation. Prolonged culture of endothelial cells resulted in increased cell senescence that correlated with increased VWF expression. VWF expression was specifically upregulated in senescent population of cultured endothelial cells and p53 knockdown prevented this upregulation. In vivo, a significantly higher proportion of VWF expressing endothelial cells exhibited senescent markers SA-β-Gal, and p53 in brain vasculature of aged mice compared to young.

CONCLUSIONS
Aging elicits a heterogenic response in endothelial cells with regard to VWF expression, leading to organ-specific increase in VWF levels, as well as alterations in its vascular tree pattern of expression. This is concomitant with increased platelets aggregate formation. Demonstration of senescent endothelial cell association with increased thrombogenicity, and identification of p53 as a participating molecule provide opportunities for targeting these cells and/or p53 towards development of potentially therapeutic approaches for combating age-associated increased thrombogenicity.

Comparison of two ultrasound contrast agents for left ventricular opacification

Waleed Alhumaid MBBS, Nojan Mannani BS, Marina Choy, Jonathan Choy MD, Ian Paterson MD, Edith Pituskin PhD, and Harald Becher MD, PhD

BACKGROUND
Several ultrasound contrast agents have been approved and used for measurement of LV ejection fraction (EF). However, there has been no direct comparison between these agents.

METHODS/RESULTS
Methods: A retrospective study was performed using recordings of the local echocardiography registry for patients undergoing chemotherapy for cancer treatment. Patients were included who underwent follow-up echocardiograms (3 months) with 2 different ultrasound contrast agents and had only minor changes in the LV ejection fraction (EF) between the studies (<5%). Qualitative and quantitative analysis of the contrast effect was performed in apical four- and two chamber views (4CV,2CV). For quantitative analysis of the LV opacification square regions of interest (ROI) were placed in the apical and basal regions of the ventricle in each echocardiographic recording and the arithmetic mean and standard deviation of pixel intensity within each ROI was recorded throughout the entire loop. Qualitative visual assessment was performed using a three step visual score in order to assess the endocardial border delineation, basal attenuation and apical swirling.
Results: 41 patients mainly with breast cancer fulfilled the inclusion criteria. The mean+standard deviation of the EF was 61+9%. Both contrast agents provided intensive LV opacification in the basal and apical cavities. The video intensities
(mean+standard deviation) in the apical and basal cavities were comparable across both contrast agents in the 2CV apical ROI (219.96+21.42 vs
224.69+20.23), the 2CV basal ROI (114.55, 42.02 vs 112.79, 42.57), the 4CV apical ROI (228.02, 17.80 vs 225.51,
20.37), and the 4CV basal ROI (100.05, 41.11 vs 92.84, 42.54). Visual assessment revealed no statistical difference between the contrast agents in terms endocardial delineation.

CONCLUSIONS
Conclusion: In patients with normal LV function both ultrasound contrast agents no clinically relevant differences were found regarding LV opacification and endocardial border delineation.

Toll-like receptor 4 activation contributes to systemic vascular dysfunction in pregnant rats fed a high cholesterol diet during pregnancy

Amanda A. de Oliveira, Amy Wooldridge, Raven Kirschenman, Floor Spaans, Christy-Lynn M. Cooke, Sandra T. Davidge

BACKGROUND
Hypercholesterolemia, an imbalance in the lipid profile, is a hallmark of cardiovascular diseases, and also a physiological process required for normal fetal development. However, excessive hypercholesterolemia during pregnancy has been linked to an increased risk of pregnancy complications (e.g., preeclampsia); still, the underlying mechanisms are unclear. Toll-like receptor 4 (TLR4) impairs vascular function in non-pregnant models of chronic dyslipidemia and atherosclerosis, but whether TLR4 activation also plays a role in pregnancies complicated by hypercholesterolemia is unknown. Hypothesis: Pathological hypercholesterolemia during pregnancy causes maternal vascular dysfunction via activation of TLR4.

METHODS/RESULTS
Sprague Dawley rats were fed a standard (CD) or high cholesterol diet (HCD; 2% cholesterol and 0.5% cholic acid) from gestational day (GD) 6 to GD20 (term=22 days; n=9-10). Blood pressure was assessed before pregnancy and on GD19, and the results are presented as delta change. On GD20, body weight and pregnancy outcomes were recorded, and mesenteric arteries were assessed using wire myography to evaluate vasoconstriction capacity to phenylephrine and endothelium-dependent vasodilation responses to methacholine. Experiments were conducted in the presence or absence of L-NAME (a pan-NOS inhibitor, 100 umol/l) and/or CLI-095 (a selective TLR4 inhibitor, 10 umol/l). Functional data were summarized as Emax (maximum response) or pEC50 (concentration required to produce 50% of Emax). The statistical tests applied were Student's t-test or two- way ANOVA with Fisher's LSD post hoc test (significance: $p<0.05$). The HCD during pregnancy prevented the late gestation systolic ($p=0.0004$) and diastolic ($p=0.0066$) blood pressure reduction observed in the CD group, and reduced male ($p=0.0062$) and female ($p=0.0352$) fetal-to-placental weight ratio. Total body weight gain during pregnancy was not different between CD and HCD dams ($p>0.05$). In mesenteric arteries, vasoconstriction responses to phenylephrine (Emax) were increased in HCD dams ($p=0.0056$), and TLR4 inhibition with CLI-095 reduced the sensitivity (pEC50) of phenylephrine in these vessels ($p=0.0147$).
Additionally, HCD dams presented higher sensitivity (pEC50) to methacholine ($p=0.0169$), which was not modified by the TLR4 inhibitor ($p>0.05$). Incubation of arteries with L-NAME abolished the increased sensitivity to methacholine ($p>0.05$), which was not further altered by CLI-095 ($p>0.05$).

CONCLUSIONS
Excessive hypercholesterolemia during pregnancy prevented the blood pressure adaptation to

pregnancy, and impaired male and female placental efficiency.
Inhibition of TLR4 (ex vivo) reduced the enhanced vasoconstriction observed in HCD dams but did not alter endothelium-dependent vasodilation responses. Thus, by blocking the vasoconstrictor effects of excessive hypercholesterolemia during pregnancy, TLR4 inhibition may be a target for future therapy development.

Understanding The Mechanisms Behind Congenital LQT2-Related Protein Destabilization Of The hERG Potassium Channel Using Molecular Dynamics Simulations

Sara AlRawashdeh, Khaled Barakat

BACKGROUND
Cardiovascular diseases are the leading cause of death worldwide, accounting for 17.9 million deaths per year and 32% of global mortality. Cardiac arrhythmias, which are often caused by faulty ion channels, contribute considerably to these fatalities. Hereditary LQTS is a cardiac repolarization condition characterised by a prolonged QT interval in the ECG. LQT2, the most common type of LQTS, is caused by gene mutations in the human ether-a-go-go-related gene (hERG), which encodes a delayed rectifier K+ current. 90% of hERG mutations cause defective hERG channel trafficking to the cell membrane, and the mechanism of intracellular retention of these channels is still unknown. Interestingly, a number of high affinity hERG channel blocking drugs can pharmacologically rescue some of these mutants, hence, restoring the hERG surface expression. Nevertheless, the mechanism of this pharmacological rescue is still unclear.

METHODS/RESULTS
Methods: In this work, we used computational techniques such as molecular dynamics simulations to learn important structural details about the effects of mutations on hERG folding, ER retention, and trafficking. Wildtype and the two mutant hERG channels R534C and N470D were simulated and analyzed to highlight the altered dynamics of hERG mutants and learn more about the causes of their structural destabilisation.
Results: Pore dimensions analysis of the mutant channel showed a significant narrowing in a portion of the channel pore. Binding site of the trafficking recure drugs was shown to be affected by this change in the pore. On the other hand, conformer clustering of the mutant simulations showed a conformational shift in the intercellular domain PAS compared to wildtype.

CONCLUSIONS
Conclusion: Our results reveal a potential mechanism of trafficking mutant dysfunction where the channel pore and PAS intracellular domain are directly affected by the mutation. Those results will aid generating new hypotheses about their lack of binding to folding chaperone proteins.

Efficacy of novel production variants for an chimeric anti-atherosclerotic antibody, chp3r99, to produce an immune response.

Gala Araujo, Yosdel Soto, Rabban Mangat, Martin-Ozimek, Spencer Proctor

BACKGROUND
Atherosclerosis is a pervasive form of cardiovascular disease (CVD) characterized by the accumulation of cholesterol-rich lipoproteins within the innermost arterial wall. Therapeutic approaches for the treatment of atherosclerosis have been largely limited to the management of atherosclerotic risk factors rather than disease prevention per se. However, a novel atheroprotective therapy has emerged in the form of a chimeric monoclonal antibody (mAb) produced in a murine myeloma (NS0) cell line known as chP3R99 mAb. chP3R99 has been shown to directly inhibit lipoprotein-proteoglycan binding by blocking chondroitin sulfate on sugar side chains of proteoglycans. Previous studies of chP3R99 have attributed these atheroprotective features to be associated with the induction of secondary Ab2 (anti-chP3R99) antibodies in the host. However, production efficiencies of chP3R99 in NS0 cells have led to the development of two novel chP3R99 variants produced from more efficacious cell lines: Chinese Hamster Ovary (CHO) and Human Embryonic Kidney (HEK). Thus, the aim of this study was to assess the effects of variant chP3R99 immunizations in healthy and pro-atherogenic rodent and swine animal models.

METHODS/RESULTS
We assessed the immunogenicity of the three chP3R99 mAb variants, HEK-R99, NSO-R99, and CHO-R99 in healthy and insulin resistant animal models. Two experimental conditions were conducted. (i) Immunizations of 4 weekly doses each of 200mg in 20 healthy 9-month-old male lean rats and 20 3-week-old male swine.(ii) Immunization of obese 9-month-old male JCR: LA-cp rats given 4 weekly doses of 200 mg each followed by two biweekly doses of 200 mg. ELISA was then employed to assess the presence of Ab2 (anti-chP3R99) antibodies in the pre-immune and post-immune (final dose) sera samples.

Results: Immunizations of rats with CHO and HEK-R99s produced an immunogenic cascade of similar strength to NSO-R99 regardless of their physiological status, as shown by the significant levels of Ab2 antibodies at the final dose detected via ELISA ($p<0.05$, CI 0.95% Mann Whitney). Administration of R99 variants also produced significant levels of Ab2 antibodies compared to their respective pre-immune sera. However, for healthy swine only immunizations of NS0-R99 and CHO-R99 produced significant levels of Ab2 antibodies.

CONCLUSIONS
The results suggest that the new production variants of chP3R99 mAb, CHO-R99 and HEK-R99 induced an immunogenic response similar to that of the original NS0-R99 variant in rodent models. The outcomes from these validation studies are critical for the evaluation and efficacy of large scale-up protocols to move to human trials.

COVID-19-associated upregulation of TNF-α increases VEGF expression in megakaryocytes and subsequent platelets: a potential risk factor for pulmonary edema

Amir Asgari, Paul Jurasz

BACKGROUND
Vascular endothelial growth factor (VEGF/VPF) has been implicated in COVID-19-induced pulmonary edema. Platelets are known to contain massive reservoirs of this factor, which our lab's recent observations suggest are upregulated in isolated platelets from COVID-19 patients. According to the reports, VEGF expression is induced by hypoxia and TNF-α Interestingly, COVID-19 patients demonstrated higher TNF-α plasma concentration compared to COVID-19 negative controls. Our preliminary data suggests the presence of a novel platelet subpopulation in healthy donors loaded with higher content of VEGF (2.5±1.1%). Since TNF-α is known to increase VEGF expression, we hypothesized that its COVID-19-associated upregulation may be responsible for inducing VEGF-enriched platelet subpopulations through modulating VEGF expression in megakaryocytes and subsequently platelets.
Aims: To determine whether COVID-19-associated upregulation of plasma TNF-α increases the proportion of VEGF-enriched platelet sub-populations when compared to COVID-19 negative controls. Additionally, we will characterize the role of TNF-α in inducing VEGF expression and the consequential elevation of VEGF-enriched platelet subpopulations in megakaryocytes.

METHODS/RESULTS
Methods: Platelets were isolated from age- and sex-matched COVID-19 ICU patients and COVID-19 negative controls. Isolated platelets and TNF-α treated Meg-01 cell line were intracellularly stained for VEGF and analyzed using flow cytometry. A multiplex assay was used to measure the concentration of plasma TNF-α.
Results: Treatment of Meg-01 cells with TNF-α leads to the formation of a distinct subpopulation with higher intracellular VEGF levels (19.8±1.7%). Additionally, isolated platelets from COVID-19 patients not only demonstrated a higher overall mean in VEGF content but also contain a greater percentage of VEGF-enriched platelet subpopulation compared to COVID-19 negative controls.

CONCLUSIONS
Preliminary data suggests incubation of Meg-01 with TNF- α results in increased VEGF expression. This phenomenon may in part contribute to the generation of a greater percentage of VEGF-enriched platelets in COVID-19 patients, predisposing them to higher vascular permeability and therefore edema, compared to COVID-19 negative controls.

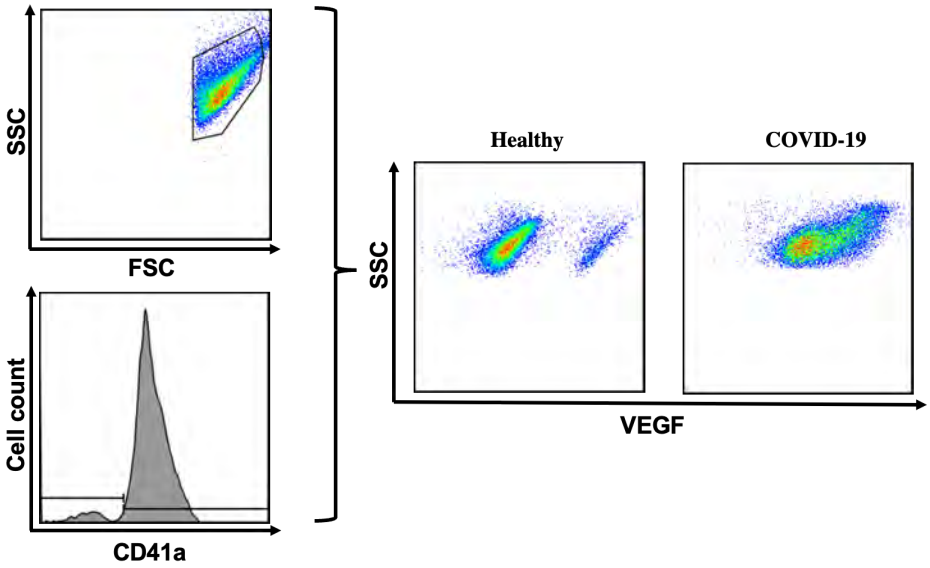

Figure 1. COVID-19 increases the overall mean expression of VEGF compared to COVID-19 negative controls, and the proportion of VEGF-enriched platelet subpopulation.

PHARMACIST-LED SHORT TERM FOLLOW-UP PILOT PROGRAM FOR ACUTE CORONARY SYNDROME PATIENTS: A RETROSPECTIVE COHORT STUDY

Hazal E Babadagli, Sheri Koshman, Michelle Graham, Marnie Wang, Glen Pearson

BACKGROUND

Rural patients have been shown to have reduced access to care, delayed discharge-prescription fills, and frequent readmissions following acute coronary syndrome (ACS) compared to urban patients. While virtual and pharmacist-led programs have shown benefit in providing efficient care to cardiac patients, to our knowledge,
their implementation in rural ACS-population have not been assessed. The purpose of this study was to determine the impact of pharmacist-led virtual follow-up program for rural ACS patients, compared to a matched control group.

METHODS/RESULTS

The intervention arm included 40 consecutive rural ACS-patients discharged from the Mazankowski Alberta Heart Institute between March-May 2022, as part of a pharmacist-led follow-up pilot-program. Structured telephone interviews were used to identify and resolve cardiac medication-related issues for each patient on day 1, 10, and 30 post discharge. Program-patients were compared to a control group (n=80) which included ACS patients (discharged November 2021-July 2022), matched for sex, zone of residence, and age within 10 years. Outcomes were collected from administrative databases and multivariable regression analyses were conducted for comparisons. The primary outcome was time to prescription fill of discharge ACS-medications within 30 days of discharge. Secondary outcomes included 30-day cardiac-related hospital readmissions, cardiac-related emergency department visits, and primary care practitioner (PCP)-visits.

During the 15-week pilot-program, 139 virtual visits were completed. Median time spent per visit was 60 (interquartile range [IQR], 50-80) minutes. A total of 255 cardiac medication-related issues (6 per patient; IQR, 3.75-8.25) were identified, and 91% were resolved by the pharmacist. Prescription errors, adverse events, and therapy optimization were most common on day 1, 10, and 30 respectively. There was no significant difference between groups in time to prescription fill (0.25 [IQR, 0.0-0.25] days vs 0 [IQR, 0.0-1.0] days; hazard ratio [HR], 1.17; 95% confidence interval [CI], 0.80-1.73), cardiac-related hospital readmissions (8% vs 5%; odds ratio [OR], 1.54; 95% CI, 0.21-9.59), or cardiac-related emergency department visits (10% vs 8%; OR, 1.37; 95% CI, 0.27-6.18). PCP-visit was higher in program
patients (90% vs 73%; HR, 3.00; 95% CI, 1.47-6.10).

CONCLUSIONS

A significant number of cardiac medication-related issues were efficiently identified and resolved by pharmacist-led early follow-up program in rural post-ACS patients. Compared to matched control group, there was no difference in the time to ACS- medication prescription

fill. Program-patients were more likely to have visits with their PCP following their ACS from program prompting, resulting in closer follow-up care. Further studies, with adequate power, are required to determine the impact on clinical outcomes.

Multiview 3D Echocardiography Fusion Using Deep Learning to Advance the Diagnostic Value of Cardiac Imaging

Sharanya Balachandran, Dr. Kumaradevan Punithakumar, and Dr. Michelle Noga

BACKGROUND

Cardiovascular disease is the second leading cause of death in Canada. Echocardiography is considered one of the best modalities to examine cardiovascular diseases as it is non-invasive, cost-effective, portable, and readily available. However, echo scans suffer from low signal-to-noise ratio and occasional signal dropout. These limitations could be overcome by developing an image fusion process where two or more images from multiple views of the heart are combined and fused to increase the information and quality of images to advance the diagnostic value of cardiac ultrasound images.

METHODS/RESULTS

A deep learning-based cardiac image fusion is proposed using U-Net, a well-known neural network used for medical image segmentation. The U-Net is trained as an auto-encoder feeding the cardiac images from different views or the same views (apical and parasternal) as the input where the network is expected to learn spatial features. Once training is completed, the weights of the encoder are used for the testing phase, so that the learned features by the network are utilized to produce encoded images of the test input. The encoded images are then added and reconstructed to the fused image by the decoder part. The proposed method is executed on the volunteer dataset of 19440 two-dimensional (2D) slices for training and 8640 2D slices for validation and 720 2D slices for testing. Quality metrics including Signal-to-Noise ratio (SNR), entropy, and Structural Similarity (SSIM) are computed and compared with other traditional fusion methods such as average fusion, maximum fusion, and wavelet fusion, and a neural network-based DenseFuse approach with L1 norm and simple addition fusion. Quantitative results are reported in Table 1, and qualitative results are presented in Fig.1 with two image samples from apical views fused using different methods which shows U-Net performance is better compared with other methods.

CONCLUSIONS

The proposed deep learning method eliminates the need for the extraction of hand-crafted features used in traditional fusion hence enabling better quality fusion results. The clinical significance of this network is assisting in accurate visualization of the focused region of heart structures including vital information such as edges of chambers and other details. As limited research has been done on ultrasound image fusion, this would be a significant contribution to clinical applications. The evaluation demonstrates the benefits of using a neural network for the fusion of 2D images. Future work will be devoted to extending the proposed network to fusing 3D echo volumes.

MMP-2 Inhibition Protects Against Mitofusin-2 Proteolysis and Mitochondrial Dysfunction During Myocardial Ischemia-Reperfusion Injury

Wesam Bassiouni, Robert Valencia, Zabed Mahmud, John M. Seubert, Richard Schulz

BACKGROUND
Impaired mitochondrial respiratory function is a major consequence of myocardial ischemia-reperfusion (IR) injury, accompanied by enhanced oxidative stress and disrupted calcium homeostasis. Tethering of mitochondria to the endoplasmic reticulum is essential for calcium transit between the two and is regulated by different proteins including mitofusin-2 which mediates mitochondrial fusion. Matrix metalloproteinase-2 (MMP-2) is a multifunctional protease that cleaves both extracellular and intracellular proteins. It is rapidly activated intracellularly in response to oxidative stress along with the de novo expression of its N-terminal truncated isoform (NTT-MMP-2) which is localized at or near mitochondria. Here we investigated whether MMP-2 proteolyzes mitofusin-2 during IR injury and impairs mitochondrial respiration.

METHODS/RESULTS
Hearts from 3 month old male C57BL/6J mice were isolated and subjected to IR injury in vitro (30 min ischemia, 40 min reperfusion) with MMP-2 preferring inhibitors ARP-100 (10 µM), ONO-4817 (50 µM) or DMSO (vehicle, 0.1% v/v). Permeabilized muscle fibers, isolated from hearts at the end of reperfusion, were used for measurement of mitochondrial respiration. Hearts subjected to IR showed a significant reduction in left ventricular developed pressure, together with reduced mitochondrial oxygen consumption and ATP production rates in fibers isolated from IR compared to aerobic hearts. ARP-100 or ONO-4817 improved post-ischemic contractile function recovery and mitochondrial respiratory function compared to vehicle-perfused IR hearts. Full length-MMP-2 activity along with mRNA expression of NTT-Mmp-2 were significantly increased in IR hearts compared to aerobic controls. There was a significant reduction in mitofusin-2 in mitochondria-enriched fractions from IR compared to aerobic hearts, while ARP-100 or ONO-4817 attenuated this reduction.

CONCLUSIONS
MMP-2 activation and induction of NTT-Mmp-2 expression following myocardial IR injury contributes to reduced contractile function and impaired mitochondrial respiration which could be attributed, at least in part, by the cleavage of mitofusin-2 by MMP-2.

Table. Changes in left ventricular developed pressure (LVDP), mitochondrial respiratory parameters, mitofusin-2 protein and *NTT-Mmp-2* mRNA levels in IR hearts.

	↵erobic (n=5)	+vehicle (n=5)	ARP-100 (n=5)	)NO-4817 (n=5)
LVDP (% of baseline at R40 min)	96.3±9.2	25.5±3.2*	50.1±3.2*#	57.3±1.6*#
Respiratory Control ratio	5.2±0.7	2.1±0.3*	4.6±0.6#	4.4±0.5#
ATP-dependent OCR (nmol O_2· min^{-1}· mg^{-1})	8.5±1.0	2.2±0.4*	7.0±1.0#	6.7±1.0#
Maximum OCR (nmol O_2· min^{-1}· mg^{-1})	11.0±1.9	2.1±0.6*	9.0±1.1#	8.5±1.5#
ATP production rate (nmol· min^{-1}· mg^{-1})	0.6±0.1	0.2±0.1*	0.5±0.1#	0.5±0.1#
Mitofusin-2/VDAC protein level	2.7±0.1	1.5±0.1*	2.0±0.1#	2.0±0.2#
NTT-Mmp-2/B2M mRNA	1.2±0.1	1.8±0.1*	1.1±0.1#	1.0±0.1#

*p<0.05 vs. aerobic. #p<0.05 vs IR+vehicle. OCR=oxygen consumption rate (ANOVA, Dunnett's
post-hoc test)

*p<0.05 vs. aerobic. #p<0.05 vs IR+vehicle. OCR=oxygen consumption rate (ANOVA, Dunnett's
post-hoc test)

Impact of Socioeconomic Status and Remoteness of Residence on Fetal Outcomes in Major CHD

Scott Bennett; Lisa Hornberger; Luke Eckersley; Deborah Fruitman; Amanpreet Kaur

BACKGROUND
Social determinants of health impact outcomes in congenital heart disease (CHD), and we recently demonstrated that remoteness of residence (RoR) and lower socioeconomic status (SES) are associated with later timing of prenatal diagnosis. Timing of prenatal diagnosis may also affect parental decision-making regarding continuation of pregnancy. In the current investigation, we sought to explore the impact of RoR and SES on rate of termination (TOP), adjusting for severity of CHD, syndromic diagnoses, and timing of prenatal diagnosis.

METHODS/RESULTS
We retrospectively identified all fetal and infant cases of major CHD undergoing surgical intervention at less than a year, as well as termination of pregnancy and intrauterine fetal demise in Alberta from 2008 to 2018. Using the maternal postal code of residence, we determined dissemination area Chan index SES quintile (1, lowest), and RoR from the closest tertiary care fetal cardiology unit categorized as <100km or >100km. CHD subtype and the presence or absence of syndromes were recorded.

We identified 130 of 803 (16%) pregnancies with a prenatal diagnosis of major CHD resulting in TOP. In a logistic model, after excluding syndromic cases, CHD seen on four chamber obstetric ultrasound view was predictive of higher risk of TOP (OR 9.9 (95% CI 1.3 – 75, p=0.03), and Chan index quintile of 1 trended to lower risk (OR 0.49 (95% CI 0.22 –1.1, p= 0.08). Interestingly RoR did not predict risk of TOP, however residence >100km from tertiary care predicted higher risk of diagnosis after 22 weeks gestation (OR 2.3, p=0.001), which in turn is a strong predictor of continuation of pregnancy (OR 0.43 (95% CI 0.2 – 0.76, p=0.004), implying that later gestation of diagnosis may be a mediator in this context. Similarly, Chan quintile 1 predicts higher risk of diagnosis >22 weeks (OR 1.72, p=0.03).

CONCLUSIONS
The major predictors of termination of pregnancy are the severity of major congenital heart disease and timing of prenatal diagnosis, although our work suggests that formal analysis exploring timing of diagnosis as a mediator of remoteness of residence and socioeconomic status is warranted.

Fetal diagnosis and management of pulmonary artery sling: A case series

Scott Bennett, Lisa K. Hornberger, Deborah Fruitman, Timothy Bradley and Gitanjali Mansukhani

BACKGROUND
Pulmonary artery sling is a rare congenital anomaly accounting for 2% of patients with vascular anomalies that cause airway obstruction. In the normal heart, the left and right pulmonary arteries (LPA and RPA) arise in the intrapericardial space. However, in pulmonary artery sling the LPA trunk arises in the extrapericardial space from the posterior aspect of the RPA and causes tracheal compression. Prenatal diagnosis of most congenital heart disease is possible however, there are few reports documenting prenatal LPA sling.

METHODS/RESULTS
We retrospectively identified all cases of prenatal LPA sling from 3 western Canadian fetal cardiology centers since 2015. Data captured included pregnancy outcome, imaging, and operative reports were reviewed. Patient A and B were monochorionic-diamniotic twins both diagnosed with LPA sling. Due to polyhydramnios and significant airway narrowing in one twin, they were delivered via Cesarian section at 35 weeks in the surgical hospital for immediate resuscitation. Both patient A and B were managed with surgical repair as infants. Patient C was a dichorionic-diamniotic twin who had intrauterine growth restriction and abnormal umbilical doppler pulsatility index. She was diagnosed postnatally with trisomy 21 and hospitalized at 4 months of age with acute respiratory distress. She underwent surgical repair shortly after. Patient D was referred for multiple fetal congenital anomalies and echocardiography demonstrated LPA sling and moderate-large ventricular septal defect. The fetus developed ascites but not hydrops, and congenital high airway obstruction due to severe tracheal stenosis. Intrauterine fetal demise occurred at 35+5 weeks. Autopsy confirmed LPA sling.

CONCLUSIONS
Prenatal detection of LPA sling is possible using the 3-vessel view and should prompt evaluation for severe airway obstruction, cardiac and extracardiac lesions, and genetic testing. Prenatal diagnosis permits counselling regarding clinical outcomes and optimized perinatal and neonatal care.

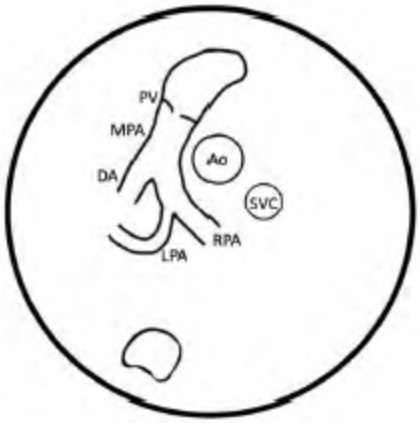
PV
MPA
DA
Ao
SVC
RPA
LPA


PV
MPA
DA
RPA
LPA
83fps

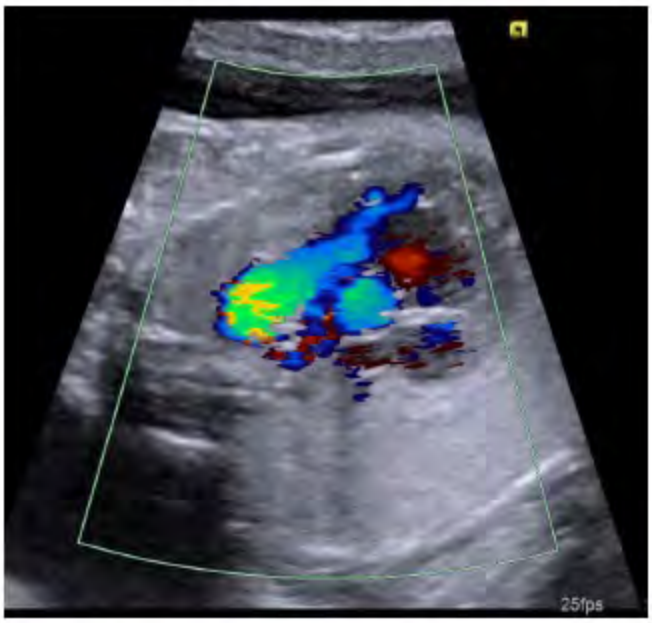

Figure 1: Fetal echocardiography images of Patient B at 33 weeks gestation. a) In the 3 vessel view and further demonstrated in the diagram, the right ventricular outflow tract and pulmonary valve (PV) was seen leading to the main pulmonary artery (MPA) which gave rise only to the right pulmonary artery (RPA) and ductus arteriosus (DA). The left pulmonary artery (LPA) was shown arising from the distal RPA coursing behind the trachea (*)and ultimately under the ductal arch towards the left lung. b) Color Doppler confirmed the abnormal course of the LPA. Ascending aorta (Ao); Superior vena cava (SVC).

SEX DIFFERENCES IN FOLLOW UP AND OUTCOMES AFTER AN ACUTE CORONARY SYNDROME IN ALBERTA, CANADA

CATHERINE BOUTET1, TODD WILSON2, MICHELLE GRAHAM1

BACKGROUND

Acute coronary syndrome (ACS) is the greatest cause of mortality (approximately 7 million deaths annually) and loss of disability adjusted life years1 . Men often receive earlier diagnosis, and more aggressive treatment then women when hospitalized for ACS2-4. This variability in initial management is well documented, however, it is unclear if differences persist during follow up. We aimed to evaluate sex differences and outcomes in the outpatient management strategies post ACS in Alberta, Canada.

METHODS/RESULTS

This study used linked administrative datasets to establish a cohort of all incident ACS patients in the province of Alberta from 2010 to 2022. Patients residing out of the province and those with previously established cardiovascular disease (CVD) were excluded. The primary endpoint was time to and frequency of follow up by sex at 30 days, 60 days, 90 days and yearly (up to 10 years). Mean comparison t-test and Wilcoxon rank-sum median comparison test between unstable angina, non-ST elevation myocardial infarction (NSTEMI), ST elevation myocardial infarction
(STEMI) were used to determine statistical differences between sexes. A Cox proportional hazard was used to determine death within one year of ACS events. Of 60 448 patients without prior CVD diagnosed with ACS, 41 799 (69.2%)
were men and 18 649 (30.8%) were women with a mean age of 61.7 years and 66.2 years in men and women, respectively. Men were more likely to be current smokers whereas hypertension and diabetes were more common in women. Women with NSTEMI were less likely to receive early primary care physician and specialist follow up than men, and had fewer total follow up visits. There was a significant decrease of missed/loss to follow up post ACS in the post pandemic period for both men and women in all three ACS pathologies (table 1). Lastly, death (5.9% vs 4.7%) and heart failure events (2.3% vs 1.5%) at one year were more common in women than men ($p<0.001$).

CONCLUSIONS

Our findings suggest that there are sex differences in follow up after an ACS event which may contribute to differences in outcomes. Further research is required to determine whether these process of care differences lead to differences in guideline directed medical therapy. Finally, we have identified a large increase in post pandemic follow up that may affect future outcomes in both sexes.

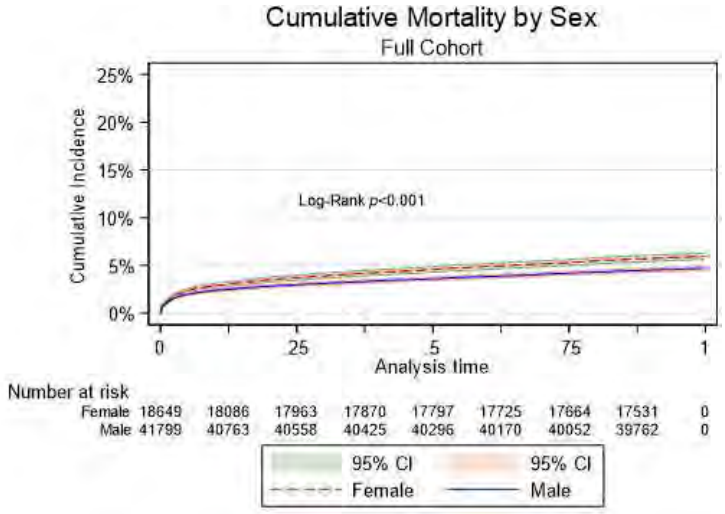

Figure 1 – Adjusted Kaplan – Meier curves for patient diagnosed with acute coronary syndrome (ACS) by sex. Blue line: men (n = 41 799). Pink line: women (n=18 649).

Table 1 - Time, type and number of follow up post ACS by sex over 10 years.

	Admission Diagnosis					
	Unstable Angina		**NSTEMI[1]**		**STEMI[2]**	
	Male (n, %)	Female (n, %)	Male (n, %)	Female (n, %)	Male (n, %)	Female (n, %)
Time to follow up[3]						
Family physician						
< 3 weeks	1,341 (83.9)	762 (82.2)	2,619 (85.7)	1,398 (82.2)	457 (80.9)	167 (81.1)
3- 6 weeks	55 (3.4)	37 (4.0)	158 (5.2)	101 (5.9)	31 (5.5)	14 (6.8)
>18 weeks	131 (8.2)	90 (9.7)	183 (6.0)	130 (7.6)	53 (9.4)	11 (5.3)
Specialists follow up[4]						
< 3 weeks	4,978 (91.8)	2,579 (90.1)	13,879 (95.5)	6,934 (95.4)	14,012 (98.7)	4,523(99.1)
3- 6 weeks	118 (2.0)	77 (2.6)	189 (1.3)	82 (1.1)	51(0.3)	11(0.2)
6 – 10 weeks	88 (1.6)	57 (1.9)	155 (1.0)	67 (0.9)	35(0.2)	8(0.1)
10 – 12 weeks	28 (0.5)	16 (0.5)	72 (0.4)	22 (0.3)	11(0.07)	3(0.06)
12 – 18 weeks	46 (0.8)	26 (0.9)	63 (0.4)	59 (0.8)	19 (0.1)	4 (0.08)

>18 weeks	162 (2.9)	105 (3.6)	169 (1.1)	100 (1.3)	58 (0.4)	12 (0.2)
Number of visits with health care provider [5]						
N	7,380 (17.6)	3,938 (21.1)	17,972 (42.9)	9,135 (48.9)	15,330 (36.6)	4,981 (26.7)
Mean (SD)	16.8 (19.1)	13.4 (18.4)	18.8 (20.3)	16.9 (20.7)	22.1 (25.2)	21.7 (23.5)
Median (IQR)	11 (4,23)	8 (3, 17)	13 (6, 24)	11 (5, 21)	17 (10, 27)	16 (10, 26)
Number of loss follow up post pandemic						
No follow post ACS	71 (34.5)	46 (29.5)	144 (63.3)	80 (36.7)	165 (37.0)	69 (40.8)

1. NSTEMI: non ST elevation myocardial infarction
2. STEMI: ST elevation myocardial infarction
3. Time to follow up P-values were the following: Family physician: Angina p = 0.348, NSTEMI = 0.025, STEMI = 0.21 Cardiologist: Angina p = 0.253, NSTEMI = 0.001, STEMI = 0.717 Internal Medicine: Angina p = 0.780, NSTEMI = 0.024, STEMI = 0.36.
4. Specialist include internal medicine physicians and cardiologist
5. Number of visits by sex in the first 12 months post ACS statistical mean comparison t-test was used and showed unstable Angina p<0.001, nSTEMI p<0.001, STEMI p=0.363. Wilcoxon rank-sum median comparison test: Unstable Angina p<0.001, NSTEMI p<0.001, STEMI p=0.006

Working toward assessment of eNOS based platelet subpopulations in Acute myocardial infarction patients vs healthy volunteers.

Diego Alberto Castaneda-Zaragoza, Paul Jurasz

BACKGROUND

Acute myocardial infarction (AMI) remains one of the main causes of mortality in Canada. Despite current antiplatelet therapies, incidence and mortality of AMI remains high. Nitric oxide (NO) plays an important role in platelet function by inhibiting platelet adhesion and aggregation. In addition, previous studies have shown that platelets of patients with acute coronary syndromes have reduced NO production.

Recently our research group identified two platelet subpopulations. One that does not produce NO due to an absence of the enzyme NO synthase (eNOSneg) which accounts for ~20% of all platelet count and a platelet subpopulation that possess the NO synthase (eNOSpos). Furthermore, previous studies have used Quartz Crystal Microbalance with dissipation (QCM-D) under flowing conditions to assess platelet function assessing aggregation and stiffness of the resulting aggregate, Nevertheless, it has not been explored the eNOS-based platelet subpopulation neither platelet function using QCM-D in patients with AMI.

METHODS/RESULTS

Platelets were isolated from healthy donors resuspended in Tyrode's buffer and supplemented with L-arginine (100uM). Platelet function was assessed by coating QCM-D with collagen (10ug/ml) for 1 hour, and then platelets

were flowed through saw)D (noitapissid dna)F (ycneuqerf ni egnahc evitagen .nim/lm14.1 ta meht measured over 7 minutes. Thereafter, platelets were Fixed, permeabilized and blocked. Platelets were incubated with primary antibodies: anti-eNOS antibody

(1.25ug/mL), or Isotype control (1.25ug/mL), for 1 hour at room temperature and secondary antibody Alexa Fluor 488 (10ug/ml), for 1 hour at room temperature. Lastly, platelets were stained with anti-CD42b-PE (0.0025ug/ml). Samples were analyzed using a Fortessa X flow cytometer and analyzed using FlowJo software.

We have started recruiting healthy participants to assess their eNOS platelet subpopulations and we have found that >92% of our sample are CD42b positive events (Figure 1a) and from those events we have measured the eNOS platelet subpopulation ratio being ~17% eNOSneg to ~83% eNOSpos (Figure 1b). In addition, platelet function under flowing condition was measured using QCM-D. We found that platelet aggregation, measured by negative change in frequency, is 49.7 and the stiffness of the resulting aggregate, measured by positive change in Dissipation, is 7.6

CONCLUSIONS

We plan to start collecting samples from AMI to identify the eNOS based platelet subpopulation and compare it with healthy controls. Additionally, we aim to assess platelet function under flowing conditions using the QCM-D and correlate with the eNOS based platelet subpopulations.

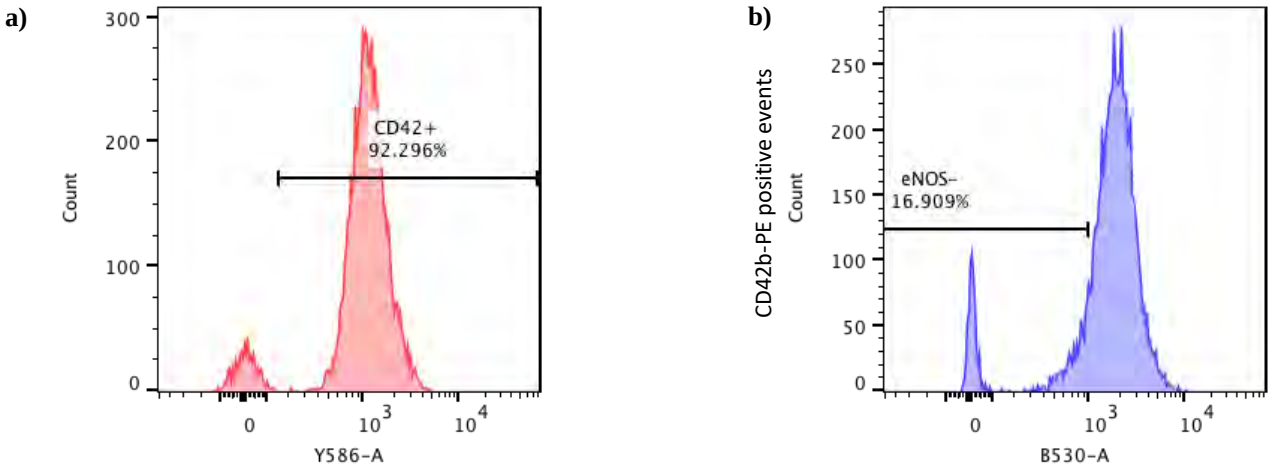
a)
300
200
100
0
Count
CD42+
92.296%
0
10^3
10^4
Y586-A
b)
250
200
150
100
50
0
CD42b-PE positive events
Count
eNOS-
16.909%
0
10^3
10^4
B530-A

Figure 1

The GLP-1 receptor agonist liraglutide alleviates type 2 diabetes-related diastolic dysfunction in a pyruvate dehydrogenase dependent manner

Jordan S.F. Chan, Amanda A. Greenwell, Christina T. Saed, Magnus J. Stenlund, Indiresh A. Mangra-Bala, Seyed Amirhossein Tabatabaei Dakhili, Kunyan Yang, Keshav Gopal, Farah Eaton, John R. Ussher

BACKGROUND

Impairments in cardiac energy metabolism are a major contributor to the pathology of diabetic cardiomyopathy (DbCM), which is characterized by diastolic dysfunction. This includes an increased reliance on fatty acid oxidation to meet the heart's energy demands, which coincides with a marked reduction in glucose oxidation. Of interest, several studies have shown that restoration of myocardial glucose oxidation improves cardiac function in type 2 diabetes (T2D). Liraglutide, a glucagon-like peptide-1 receptor (GLP-1R) agonist used for the treatment of T2D that also improves cardiovascular outcomes, can alleviate diastolic dysfunction and increase myocardial glucose oxidation in experimental T2D. However, whether these increases in glucose oxidation explain the liraglutide-mediated alleviation of DbCM remains enigmatic. Thus, we hypothesized that the cardioprotective actions of liraglutide would be abolished in mice with T2D and a cardiac-specific deletion of pyruvate dehydrogenase (PDH; PDH cardiac KO mice), the rate-limiting enzyme of glucose oxidation.

METHODS/RESULTS

Male PDH cardiac KO mice and their myosin heavy chain-α Cre expressing littermates (αMHC Cre mice) were subjected to experimental T2D via 10-weeks of high-fat diet supplementation (60% kcal from lard) with a single low-dose injection of streptozotocin (75 mg/kg) provided at week 4. After the induction of experimental T2D, αMHC Cre and PDH cardiac KO mice were randomized to treatment with either vehicle control (VC; saline) or liraglutide (30 µg/kg) twice daily during the final 2-weeks of the protocol, with cardiac function assessed via ultrasound echocardiography pre- and post-treatment. As expected, liraglutide treatment improved glucose homeostasis in both αMHC Cre and PDH cardiac KO mice with T2D but did not produce any notable weight loss. Furthermore, parameters of systolic function were unaffected by liraglutide treatment in both groups. In contrast, liraglutide treatment alleviated diastolic dysfunction in αMHC Cre mice with T2D, as indicated by an increase and decrease in the e'/a' ratio (1.63 vs. 1.32; $p<0.05$) and E/e' ratio (25.25 vs. 31.52; $p<0.05$), respectively, when compared to VC-treated αMHC Cre mice with T2D. Consistent with our hypothesis, liraglutide failed to rescue diastolic dysfunction in PDH cardiac KO mice with T2D, as evidenced by a lack of improvement in either the e'/a' ratio (1.34 vs.1.24) or E/e' ratio (30.46 vs. 31.29) relative to VC-treated PDH cardiac KO mice with T2D.

CONCLUSIONS

Our findings suggest that increases in myocardial glucose oxidation are necessary for GLP-1R agonist-mediated improvements of diastolic function in T2D. Therefore, strategies aimed at increasing PDH activity may represent a novel approach for DbCM management.

A deep learning approach to left ventricular segmentation from 3D echocardiography

Ishani DasGupta, Michelle Noga, Kumaradevan Punithakumar, Nilanjan Ray

BACKGROUND

Echocardiography is a non-invasive, non-ionizing, cost-effective medical imaging modality that uses ultrasound (US) waves to evaluate heart function. Analysis of the left ventricle (LV) and estimating its function are crucial in diagnosing cardiac diseases. Quantitative volumetric analysis of the LV involves time-consuming delineation of endocardial borders. Semi- and fully-automated methods developed for LV segmentation utilize a variety of approaches: surface fitting, atlas-based methods, and more. Although machine learning has shown promise when predicting measurements in multiple medical imaging tasks, it has not been explored extensively for 3D echocardiography (3DE). The proposed research utilizes neural networks to automatically generate and predict segmentation labels from 3DE scans, reducing diagnosing time. The tested nnU-Net, a neural network (NN) based on U-Net, generated segmentation labels that achieved an 82% overall Dice score when compared to expert clinicians' ground truth annotations.

METHODS/RESULTS

As a first step, nnU-Net extracts a dataset fingerprint, which includes a set of properties, e.g., voxel spacings and image sizes, which are data-specific. Model configurations undergo training in a 5-fold cross-validation format, which enables nnU-Net to determine the postprocessing on the training dataset. After completing cross- validation, nnU-Net selects the optimal ensemble or configuration based on performance metrics. Averaging the Dice scores for all foreground classes results in a scalar value which nnU-Net then uses to evaluate the model performance.

The 3DE dataset used for training the neural network comprised nine patients (7 for training and 2 for testing). Each 3DE scan included multiple image slices of the 3D volume resulting in 213 temporal volume sequences. Two nnU-Net configurations, 2d and 3d_fullres, were used to generate 3D segmentation labels from the test images. The degree of accurate segmentation was measured by comparing these predicted 3D labels with the ground truth annotations. For the higher resolution 3d_fullres model, precision, recall, Dice score, and Jaccard index values were at 84.5%, 80.7%, 82.5%, and 70.3%, respectively.

CONCLUSIONS

Although nnU-Net performed remarkably well, it primarily targets computed tomography (CT) and magnetic resonance imaging (MRI) and does not exploit prior information associated with echocardiography, e.g., temporal consistency. nnU-Net for automatic segmentation of the LV from 3DE scans has achieved reasonably well results, with an overall Dice score of 82%. The study provides a favourable foundation for developing more accurate and efficient automated segmentation methods for 3DE images. Future work includes exploring other NN architectures that incorporate echocardiography-specific features to train the proposed NN, leading to further improvements in segmentation accuracy.

Modulation of cardiac cytochromes P450 in C57BL/6 mice by acute exposure to the anti-leukemic arsenic trioxide

Mahmoud A. El-Ghiaty**, Sara R. El-Mahrouk**, and Ayman O.S. El-Kadi

BACKGROUND
Arsenic trioxide (ATO) is a hazardous arsenical whose toxicity has been successfully harnessed for treating acute promyelocytic leukemia (APL), and probably for fighting other cancers in the future. Despite its high therapeutic efficacy, the innate toxicity of ATO results inevitably in serious side effects such as cardiotoxicity. Because polypharmacy is very common among cancer patients, they become vulnerable to drug-drug interactions that may result in critical adverse events. These interactions are usually attributed to alterations in drug metabolism, at the core of which is the superfamily of cytochrome P450 (CYP) enzymes. Moreover, these enzymes are also involved in the metabolism of arachidonic acid (AA), and other endobiotics, thus generating metabolites that might, at least partly, contribute to cardiovascular toxicity. The current study was conducted to characterize the effect of ATO on different CYP enzymes in the heart.

METHODS/RESULTS
10-week-old male C57BL/6 mice were injected intraperitoneally with either normal saline or ATO (8 mg/kg) for 6
h. Hearts were isolated, and real-time PCR (qPCR) analysis was performed to determine mRNA expression levels for various CYP enzymes. Our results showed that after 6 h-exposure, ATO significantly increased mRNA expression levels of Cyp1a2, 1b1, 2a5, 2b9, 2b19, 2c29, 2c38, 2c39, 2c40, 2c65, 2c66, 2d10, 3a11, 4a10, 4f15, and 4f18 by 3.9, 2.7, 3, 1.7, 2.1, 3.1, 1.8, 2.8, 2.9, 2.7, 2.7, 2.9, 2.5, 2.8, 2.9, and 1.6 folds, respectively; while decreased Cyp2c44, 2j9, 2j13, 3a13, and 4f16 mRNAs.

CONCLUSIONS
This study demonstrates that ATO modulates the expression of a wide array of cytochrome P450 enzymes, which may be implicated not only in altered drug biotransformation, but also in deranged AA metabolism. Upregulation of Cyp1a2, 1b1, and 4a10 coupled with downregulating Cyp2j9 and 2j13 may result in unfavorable pattern of AA-derived eicosanoids production that entails cardiotoxicity rather than cardioprotection.

SUPPORT: This work was supported by the Natural Sciences and Engineering Research Council of Canada (NSERC) Discovery Grant [RGPIN 250139] to A.O.S.E. M.A.E. is a recipient of the Rachel Mandel Scholarship in Lymphoma and Other Blood Cancers and the Alberta Innovates Graduate Student Scholarship. S.R.E. is a recipient of the Egyptian Government Scholarship.

Discontinuation of Heart Failure Therapy in patients Undergoing Non-Cardiac surgery: Data from a Real-world Cohort

Malik Elharram, Xiaoming Wang, Pishoy Gouda, Michelle M.Graham

BACKGROUND
Patients with heart failure (HF) with reduced ejection fraction (HFrEF) are at high risk for cardiovascular events following non-cardiac surgery. The perioperative period represents many challenges to maintain guideline directed medical therapy (GDMT). We examined GDMT use in HFrEF patients following non-cardiac surgery, and the association of medication changes with cardiovascular outcomes.

METHODS/RESULTS
Using linked administrative databases, a retrospective cohort of HFrEF patients undergoing major non-cardiac surgery between 2008 and 2020 was formed. Pre-operative use of GDMT was determined by outpatient prescriptions up to 90 days prior to surgery. Changes in GDMT was defined as discontinuation or a dose reduction (≥50%) of baseline therapies at 90 days after discharge. The primary composite outcome was HF hospitalization or all-cause mortality at one-year adjusted for age, sex, components of the Revised Cardiac Risk Index and the Charlson Comorbidity index.

Of 397,829 index surgeries, there were 7667 (2%) patients with pre-existing HFrEF on at least one GDMT (50.6% female; mean age: 75 +/- 12 years). At 90 days post-operatively, 46% of patients had undergone major changes to GDMT. Compared to patients who continued GDMT, patients with any change to therapy had a higher incidence of the primary outcome (52% vs. 46%, aOR: 1.14, 95% CI: 1.03-1.25) and all-cause mortality at one year (8.5% vs. 4.9%, aOR: 1.57, 95% CI: 1.3-1.90).

CONCLUSIONS
Among patients with HFrEF undergoing major non-cardiac surgery, few are on optimal GDMT, and perioperative changes to GDMT is associated with higher odds for HF hospitalization or death.

Sexual dimorphism in cardiorenal protective effect of soluble epoxide hydrolase genetic deletion in aged mice following myocardial infarction

Liye Fang, Ala Yousef, Faqi Wang, Jia You, Zamaneh Kassiri, John M.Seubert

BACKGROUND
Cardiovascular disease (CVD) is a leading cause of death in both females and males resulting in significant health and economic burdens. While differences in CVD between males and females are recognized, it remains understudied. Cardiorenal syndrome encompasses a spectrum of disorders where acute or chronic dysfunction of 1 organ can induce dysfunction in the other organ, reflecting the interdependent relationship between the heart and kidney. However, our understanding of age- and sex-differences remains limited. CYP450 enzyme metabolizes N-3 and N-6 polyunsaturated fatty acids (PUFAs) into various bioactive lipid mediators, with cardioprotective properties. These lipids are further metabolized into less active or toxic diols by soluble epoxide hydrolase(sEH). We, and others, have reported the inhibition of sEH significantly attenuates the adverse effects of myocardial infarction but its role in protecting the kidney following cardiac MI is unknown. The objective of this study was to investigate cardiorenal protective effects of the global sEH genetic deletion on both aged male and female following MI.

METHODS/RESULTS
Method: Male and female WT and sEH null mice (15-18 mo) were subjected to permanent left anterior descending artery ligation to induce myocardial infarction. Echocardiography was used to assess the cardiac function at baseline and 7 days post MI. Frailty index was collected as a marker for aging/body condition. Plasma, hearts and kidneys were collected for molecular and biochemical analyses.

Result: Echocardiography analyses demonstrated a reduced systolic and diastolic cardiac function after LAD surgery in all mice. However, female sEH null mice showed significantly better ejection fraction compared to all other groups. Overall markers such as frailty index and plasma glucose levels (acute hyperglycemia) were attenuated in sEH null mice post MI. Activation of NLRP3 was observed in only WT mice post MI suggesting genotype differences in the innate immune response. Sex-dependent differences in mitochondrial antioxidant gene expression demonstrated female mice had significantly lower GPX1 gene expression. While aged sEH null female mice exhibited preserved markers of cell injury, ICAM-1 and KIM-1, compared to their WT counterparts. Interestingly, all groups had significantly higher levels of mitochondrial DNA transcription factor Tfam post MI but increased mitochondrial DNA content was only observed in sEH null mice, suggesting better mitochondrial quality control in sEH null mice.

CONCLUSIONS
Our data highlight both sex- and genotype-differences in renal injury following myocardial infarction in aged mice. Importantly, these preliminary data demonstrated aged female sEH null mice had better cardiac and renal protection.

Myosteatosis is associated with disease burden and decreased aerobic endurance in adults recovered from COVID-19

Stephen J Foulkes, David I Paterson, Rachel Sherrington, Christian Beaulieu, Caroline Gendron, Peter Seres, Justin Grenier, James White, Mark J Haykowsky, Richard B Thompson

BACKGROUND
Skeletal muscle fat infiltration (myosteatosis) is associated with reduced aerobic endurance and increased morbidity in chronic disease populations, and may be predictive of disease burden following coronavirus disease 2019 (COVID-19). Therefore, we sought to investigate the association between myosteatosis with acute and persistent COVID-19 burden and aerobic endurance in adults (n=203) with a previous COVID-19 diagnosis.

METHODS/RESULTS
Adults >12-weeks following diagnosis with COVID-19 (n=203, 65% female, 51±14 years; 29.1±6.0 kg/m2) were recruited for a comprehensive MRI scan, including chemical-shift encoded fat and water separated imaging of the mid-thigh. Myosteatosis was measured as the muscle fat fraction (MFF, %), which was calculated as the total volume of fat divided by the total muscle and fat volume within the muscle boundary of the mid-thigh. These were compared to reference data for age-matched healthy controls from our laboratory (n=99; 43% female; 49
±14 years; 24.8±3.7 kg/m2). Aerobic endurance was quantified by the distance covered in a 6-minute walk test (6MWd). Duration of COVID-19 symptoms at the time of infection was stratified into 0-7, 8-14 and >14 days, with the impact of persistent COVID-19 symptoms on activities of daily living (ADLs) classified on a 5-point scale as not at all (1), mild-to-moderately limited (2-3) and significantly limited (4-5). All comparisons were made with adjustment for age and sex using analysis of covariance.

Participants were assessed 162±54 days post COVID-19. After adjustment for age and sex, the COVID-19 cohort had higher MFF than healthy controls (Figure 1A). Fifty-three participants (26%) were hospitalized due to COVID-19, and had a markedly increased MFF compared to those not hospitalized (Figure 1B). Increasing duration of initial COVID-19 symptoms (Figure 1C), and the impact of persistent symptoms on ADLs (Figure 1D) was associated with increased MFF, which was negatively correlated with 6MWd (r=-0.53, P<0.001).

CONCLUSIONS
Thigh myosteatosis is a marker of disease burden and decreased aerobic endurance in adults recovered from COVID-19 infection.

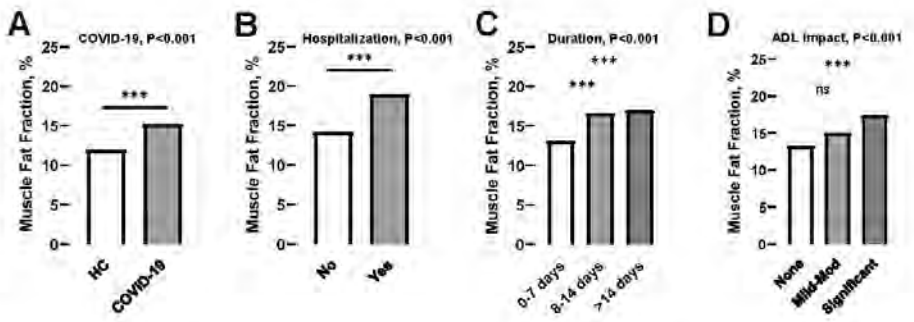

Figure 1. Differences in myosteatosis between A) Reference data for healthy controls (HC) from our laboratory and individuals recovered from COVID-19; and across B) whether individuals were hospitalized as a result of COVID-19; C) increasing duration of COVID-19 symptoms at the time of infection; and D) increasing impact of persistent COVID-19 symptoms on ADLs. Data are estimated marginal means with 95% CI adjusted for age and sex. Post-hoc: *** P<0.001 relative to first category for each panel.

Effect of angiostatin and its neutralization on cell death and cellular infection by SARS-CoV and SARS- CoV-2

Aleksandra Franczak, Michael Joyce, Sophia Li, Khaled Barakat, Lorne Tyrrell, Paul Jurasz

BACKGROUND
Angiostatin is constitutively generated angiogenesis inhibitor important for endothelial cell homeostasis. High angiostatin concentrations, such as those observed in COVID-19 patient plasma, promote cell death in acidotic microenvironment - characteristic of severe COVID-19, and thus might contribute to lung endothelial barrier failure. Conversely, COVID-19-relevant angiostatin concentrations reduce SARS-CoV-2 (D614G) cellular entry, most likely by interacting with abundant spike protein lysine residues and preventing spike protein cleavage, that is essential for SARS-CoV-2 infection. The aim of the study was 1) To assess if angiostatin prevents entry of other SARS-CoV-2 variants and SARS-CoV, 2) To assess effect of selective angiostatin neutralization on cell death and cellular infection by SARS-CoV-2, 3) To model 3D structure of angiostatin-spike complex, 4) To assess if inhibition of PV cellular infection is lysine-dependent.

METHODS/RESULTS
HEK293-ACE2 cells were infected with replication-incompetent SARS-CoV-2 pseudo-viruses (PV, GFP-expressing; SARS-CoV-2 Omicron, SARS-CoV Urbani) with/without angiostatin (140microg/ml) and analyzed by flow cytometry. VeroE6 cells were infected with wild-type SARS-CoV-2 and treated with angiostatin (140microg/ml) in the presence/absence of selective angiostatin neutralizing (Alpha) or control peptides (Delta) for 24h at pH 6.9. Cell death was quantified by TUNEL and percentage of detached cells. Immunofluorescent staining against spike protein was used to confirm cellular infection. In silico modeling was used to confirm binding of angiostatin to spike protein. To test if inhibition of infection is lysine-dependent, Omicron PV infection was carried out with angiostatin in the presence/absence of epsilon-aminocaproic acid (EACA, lysine analogue). Angiostatin lowered the percentage of GFP-expressing HEK293-ACE2 cells
(Omicron: 23±5.6 vs 1.5±0.3%, p=0.0148; Urbani: 73.1±5.8 vs 7.2±4.9%,
p=0.0095). Angiostatin neutralizing peptides reduced % of detachment (cell death) of SARS-CoV-2-infected VeroE6 in the presence of angiostatin by approximately half compared to concentration matched peptides. Angiostatin reduced the percentage of TUNEL and spike protein positive cells, and these reductions were maintained in the presence of peptides (Figure 1). In silico molecular binding study predicted angiostatin bind to spike protein lysine residues near the S1/S2 cleavage site. EACA reversed angiostatin's effect on reducing % of infection by 20% (p = 0.002).

CONCLUSIONS
Angiostatin inhibits cellular infection not only by multiple variants of SARS-CoV-2, but also by SARS-CoV, suggesting its importance in the pathophysiology of other SARS-like beta coronaviruses. Selective angiostatin neutralizing peptides may be potential new therapeutic strategy to reduce angiostatin-induced cell death within COVID-19 without interfering with angiostatin's ability to reduce SARS-CoV-2 cellular infection. Angiostatin binding to spike protein and inhibition of cellular infection is partially lysine-dependent.

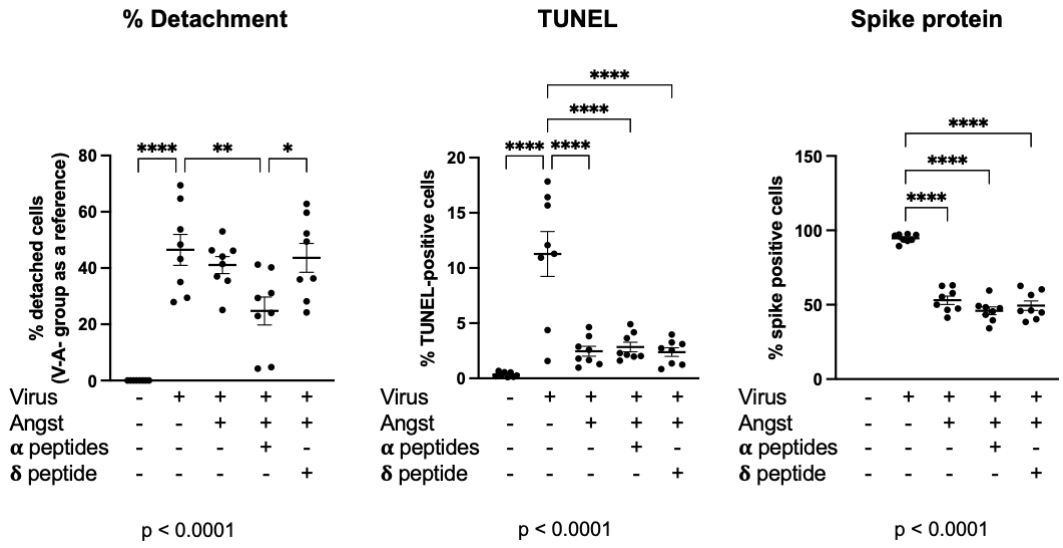

Figure. Effect of selective angiostatin neutralization on Vero E6 cell death and cellular infection by SARS-CoV-2.

FEASIBILITY OF UTILISING QUALITY OF LIFE ADJUSTED DAYS ALIVE AND OUT OF HOSPITAL IN HEART FAILURE CLINICAL TRIALS

PISHOY GOUDA, SARAH RATHWELL, ELOISA COLIN-RAMIREZ, MICHAEL FELKER, HEATHER ROSS, JORGE ESCOBEDO, PETER MACDONALD, RICHARD TROUGHTON, CHRIS O'CONNOR, JUSTIN EZEKOWITZ

BACKGROUND
Clinical trials in heart failure (HF) identify treatment differences using objective measurement of morbidity and mortality, such as death and hospitalisations and quality of life. Integrating these elements in clinical trials, including via days alive and out of hospital (DAOH) and quality of life in a single metric may provide a useful way of evaluating therapies.

METHODS/RESULTS
Using data from two clinical trials in HF [Guiding Evidence Based Therapy Using Biomarker Intensified Treatment in Heart Failure (GUIDE-IT) and Study of Dietary Intervention under 100mmol in Heart Failure (SODIUM-HF)] we explored the feasibility of assessing treatment difference using %DOAH adjusted for quality of life at 18-months as the primary outcome. For each participant %DAOH was calculated as a ratio between DAOH / total follow-up. Using a one inflated beta regression model, %DAOH was subsequently adjusted for quality of life measured by the Kansas City Cardiomyopathy Questionnaire Overall Summary Score (KCCQ-OSS). In the GUIDE-IT trial, 847 participants were included with a median baseline KCCQ-OSS score was 59.0 [Interquartile range (IQR) 40.8-74.3]. No change in KCCQ-OSS was observed at 18-months in either arm. %DAOH was 90.76% +/- 22.09% in the biomarker-guided arm and 88.56% +/- 25.27% in the usual care arm. Using the one-inflated beta regression model and adjusting for quality of life, no significant difference QoL adjusted %DAOH was observed [1.09% (-1.57
%, 3.97%)]. In the SODIUM-HF trial, 796 were included with a median baseline KCCQ-OSS score was [69.8 (IQR 49.3-84.3]. No change in KCCQ-OSS was observed at 18-months in either arm. %DAOH was 95.69% +/- 16.31% in the low-sodium arm and 95.95% +/-14.76% in the usual care arm. Using the one-inflated beta regression model and adjusting for quality of life, no significant difference QoL adjusted %DAOH was observed [1.91% (-0.85 %, 4.77%)].

CONCLUSIONS
Adjusting %DOAH for quality of life is feasible and may provide complementary information on treatment effects in heart failure clinical trials.

Table 1 – Demographics of Trial Participants

Characteristic	GUIDE-IT (N=847)	SODIUM HF (N=796)
Age, median (IQR), y	63.00 (53.00, 72.00)	67.00 (58.00, 74.00)
Women, N (%)	266 (31.4%)	264 (33.2%)
Ejection fraction, median (IQR), %	24.00 (20.00, 30.00)	35.85 (27.00, 49.00)
NYHA class at enrollment, N (%)		
I	54 (6.4%)	8 (1.0%)
II	426 (50.8%)	570 (71.8%)
III	342 (40.8%)	213 (26.8%)
IV	16 (1.9%)	3 (0.4%)
Risk factors, N (%)		
Ischemic heart disease	426 (50.3%)	307 (38.6%)
Diabetes mellitus	390 (46.0%)	284 (35.7%)
Atrial fibrillation	137 (16.2%)	327 (41.6%)
Chronic kidney disease	311 (36.7%)	400 (51.3%)
Systolic BP, median (IQR), mm Hg	114.00 (101.00, 129.00)	118.00 (105.00, 129.00)
Heart rate, median (IQR), beats/min	76.00 (67.00, 86.00)	69.00 (61.00, 76.00)
NT-proBNP, median (IQR), pg/mL	2648.00 (1461.00, 5339.00)	763.00 (335.00, 1552.00)
Creatinine, median (IQR), mg/dL	1.30 (1.05, 1.70)	1.14 (0.94, 1.46)
Treatments, N (%)		
Beta Blocker	789 (93.2%)	694 (87.3%)
ACE/iARB	651 (76.9%)	534 (67.2%)
Mineralocorticoid antagonist	415 (49.0%)	454 (57.1%)
Implantable cardioverter-defibrillator	338 (39.9%)	182 (22.9%)
Cardiac resynchronization therapy	156 (18.4%)	73 (9.2%)
Treatment arm, N (%)		
Intervention	422 (49.8%)	390 (49.0%)
Usual care	425 (50.2%)	406 (51.0%)
Outcomes		
KCCQ-PLS, median (IQR)	65.00 (41.67, 85.00)	75.00 (54.17, 87.50)
KCCQ-CSS, median (IQR)	75.00 (50.00, 100.00)	74.74 (56.65, 88.54)
KCCQ-OSS, median (IQR)	59.03 (40.80, 74.31)	69.79 (49.35, 84.38)
Unadjusted DAOH, mean (SD)	375.78 (185.77)	522.55 (89.91)

Abbreviations: IQR – interquartile range; NYHA – New York heart association; BP – blood pressure; ACEi – angiotensin converting enzyme inhibitor; ARB – angiotensin II receptor blocker; KCCQ – Kansas City Cardiomyopathy Questionnaire; PLS – physical limitations score; CSS – clinical summary score; OSS – overall summary score; DAOH – days alive and out of hospital

Figure 1 – Estimated difference in %DAOH at 18-months

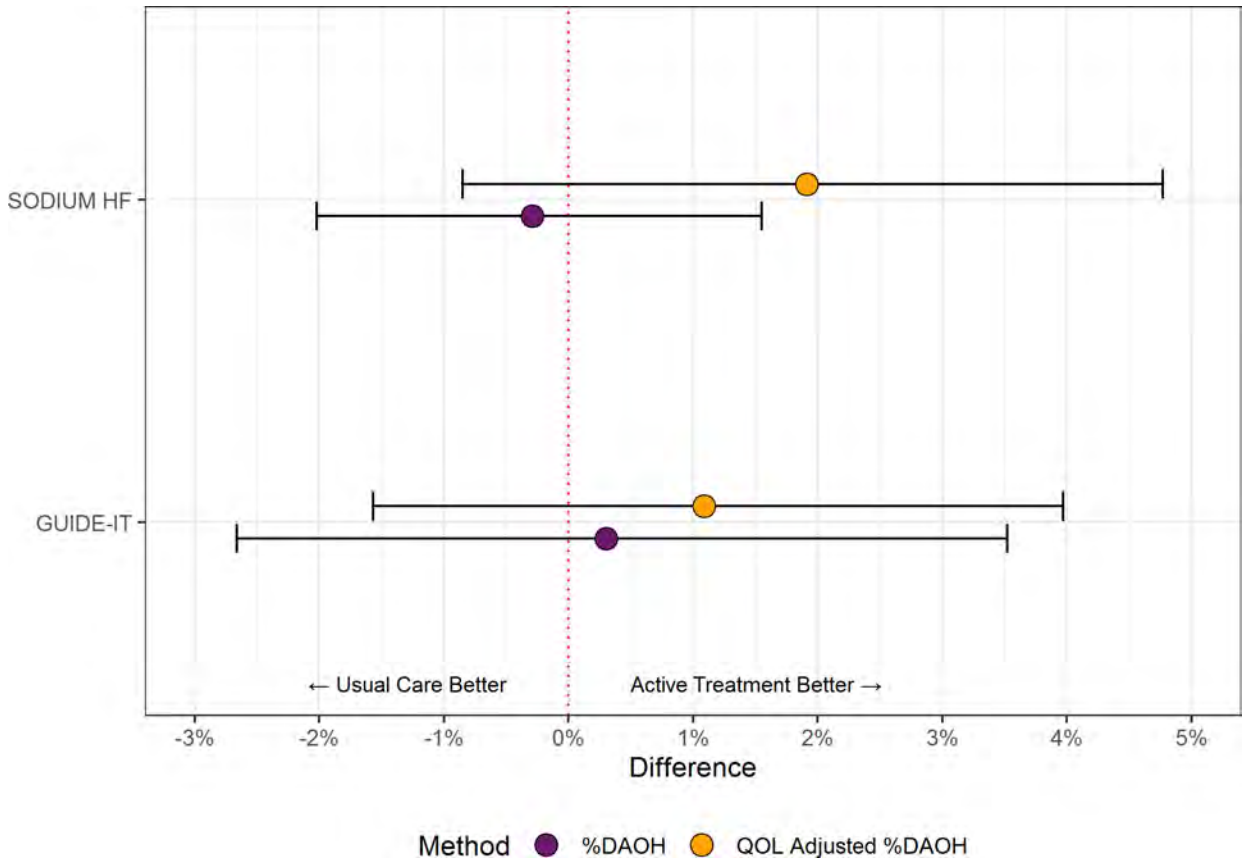

Figure Legend: Estimated difference in %DAOH at 18 months using a one-inflated beta regression model with bootstrapped 95% confidence with (yellow) and without (purple) adjustment for quality of life. Abbreviations: %DAOH – percentage days alive and out of hospital; QOL – quality of life.

Prenatal hypoxia increases thromboxane-mediated vasoconstriction in mesenteric arteries of only female adult offspring, which is prevented by a prenatal placental antioxidant treatment

Murilo E. Graton1, Floor Spaans1, Rose He1, Raven Kirschenman1, Paulami Chatterjee1, Anita Quon1, Thomas Phillips2, Patrick Case3, Sandra T. Davidge1 1University of Alberta, Canada, 2Cardiff University, UK, 3University of Bristol, UK

BACKGROUND

Introduction: Fetal hypoxia, a common pregnancy complication, increases the risk of later-life cardiovascular disease. Mesenteric resistance arteries (important for blood flow and blood pressure regulation) of adult offspring exposed to prenatal hypoxia have increased responsiveness to endogenous vasoconstrictors. Nitric oxide (NO) is an endogenous vasodilator, and a reduction in NO bioavailability contributes to increased vasoconstrictor responses. We previously showed that a placenta-targeted antioxidant treatment (nMitoQ) during pregnancy improves offspring cardiovascular outcomes. However, whether nMitoQ reduces vasoconstrictor responses in mesenteric arteries of prenatal hypoxia offspring, and the role of NO as a modulator, is not known. We hypothesized that prenatal hypoxia increases vasoconstrictor responses in mesenteric arteries from adult offspring via decreased NO modulation, which is improved by nMitoQ treatment.

METHODS/RESULTS

Methods/Results: On gestational day (GD)15, rats received a single i.v. injection of ro)2O %12(aixomron ot
desopxe erew dna)M 521(QotiMn ro)enilas(elcihev hypoxia (11% O2) until GD21 (term=22 days). Mesenteric arteries from 4-month-old offspring were isolated and mounted on a wire myograph, and vasoconstriction responses to U46619 (thromboxane A2 analogue) were assessed. Contribution of NO to vasoconstriction was measured by pre-incubation with L-NAME [NO synthase (NOS) inhibitor] before the U46619 response curve.
Thromboxane prostanoid (TP) receptor and endothelial (e)NOS expression were assessed with immunofluorescence in mesenteric artery sections. Data were analyzed by two-way ANOVA (Sidak's post-hoc test, significance: $p<0.05$); n=6-14/group. In female offspring, prenatal hypoxia increased U46619 responsiveness ($p=0.009$), which was prevented by prenatal treatment with nMitoQ ($p=0.03$). Pre-incubation with L-NAME further increased U46619 responsiveness in both normoxia groups (saline, $p=0.003$; nMitoQ, $p=0.0003$), and hypoxia nMitoQ-treated offspring ($p=0.005$), but not in the hypoxia saline group in female offspring, In male offspring, U46619 vasoconstriction responses were similar across all groups, and the presence of L-NAME enhanced U46619 responsiveness to the same extent in all male normoxia (saline, $p=0.0390$; nMitoQ, $p=0.0167$) or hypoxia (saline, $p=0.0002$; nMitoQ,
$p=0.0028$) groups. Surprisingly, TP receptor or eNOS expression was not altered in either the female or male offspring.

CONCLUSIONS

Conclusions: In female, but not in male offspring, prenatal hypoxia increased mesenteric artery thromboxane- mediated vasoconstriction responses. Moreover, a placental-targeted antioxidant

treatment with nMitoQ during pregnancy reduced the enhanced vasoconstriction observed in mesenteric arteries of adult offspring exposed to prenatal hypoxia, via increasing NO contribution to vasoconstriction. Our data suggest that prenatal hypoxia impairs systemic vasoconstrictor capacity

Ertugliflozin does not inhibit the late component of the cardiac voltage-gated sodium channel

Brittany Gruber, Mohammad Fatehi, Arkapravo Chattorpadhyay, Khaled Barakat, Peter E. Light

BACKGROUND
Patients with diabetes experience cardiovascular disease at a higher rate including a more than 2-fold increased risk of heart failure. Thus, when choosing treatment there is strong motivation to use pharmacotherapies that prioritize cardioprotection. The sodium-glucose transport-2 inhibitors (SGLT2is) prevent glucose reabsorption in the kidney reducing blood glucose. Surprisingly, SGLT2is such as dapagliflozin were also found to be highly cardioprotective in patients with or without type-2 diabetes. Our research has shown that the late component of the cardiac voltage gated sodium channel (late-INa) is a molecular target for the SGLT2is that may contribute to cardioprotection (Philippaert et al., Circulation, 2021). However not all SGLT2is are equally effective at protecting against heart failure and cardiovascular death. Ertugliflozin, was shown to be no better than placebo at preventing death from cardiovascular cause or heart failure (11.9% vs 11.9%) or preventing stroke (3.4% vs 3.2%) or myocardial infarction (6.0% vs 5.8%) (VERTIS-CV trial). Therefore, we proposed that structural differences of ertugliflozin compared to dapagliflozin may impact binding to Nav 1.5 and affect the ability of ertugliflozin to inhibit late-INa and therefore help to explain the reduction in cardioprotection observed in clinical trials.

METHODS/RESULTS
Cardiac Nav1.5 channels were recombinantly expressed in HEK293 cells and whole cell patch clamp was used to measure sodium channel currents. In silico docking techniques using the cryo-EM structure of Nav1.5 were used to predict differences in binding affinity of ertugliflozin and dapagliflozin. Our results show that ertugliflozin is a poor inhibitor of late-INa when compared to dapagliflozin and that small structural changes in ertugliflozin interfere with its interaction with the putative binding region in Nav1.5

CONCLUSIONS
Ertugliflozin is less effective than dapagliflozin at inhibiting late-INa which may help to explain clinical observations that show ertugliflozin is less cardioprotective than other SGLT2is.

Proteomic and degradomic approaches to assess the implications of matrix metalloproteinase-2 in the heart

Bridgette Hartley, Wesam Bassiouni, Andrej Roczkowsky, Richard Schulz, and Olivier Julien

BACKGROUND
The reintroduction of blood supply to ischemic heart muscle results in ischemia-reperfusion (IR) injury. One form of IR injury is myocardial stunning caused by short duration of ischemia (~20 min) followed by reperfusion. While cell death is not involved, the mechanism of stunning injury is not fully understood. Part of the damage is caused by the activation of proteases, including matrix metalloproteinases (MMPs). For example, MMP-2 cleaves intracellular proteins in cardiac myocytes, including cardiac troponin I, titin, sarco/endoplasmic reticulum calcium ATPase2a and junctophilin-2.

METHODS/RESULTS
The purpose of this study is to use mass spectrometry to quantify proteome changes following myocardial
stunning injury between three experimental groups: A)eW .rotibihni 2-PMM yrujni gninnuts)C dna ,yrujni gninnuts)B ,lortnoc ciborea used a second mass spectrometry method to assess the proteolytic events (degradomics) that occurred in each of the three groups. Our third method is to express a novel MMP-2 construct to identify MMP-2 specific substrates in the myocardium.

Using N-terminal labelling, we identified a total 292 proteolytic cleavage sites (yrujni gninnuts gniwollof deifitnedi erew hcihw fo 601 .selpmas lla ssorca MMP-2 inhibitor treatment) with 42 of which only identified without MMP-2 inhibition. We then designed a novel MMP-2 protein construct which is constitutively active and cleaves known native substrates including collagen and gelatin. Using N-terminal labelling on heart tissue incubated with this purified MMP-2, we identified 95 cleavage sites in proteins primarily involved in metabolism and mitochondrial function.

CONCLUSIONS
Changes in the proteome are evident following stunning injury with the abundance of 98 proteins increasing and 179 proteins decreasing. We show for the first time a global proteolytic analysis identifying cleavage sites following myocardial stunning injury which may be caused by MMP-2. We then confirmed MMP-2 cleavage sites by incubating heart tissue with recombinant MMP-2. Our methodology and results will aid in the identification of MMP-2 and other proteases and their substrates following IR injury and could help identify new therapeutic targets to prevent the damage occurring during IR injury.

The Enantioselective Separation and Quantitation of the Hydroxy-Metabolites of Arachidonic Acid by Liquid Chromatography – Tandem Mass Spectrometry

Fadumo Isse, MSc, Ahmad Alammari, MSc, Ahmed El-Sherbeni, PhD, Dion Brocks, PhD, Ayman El-Kadi, PhD

BACKGROUND

Arachidonic acid (AA) is a polyunsaturated fatty acid with a structure of 20:4(ω-6). Cytochrome P450s (CYPs) metabolize AA to several regioisomers and enantiomers of hydroxyeicosatetraenoic acids (HETEs). The HETEs exist as enantiomers in the biological system. The chiral assays developed for HETEs are so far limited to a few assays reported for midchain HETEs

METHODS/RESULTS

A chiral stationary phase column REFLEC C-AMYLOSE A column was used to separate HETE enantiomer pairs. Gradient elution consisted of organic phase: acetonitrile, methanol, and isopropyl alcohol (88:6:6, v/v) + 0.1% acetic acid and aqueous phase: water + 0.1% acetic acid was the operating condition of liquid chromatography. The tandem mass spectrometry ionization mode was negative electrospray ionization. The selective multiple reaction monitoring was set for monitoring different precursor and product ions of HETE analytes, and the internal standards. The instrument-specific interface voltage, current, and temperature were 3 kV, 0.8 µA, and 300 ^{o}C, respectively. The nebulizing, drying, and heating gas flow rates were 2, 10, and 10 L/min, respectively. The desolvation and heat block temperatures were 250, and 400 ^{o}C, respectively. The collision-induced dissociation was 270 KPa. Single liquid-liquid extraction method was used to extract analytes from rat microsomal matrix. The developed method is capable of quantitative analysis for midchain-, subterminal-HETE enantiomers, and terminal-HETEs in microsomes. The peak area or height ratios were linear over concentrations ranging (0.01 -0.6 µg/ml) with r2 > 0.99.The intra-run percent error and coefficient of variation (CV) were ≤
±12%.The inter-run percent error and CV were ≤ ±13%, and ≤15%, respectively. The matrix effect for the assay was also within the acceptable limit (≤ ±15%,). The recovery of HETE metabolites ranged from 70-115 %.

CONCLUSIONS

The method showed a reliable and robust performance for chiral analysis of CYP-mediated HETE metabolites.

Pathways of Proprotein Convertase Subtilisin/Kexin type-9 (PCSK9) Mediated LDL Receptor (LDLR) Degradation

Suha Jarad, Hong-mei Gu, Ziyang Zhang, Govind Gill, Da-wei Zhang

BACKGROUND
Elevated plasma low-density lipoprotein cholesterol (LDL-C) levels are a major risk factor for cardiovascular diseases, and low-density lipoprotein receptor (LDLR) is the main protein responsible for the uptake of LDL-C from the circulation. Proprotein convertase subtilisin/kexin type 9 (PCSK9) is a secreted protein that promotes the degradation of LDLR via endocytosis and thereby can regulate the plasma levels of LDL-C. Endocytosis of PCSK9/LDLR complex has been known to be through clathrin-coated pits. Until recently, a clathrin-independent but caveolae-dependent endocytosis was introduced as an alternative pathway for mediating PCSK9/LDLR endocytosis.

METHODS/RESULTS
Methods
Human hepatoma-derived cell lines Huh7 and HepG2 were used since they are commonly used to study PCSK9- promoted LDLR degradation. Knockdown of proteins involved in clathrin or caveolae endocytosis was done by small interfering RNA (siRNA). Recombinant PCSK9, overexpression of PCSK9 or conditioned media from cells stably expressing PCSK9 was used to determine its effect on LDLR protein levels in cultured cells using immunoblot and cell imaging. Primary hepatocytes are the current step to investigate.
Results
We found that in Huh7 cells, PCSK9-promoted LDLR degradation with increasing PCSK9 concentrations in caveolin-1 or clathrin heavy chain knockdown, but to a lesser extent than the control. On the other hand, degradation was significantly disrupted in knockdown of both caveolin-1 and clathrin heavy chain. In HepG2 cells, however, knockdown of clathrin heavy chain but not caveolin-1 significantly impaired the ability of PCSK9 to stimulate LDLR degradation.

CONCLUSIONS
We show that endocytosis of the PCSK9/LDLR complex appears to be cell type dependent. Both clathrin and caveolae-mediated endocytosis are involved in PCSK9-promoted LDLR degradation in Huh7 cells, whereas HepG2 cells only require clathrin-mediated endocytosis for PCSK9's action on LDLR. These findings indicate the complexity of mechanisms underlying PCSK9-promoted LDLR degradation.

Mitral Valve Repair on Patients with Chronic Kidney Disease: Long Term Outcomes and Cardiac Remodelling

Jimmy JH. Kang, MD., Sabin J. Bozso, MD, PhD., Ryaan EL-Andari, MD., Nicholas M. Fialka, MD., Dana Boe, MD., Yongzhe Hong, MD, PhD., Michael C. Moon, MD., Darren H. Freed, MD, PhD., Jayan Nagendran, MD, PhD., and Jeevan Nagendran, MD, PhD

BACKGROUND

Although the relationship between chronic kidney disease (CKD) and valvular heart disease (VHD) is well established, the literature examining mitral valve repair (MVr) outcomes in CKD patients is largely limited to short-term outcomes and percutaneous approaches. This study is the first to present long-term outcomes of mortality and morbidity with paired cardiac remodelling data on CKD patients undergoing surgical MVr.

METHODS/RESULTS

Methods: Patients with varying stages of CKD undergoing MVr from 2004-2018 were compared. Patients were grouped by estimated glomerular filtration rate
(eGFR) >90 (n=90), 60-89 (394), 30-59 (204), and <30 (5). The primary outcome was all-cause mortality. Secondary outcomes included measures of postoperative morbidity and cardiac remodelling.
Results: Every 10-unit increase in eGFR was associated with a significant reduction in all-cause mortality at 5 years (HR 0.81 95% CI 0.67-0.98) p=0.028), 10 years
(HR 0.82 CI 0.72-0.94 p=0.004), and at 15 years (HR 0.78 CI 0.69-0.88 p<0.001) Moderate CKD group had significantly higher rates of all-cause mortality at 15 years (HR 3.38 CI 1.28-8.98 p=0.014). eGFR was a significant predictor for residual moderate to severe mitral regurgitation (MR) at 1 year (HR 0.74 CI 0.57-0.96
p=0.024). There was positive cardiac remodelling following MVr for CKD patients with a significant reduction in LV size and LA volume

CONCLUSIONS

Conclusion: In patients with CKD undergoing MVr, eGFR is a predictor of decreased long-term survival and residual MR at 1 year. Positive cardiac remodelling followed MVr. Further investigation is required for optimizing postoperative outcomes in this patient population.

Dissecting the role of branched-chain amino acids and branched-chain keto acids in modulating cardiac adverse remodelling in heart failure

Qutuba G. Karwi, Liyan Zhang, Cory S. Wagg, Keshav Gopal, Golam Mezbah Uddin, Kim L. Ho, Qiuyu Sun, Sai Panidarapu, Kaya Persad, Shaden Deman, Jody Levasseur, John R. Ussher, Jason R. B. Dyck, Gary D. Lopaschuk

BACKGROUND
Branched-chain amino acids (BCAAs), namely leucine, isoleucine and valine, act as mitochondrial oxidative substrates and signalling molecules. While their contribution to overall cardiac ATP production is minimal (~2-4%) compared to other oxidative substrates such as fatty acids, glucose and ketones, perturbations in cardiac branched-chain amino acid (BCAA) oxidation have been linked to triggering the activity of the
mammalian target of rapamycin (mTOR) signalling pathway and aggravating adverse cardiac remodelling in the failing heart. Interestingly, impaired cardiac BCAA oxidation is associated with the accumulation of BCAAs and their metabolites, namely branched-chain keto acids (BCKAs), which makes it challenging to ascertain whether BCAAs or BCKAs are exacerbating adverse cardiac remodelling. We have recently demonstrated that cardiac- specific deletion of mitochondrial branched-chain aminotransferase (BCATmCardiac-/-), the rate-limiting enzyme that converts BCAAs into BCKAs and vice versa, enhances cardiac BCAA levels and increases left ventricular (LV) mass. We hypothesized that selective augmentation of BCAA levels would aggravate adverse cardiac remodelling in the failing heart.

METHODS/RESULTS
We investigated the impact of high BCAA or high BCKA levels on differentiated H9C2 cells in the presence and absence of phenylephrine to induce cell hypertrophy in vitro. We also used BCATmCardiac-/- male mice, where mice underwent a sham or transverse aortic constriction (TAC) surgery to induce hypertrophy and heart failure. Changes in cardiac function and structure were monitored pre-and post-TAC using echocardiography, and cardiac energy metabolism was accessed using flux tracing in isolated working hearts. In vitro, high BCAA or BCKA levels did not significantly affect cell surface area in differentiated H9C2 cells. However, high BCAA, not BCKA, levels caused further aggravation of cell hypertrophy in phenylephrine-treated cells. Five weeks post-TAC, BCATm deletion exacerbated adverse cardiac hypertrophy, as evidenced by increased left ventricular mass, compared to the WTCre+ failing hearts in vivo or ex vivo. The mTOR/P70S6K/4E-BP1 signalling pathway was also triggered in BCATmCardiac-/- mice hearts. BCATm deletion did increase insulin-stimulated glucose oxidation rates and cardiac efficiency in the failing hearts, which was associated with enhanced mitochondrial Akt activity. This was probably due to a lowering of BCKAs, which impair cardiac insulin signalling.

CONCLUSIONS
Augmented cardiac BCAA levels in the failing heart worsen adverse cardiac remodelling and offset any potential beneficial effects of lowering BCKA in the failing heart. This aggravation in adverse cardiac remodelling is mediated by triggering the mTOR/P70S6K/4E-BP1 signalling pathway.

A look at Inpatient Outcomes of New LBBB post TAVI with a balloon expandable valve (A single center retrospective analysis)

Robert Kay MD, Haran Yogasundaram MD MSc, Ahmed Almarzuqi MD, Ben Tyrrell MD, Jeevan Nagendran MD PhD, Anoop Mathew MD, Robert Welsh MD

BACKGROUND

TAVI has emerged as the standard of care for treating many patients with aortic stenosis. Cardiac conduction system damage is a common procedural complication. The most common conduction disturbance post TAVI is new LBBB which has an incidence of approximately 20-30%1. Furthermore, 15% of patients with NOP-LBBB at discharge have a high grade AV block event within 12 months with half occurring in the first month and half being clinically silent3. Management pathways for NOP-LBBB patients have been published with strategies varying from outpatient monitoring to inpatient prophylactic permanent pacemaker implantation2. We retrospectively assessed our TAVI population for incidence of new LBBB post TAVI in order to attempt to delineate current practice patterns and attempt to uniform practice to improve patient care.

METHODS/RESULTS

A retrospective chart review of patients who underwent TAVI between 2010-2020 at the Mazankowski Alberta Heart Institute was undertaken. The study included 355 patients without evidence of baseline conduction disease. Average age was 83, and 42% were female. Post-TAVR, 27.6% of patients developed new-onset LBBB, depicted in Figure 1. Among those, 54.3% had NOP-LBBB. Of the patients who experienced spontaneous resolution of LBBB, 38.8% had a sustained recovery at discharge, while 10.2% had transient recovery but reverted back to LBBB prior to discharge and 10.2% had progression to high-grade AV block. Approximately 1 in 5 (22.4%) patients with new LBBB received a permanent pacemaker before discharge, shown in Figure 2. Of these patients, 60% received prophylactic pacemaker insertion due to the perceived risk of high-grade AV block.

Neither QRSd > 150 ms or PR > 240 ms was associated with prophylactic pacemaker insertion (X2 P=0.053)(X2 P=0.067). The average pacing rates were 12.6% at first follow-up and 21% at 12 months in patients with prophylactic pacemaker insertion, 41.6% of these patients were paced < 1% during follow-up.

CONCLUSIONS

New LBBB post TAVI is common and 15% of patients without any baseline bundle branch block will be discharged with NOP-LBBB3. At our center where there is no easy access to prolonged outpatient monitoring or EPS, the majority of patients are discharged without further investigation or outpatient monitoring with a minority receiving prophylactic permanent pacemaker implantation of which the majority have the minimum pacing requirement of <1%. Delineating which patients would truly benefit from a prophylactic device is a current topic of investigation with ongoing clinical trials and every effort should be undertaken to enroll patients prior to inserting a prophylactic device.

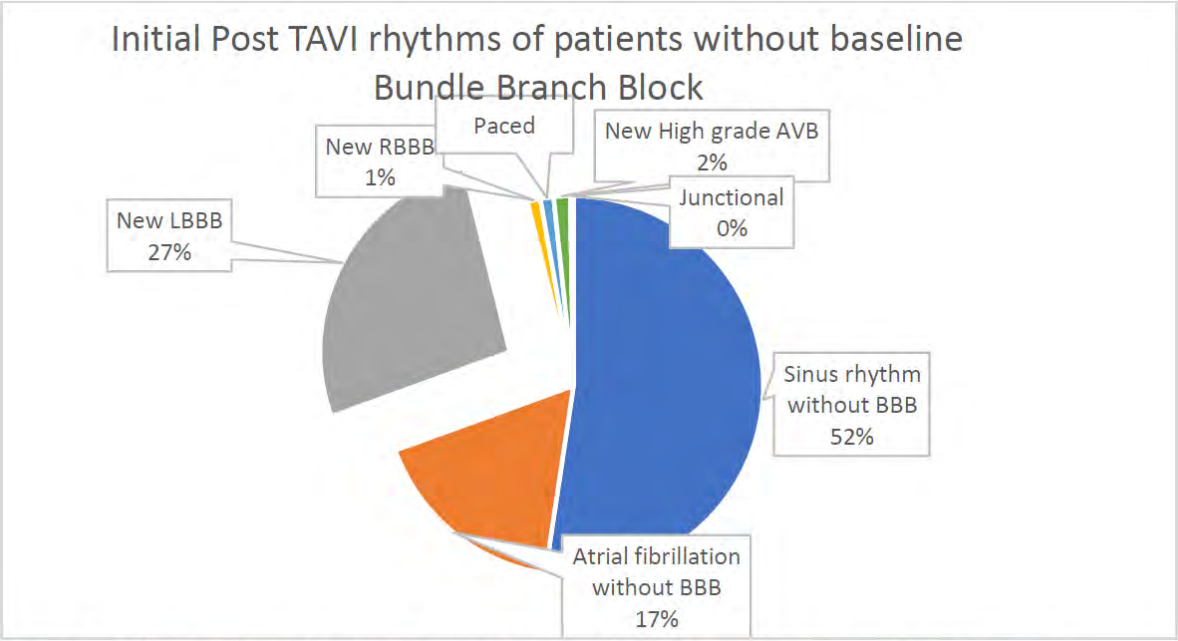

Figure 1: POD0 Rhythms of patients without bundle branch block on pre-TAVI baseline ECG.

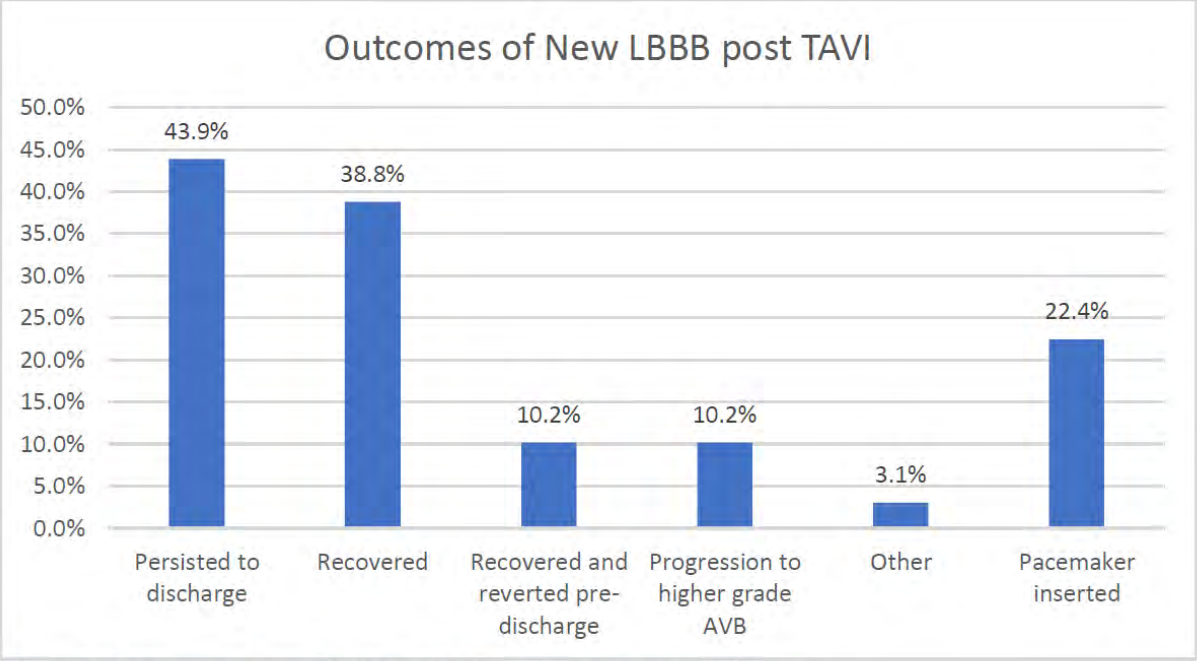

Figure 2: Outcome of post TAVI new LBBB patients prior to discharge.

Right Ventricular Segmentation in Cardiac MRI using Deep Learning

Varsha Kesavan, Kumaradevan Punithakumar, Michelle Noga

BACKGROUND
In cardiovascular disease diagnosis, non-invasive imaging techniques such as magnetic resonance imaging (MRI) are often used to assess the anatomy and function of the heart. MRI provides high-resolution images, allowing for accurate delineation of ventricular boundaries and quantification of ventricular volumes. This aids in early diagnosis of cardiac disease, improves treatment planning, and reduces associated mortality rates. Automating segmentation is preferred over manual segmentation because it is faster and has no interobserver variability.
The complex anatomy and motion of the right ventricle (RV) makes automated segmentation particularly challenging and less studied compared to the left ventricle (LV).

METHODS/RESULTS
An end-to-end machine learning model for delineating RV from MRI is developed using data from the Multi- Disease, Multi-View, and Multi-Center Right Ventricular Segmentation challenge. The dataset comprised 360 patients, with 160, 40, and 160 patients used for training, validation, and testing, respectively. The long axis (LA) view of each patient's heart at the end-systolic and end-diastolic phases is available as 2D images and that for short axis (SA) view is available as a stack of 2D slices. The dataset includes multiple RV and LV-related pathologies, comprising 8 pathologies in total, with the training set covering 6 and the validation and test sets including all 8. Two separate deep learning models - a 2D U-Net for LA images and a 3D U-Net for SA volumes, are implemented. Evaluating model performance on unseen pathological data enables assessing generalisability. Dice similarity coefficient, precision, and recall evaluated for predicted segmentation masks against their ground truth masks show a mean Dice coefficient of 0.703 for 3D SA view and 0.796 for 2D LA view; mean ± standard deviation precision and recall of 0.831 ± 0.182 and 0.653 ± 0.254 for 3D SA view, and that for 2D LA view is 0.814 ± 0.213 and 0.813 ± 0.246. Results for 2 unseen pathologies indicate high generalisability of SA and LA models.

CONCLUSIONS
The UNet-based segmentation models developed in this study have shown promising results in automating right ventricle delineation in cardiac MRI using only 160 patient exams for training, and demonstrating capability to delineate RV on unseen pathologies. Development of such automated segmentation models could eventually lead to earlier detection of cardiovascular diseases, a reduction in the subjectivity and variability of manual segmentation, and more reliable and consistent diagnoses. Overall, automated ventricular segmentation has the potential to improve clinical decision-making in cardiology while decreasing healthcare costs and improving patient outcomes.

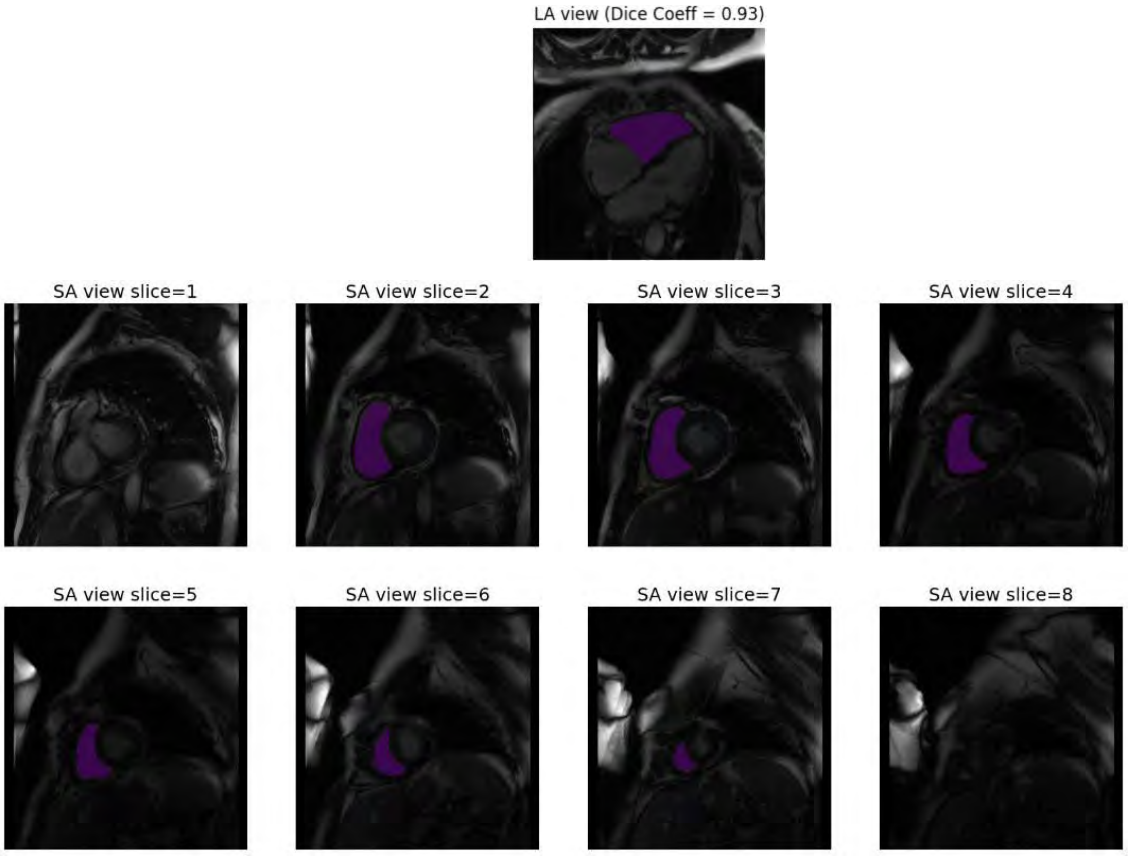

Figure 1: Right ventricle segmentation results, LA (Top) and SA (Bottom) for patient number

346. Dice coefficient for SA = 0.95

	Dice coefficient			
	SA		LA	
	Mean	Std	Mean	Std
Normal subjects	0.649	0.21	0.735	0.31
Dilated LV	0.695	0.202	0.865	0.09
Hypertrophic Cardiomyopthy	0.520	0.29	0.833	0.17
Congenital Arrhythmogenesis	0.583	0.21	0.760	0.28
Tetralogy of Fallot	0.801	0.187	0.844	0.18
Interartiel Comunication	0.767	0.169	0.713	0.31
Dilated RV (Not used in train set)	0.826	0.095	0.757	0.23
Tricuspidal Regurgitation (Not used in train set)	0.817	0.171	0.832	0.13
Overall	**0.703**	**0.228**	**0.796**	**0.226**

Table 1: Testing results – Mean and standard deviation of dice coefficient for each pathology as well as overall.

CD38 inhibition decreases myocardial glucose utilization without altering NAD+ levels and protein acetylation

Ezra B. Ketema, Muhammad Ahsan, Liyan Zhang, Qutuba G. Karwi, and Gary D. Lopaschuk

BACKGROUND
Perturbations in myocardial energy substrate metabolism is one of the main contributors to the pathogenesis of heart failure. However, the underlying causes for these metabolic alterations remain poorly understood.
Recently, post-translational acetylation modification of metabolic enzymes has emerged as one of the essential regulatory mechanisms for cardiac metabolic changes. NAD+ is a critical cofactor for sirtuins (deacetylase enzymes), and a decrease in NAD+ levels, partly due to an upregulation of CD38 (a NAD+ consuming enzyme), may contribute to an altered mitochondrial protein acetylation status. However, it is unknown whether decreasing acetylation can improve metabolic flexibility and cardiac function in the heart. This study aimed to determine if inhibiting CD38 can enhance SIRT3 activity (thereby reducing acetylation) and modify the activity of cardiac metabolic enzymes and heart function.

METHODS/RESULTS
Heart from Sprague Dawley rats were isolated and perfused aerobically or subjected to 30 minutes of ischemia followed by 40 minutes of reperfusion in the ex vivo working mode in the presence or absence of a CD38 inhibitor (10-50 µM Compound 78c). Alterations in cardiac function, as well as rates of fatty acid oxidation, glucose oxidation and glycolysis, were measured. Changes in the acetylation status of enzymes and proteins involved in glucose and fatty acid metabolism, metabolic rates, and functional changes were compared between non-ischemic and ischemic hearts and between treatment and control groups at the end of the perfusion. H9c2 cell lines were also cultured in proliferating and differentiating settings in the presence or absence of the CD38 (10 µM) inhibitor. By the end of the cell culture growth/treatments, H9c2 cells were perfused to determine the metabolic fluxes and acetylation status of the cardiac metabolic enzymes.

Inhibition of CD38 has no significant effect on ex-vivo cardiac function in aerobically perfused hearts. However, the CD38 inhibitor decreased post-ischemic recovery of heart function. CD38 inhibition significantly reduced the glycolysis rate in both isolated hearts and H9c2 cells but had no effect on fatty acid oxidation rates. Neither NAD
+ levels nor the acetylation status of metabolic enzymes were altered by CD38 inhibition.

CONCLUSIONS
CD38 inhibition significantly decreases glycolysis rates both in isolated working rat hearts and H9c2 cells. However, CD38 inhibition does not affect post-translational protein acetylation status and NAD+ levels in isolated working rat hearts or H9c2 cells.

Machine Learning-based Approach for Predicting Post-treatment Survival for CAD Patients

Anita Khalafbeigi, Sunil V Kalmady, Kevin Bainey, Robert Welsh, Padma Kaul, Russ Greiner

BACKGROUND
Coronary artery disease (CAD) is a leading cause of mortality worldwide. Coronary artery bypass graft surgery (CABG) and percutaneous coronary intervention (PCI) are two commonly used treatments for CAD, each with its own risks and benefits. Predicting patient survival is critical for developing personalized treatment plans and improving medical decision-making. In this study, we aimed to predict the survival of each patient with CAD based on a range of clinical features, including patient covariates, cardiovascular problems, previous treatments, and relevant medical history, which are collected prior to the treatment, as well as the treatment type (PCI or CABG) received by each patient.

METHODS/RESULTS
We conducted a survival analysis on a cohort of patients with CAD who received either PCI or CABG treatment. For this project, we employed neural multi-task logistic regression (MTLR) to predict patient survival after receiving PCI or CABG, using clinical features such as patient demographics, cardiovascular history, and treatment type as input variables. This study utilizes real-world datasets collected by the Canadian VIGOUR Centre from 2002 to 2019 that we used to train our model.
In this study, we investigated the survival of patients with stable angina as their indication type. Of the 27199 patients, 70% received PCI, and the rest received CABG. The age of the patients ranged from 16 to 96 years old, with an average age of 65.1 years old; also 18.9% were female. The observed mortality rates for patients who underwent PCI and CABG were 18% and 26%, respectively. Our survival model showed promising performance in predicting patient survival, with a concordance index of 0.896. These findings highlight that our algorithms can predict individual survival and assist in clinical decision-making for patients with CAD.

CONCLUSIONS
Our study findings suggest that the survival model employed in this research is effective in predicting the survival of patients receiving the target treatment by leveraging their pertinent medical history and cardiovascular conditions. Our approach integrates patient-specific information to determine their potential for survival. As a potential direction for future work and applications, the information gathered from this approach can assist clinicians in making informed decisions regarding the most suitable treatment options. Overall, our study highlights the importance of personalized medicine and the need for accurate predictive models to assist healthcare providers in delivering optimal care.

Cardioprotective Properties of the Synthetic 19,20-Epoxydocosapentaenoic Acid Analogue SA-22

Joshua Kranrod, Ahmed Darwesh, Wesam Bassiouni, Liye Fang, Jacob Korodimas, Adeniyi Michael Adebesin, Abdul Sattar Mohammad, John Falck, John Seubert

BACKGROUND
Evidence suggests that CYP epoxygenase metabolites of docosahexaenoic acid (DHA), called epoxydocosapentaenoic acids (EDPs), limit mitochondrial damage following cardiac injury. In particular, the 19,20-EDP isomer has demonstrated potent cardioprotective action. We investigated our novel synthetic 19,20-EDP analog compound SA-22 for protection against cardiac ischemia-reperfusion (IR) injury.

METHODS/RESULTS
Isolated C57BL/6 mouse hearts were perfused via Langendorff apparatus with vehicle, SA-22, and nicotinamide (NAM) (30 µM) for 20 minutes baseline, 30 minutes of global ischemia followed by 40 minutes of reperfusion. We continuously assessed IR injury-induced changes in recovery of myocardial function, using left ventricular developed pressure, systolic and diastolic pressure change. Tissues were assessed for electron transport chain function, SIRT-1 and -3, optic atrophy type-1, manganese superoxide dismutase (MnSOD), caspase-1, IL-1B, and Gasdermin D. H9c2 cells were used in an in vitro model of hypoxia/reoxygenation injury. Perfusion with SA-22 significantly enhanced postischemic functional recovery, preserved ETC function, SIRT activity and reduced activation of pyroptosis. Interestingly, while NAM (SIRT3 inhibitor) co-treatment worsened functional outcomes, cell survival, and attenuated sirtuin activity, it partially attenuated SA-22-induced protection against pyroptosis, suggesting involvement of other protective mechanisms.

CONCLUSIONS
The data demonstrate cardioprotective effects of our novel synthetic 19,20-EDP analog against IR injury. Treatment resulted in improved postischemic cardiac function correlated with evidence of limited mitochondrial degradation and enhanced SIRT3 activity. This pilot data provides the framework for the development of superior therapeutic agents.

Vascular dysfunction in congenital heart disease: a systematic review and meta-analysis

J. Lasso-Mendez, C. Spence, LK. Hornberger, A. Sivak, MH. Davenport

BACKGROUND
Congenital heart disease (CHD) affects 1% of live births. Advances in medical care have increased survival, but individuals with CHD remain at higher risk for cardiovascular disease and reduced life expectancy compared to those without CHD. The etiology is unclear; however, a small number of studies have reported impaired vascular structure and function in individuals with CHD. We performed the first systematic review and meta-analysis to further explore the impact of CHD on vascular health and to understand which CHD is most at risk.

METHODS/RESULTS
Eight electronic databases were searched up to September 26, 2022. Studies of all designs (except case studies and review articles) were included which contained the appropriate population (CHD patient), comparator (no CHD), and outcomes of interest: arterial stiffness (pulse-wave velocity (PWV), augmentation index (AIx), distensibility and compliance), carotid intima-media thickness (cIMT) and endothelial dependent (flow-mediated vasodilation (FMD%), reactive hyperemia index (RHI)) and independent (nitroglycerine mediated dilation (NMD
%)) function presented as standardized mean differences and 95% confidence intervals.

Eighty-eight studies were included in the meta-analysis. Patients with CHD had higher metrics of arterial stiffness including PWV (0.61 [0.43, 0.78], p<0.00001), SI (0.68 [0.53, 0.83], p<0.00001) and AIx (1.06 [0.73, 1.39],
p<0.00001), lower distensibility (-0.88 [-1.05, -0.70], p<0.0001) and compliance (-1.01 [1.55, -0.47], p<0.0001) compared to those without CHD. Subgroup analyses showed that transposition of the great arteries (TGA) patients (1.19 [0.64, 1.74]) had highest PWV, followed by tetralogy of Fallot (ToF) (0.70 [0.32, 1.08]), coarctation of the aorta (CoA) (0.63 [0.41, 0.85]) and Fontan or single ventricles (V1) (0.34 [0.04, 0.65]). SI was the highest among TGA (1.37 [0.31, 2.43]) and bicuspid aortic valve (BAV) (0.81 [0.50, 1.13]). Followed by CoA (0.72 [0.44,
0.99]), ToF (0.67 [0.45, 0.89]) and Fontan/V1 (0.48 [0.19, 0.78]).
Patients with CHD exhibited decreased vascular function compared to those without CHD including decreased FMD% (-1.11 [-1.44, -0.78], p<0.00001), RHI
(-3.94 [-6.21, -1.66], p=0.0009) and NMD% (-1.34 [-1.87, -0.81], p<0.00001) suggesting endothelial dependent and independent vascular dysfunction in CHD. Subgroup analysis demonstrated significantly lower FMD in ToF (-2.33 [-3.34,
-1.33]), Fontan (-1.29 [-2.28, -0.29]) and CoA (-1.15 [-1.50, -0.79) patients relative to controls. Finally, cIMT was found to higher in CHD (0.69 [0.48, 0.89], p<0.00001) compared to those without CHD, especially among CoA (1.21 [0.90, 1.52]) and TGA (0.78 [0.35, 1.21]).

CONCLUSIONS
Patients across a spectrum of CHD demonstrate increased arterial stiffness, reduced endothelial dependent and independent vascular function and increased cIMT.

Enhanced hepatic mitochondrial respiration in the hyperacute phase of late-onset sepsis may be a protective mechanism

Si Ning Liu, Forough Jahandideh, Jad-Julian Rachid, Claudia Holody, Hélène Lemieux, Kimberly Macala, Stephane Bourque

BACKGROUND
Late-onset sepsis (LOS) is defined as the dysregulated host response to an infection after 72h of life. Sepsis is characterized by a disturbance to metabolic homeostasis and hypoperfusion that could lead to multi-organ dysfunction. At the center of metabolic homeostasis, the mitochondrion is a critical hub for energy production and signaling. Even though investigating the mitochondrial response to LOS may seem intuitive, it has yet to be explored.
Objective: We sought to explore the effects of LOS on mitochondrial function in the developing liver, as it is a highly metabolic organ.

METHODS/RESULTS
Methods: Three-day-old Sprague Dawley pups received an intraperitoneal injection of fecal slurry (FS, 1.0 mg/g body weight) or vehicle (5% dextrose). All pups received buprenorphine for pain control and antibiotics at 4h and 16h post-FS. Pups were euthanized at 4h, 8h, and 24h post-FS, and fresh liver was harvested and homogenized for assessment of mitochondrial function (O2 consumption) by high resolution respirometry. Remaining tissues were flash frozen for protein assays and Western blotting.
Results: FS reduced pup bodyweight by 4% ($P<0.0001$) by 24h but did not affect absolute liver weights. Blood glucose rose 4-fold at 4h and 8h post-FS, and normalized by 24h. Mitochondrial NADH pathway respiration increased by 62%
($P=0.004$) in male pups at 4h. This was accompanied by 1.8-fold upregulation of total AMPK ($P=0.02$) and 30% increase in phospho-AMPK/AMPK ($P=0.03$) in males. Enhanced NADH pathway respiration was observed at 8h in both sexes ($P<0.0001$), but increased AMPK protein expression was only observed in males with no changes to phospho-AMPK/AMPK. Succinate pathway respiration was enhanced by 65% ($P=0.005$) in male pups at 4h and continued through 8h. By 24h post-FS, neither NADH nor succinate pathway respiration differed from controls. However, total AMPK remained upregulated by 2.7-fold ($P<0.0001$) in both sexes while phospho-AMPK/AMPK was reduced by 50% ($P=0.006$) in males. No change to complex IV respiration was observed at any time point.
Liver NAD/NADH ratio did not differ between control and FS pups at 4h and 8h. However, FS pups had increased succinate levels ($P=0.05$) at 4h and 8h.

CONCLUSIONS
Sex-dependent increase in mitochondrial respiration was associated with increased total AMPK at 4h and 8h and increased AMPK activation at 4h, which suggests an adaptive mechanism to supply energy and metabolites in response to the infection.

TRIM35-Mediated Histone 2B Ubiquitination; An Epigenetic Modification that Reveals P53 Transcriptional Targets in Heart Failure

Maria Areli Lorenzana-Carrillo, Saymon Tejay, Joseph Nanoa, Yongneng Zhang, Yongsheng Liu, Alois Haromy, Michelle Mendiola Pla, Dawn E. Bowles, Evangelos D. Michelakis and Gopinath Sutendra

BACKGROUND
The pro-apoptotic transcription factor P53 is induced in several forms of heart failure (HF), but the precise mechanism coordinating its induction with accessibility to its transcriptional promoter sites remains unresolved. E3-ubiquitin ligase TRIM35 has been implicated in heart failure by stabilizing P53, but its exact role in regulating P53 transcriptional activity remains unclear. Ubiquitination-modified H2B at Lysine120 (K120Ub-H2B) can reveal P53 transcriptional promoter sites. We hypothesize that TRIM35 may coordinate P53 induction with increased transcriptional activity by ubiquitinating H2B, which would promote accessibility to its promoters.

METHODS/RESULTS
Cardiomyocyte(CM)-specific TRIM35 overexpressing mice (TRIM3-OE) were generated to evaluate its biological role. Co-immunoprecipitation, ubiquitination enrichment and chromatin immunoprecipitation were used to assess TRIM35 interaction, ubiquitination targets and chromatin remodeling. Dilated Left Ventricle biopsies were used to translate findings into a clinical setting.

TRIM35 is expressed in both the cytoplasm and the nucleus of cardiomyocytes. To investigate its function, we used the TRIM3-OE model, which develops cardiac dysfunction and heart failure. TRIM3-OE cardiomyocytes showed increased levels of K120Ub-H2B and P53 compared to controls, while knockdown of TRIM35 in cardiomyocytes resulted in decreased levels of K120Ub-H2B. TRIM35 interaction with H2B and subsequent ubiquitination lead to increased P53 chromatin binding and increased expression of P21 and PUMA. Interestingly, K120Ub-H2B was found to be positively correlated with p21 or Puma mRNA levels. Overall, these findings suggest that TRIM35 promotes P53 transcriptional activity through its ability to enhance H2B ubiquitination.
To provide translational evidence, in a small cohort of patients with dilated left ventricles, we found that TRIM35, K120Ub-H2B, P53, P21 and PUMA levels were significantly increased compared to non-failing controls.

CONCLUSIONS
TRIM35 is involved in HF progression by stabilizing P53 and promoting its transcriptional activity through K120Ub-H2B. This highlights a potential mechanism and provide a potential target for future therapies.

Investigating SGLT2 inhibitors as a potential novel therapy for patients with congential Long QT syndrome 3: A precision medicine approach.

Lynn Lunsonga, Mohammad Fatehi, Wentong Long, Amy Barr, Andre Edwards and Peter E. Light.

BACKGROUND
Congenital long QT syndrome (LQTS) is a hereditary cardiac disease characterized by a prolongation of the ECG QT interval and by a high risk of life-threatening arrhythmias. Gain of function mutations in the cardiac Nav1.5 channel underlie LQT3 (about 10-15% of LQT cases) and induce a persistent/late sodium current
(late-INa). Patients with LQT3 mutations have a 20% risk of death compared to
3-4% in LQT1 and 2. Current treatment options for LQT3 are limited as there are no drugs that specifically target late- over peak-INa. We have recently shown that the SGLT2 inhibitor (SGLT2i) class of diabetes medication are potent inhibitors of late-INa that may contribute to cardiovascular benefits of these drugs against heart failure and sudden cardiac death. Hypothesis. That the SGLT2is inhibit late-INa in cardiac sodium channels containing LQT3 mutations and that this inhibition is mutation-specific.

METHODS/RESULTS
Methods. We generated 13 known LQT3 mutations in the cardiac sodium channel Nav1.5 that were then expressed in HEK293 cells. Using the whole-cell patch-clamp technique, we then tested the effects of 10 uM empagliflozin (empa) on late-and peak-INa as well as activation and inactivation kinetics. Mutations were stratified into 3 classes: Class 1 are located in the inactivation gate region, Class 2 are located in the S4 voltage- sensing segments and Class 3 are located in the predicted binding region for the SGLT2is.
Results. Empa is an effective inhibitor of late-INa in Class 1 mutations and did not alter peak INa or activation/ inactivation kinetics. In Class 2 mutations, empa inhibited both late- and peak-INa and shifted the inactivation curve to more negative potentials. Empa was unable to inhibit either late- or peak-INa in Class 3 mutations.

CONCLUSIONS
We demonstrate that empa is able to selectively inhibit late-INa in Nav1.5 channels containing Class 1 mutations. Therefore, our results provide a plausible mechanistic rationale for testing the anti-arrhythmic efficacy of the SGLT2is in patients harbouring Class 1 LQT3 mutations, which are the most common class of LQT3 mutation.

Acute Kidney Injury and Renal Recovery Following Fontan Surgery

Anna Marosi, Jennifer Conway, Catherine Morgan, Maryna Yaskina, Rae Foshaug, Alyssa Chappell, Lindsay Ryerson, Billie-Jean Martin, Alanna Ash, Mohammed Al Aklabi, Kim Myers, Andrew S. Mackie

BACKGROUND

Acute kidney injury (AKI) is a common complication following the Fontan operation. AKI is defined as a rise in serum creatinine (SCr) of 1.5 times or more above baseline. Despite its common occurrence post Fontan, the duration and outcomes of AKI have not been previously reported. Duration of AKI has been defined as transient (reversal of SCr < 1.5 x baseline within 48 hours), persistent (SCr < 1.5 x baseline in 2 - 7 days), and acute kidney disease (SCr >1.5 x baseline after day 7). We sought to describe the incidence of and risk factors for AKI, the phenotype of renal recovery, and evaluate the impact of AKI phenotype on outcomes.

METHODS/RESULTS

All children who underwent a Fontan at a single center between 2009-2022 were included. Data collected from electronic medical records included Fontan characteristics, vasopressor use, all measures of SCr, and post- operative outcomes. We excluded those who had no preoperative SCr within 90 days of surgery. Every postoperative SCr was collected until the time of discharge, or 30 days postoperatively, whichever came first. Logistic regression models were used to assess predictors of AKI as well as the association between AKI and outcomes. We enrolled 141 children (45% female). AKI occurred in 100 (71%) patients. First onset of AKI was most common on postoperative day (POD) 0 in 81% or POD 1
(9%). All cases of AKI occurred by POD 7. AKI duration was transient (<48 hours) in 77 (55%), persistent (2-7 days) in 15 (11%), >7 days in 4 (3%), and of uncertain duration in 4 (3%). Risk factors for AKI were higher preoperative indexed pulmonary vascular resistance (OR 3.9, p = 0.004) and higher postoperative inotrope score on day 0 (OR 1.13, p = 0.047). Risk factors for AKI duration >48 hours included absence of a fenestration (OR 3.43, p=0.03) and longer duration of cardiopulmonary bypass (OR 1.22 for each 15-minute increase, 95% CI 1.04, 1.43, p=0.01).
Median length of stay (LOS) was 11 days (IQR 8-18) vs. 8 days (7-10) among those with vs. without AKI (p=0.001). AKI duration >48 hours was associated with longer LOS compared to transient AKI [median 18 days (9-62) versus 10 days (8-16), p=0.006] and more sternal wound infections (17% vs. 4%, p=0.049).

CONCLUSIONS

AKI after the Fontan operation is common. The occurrence and duration of AKI has significant implications for postoperative outcomes.

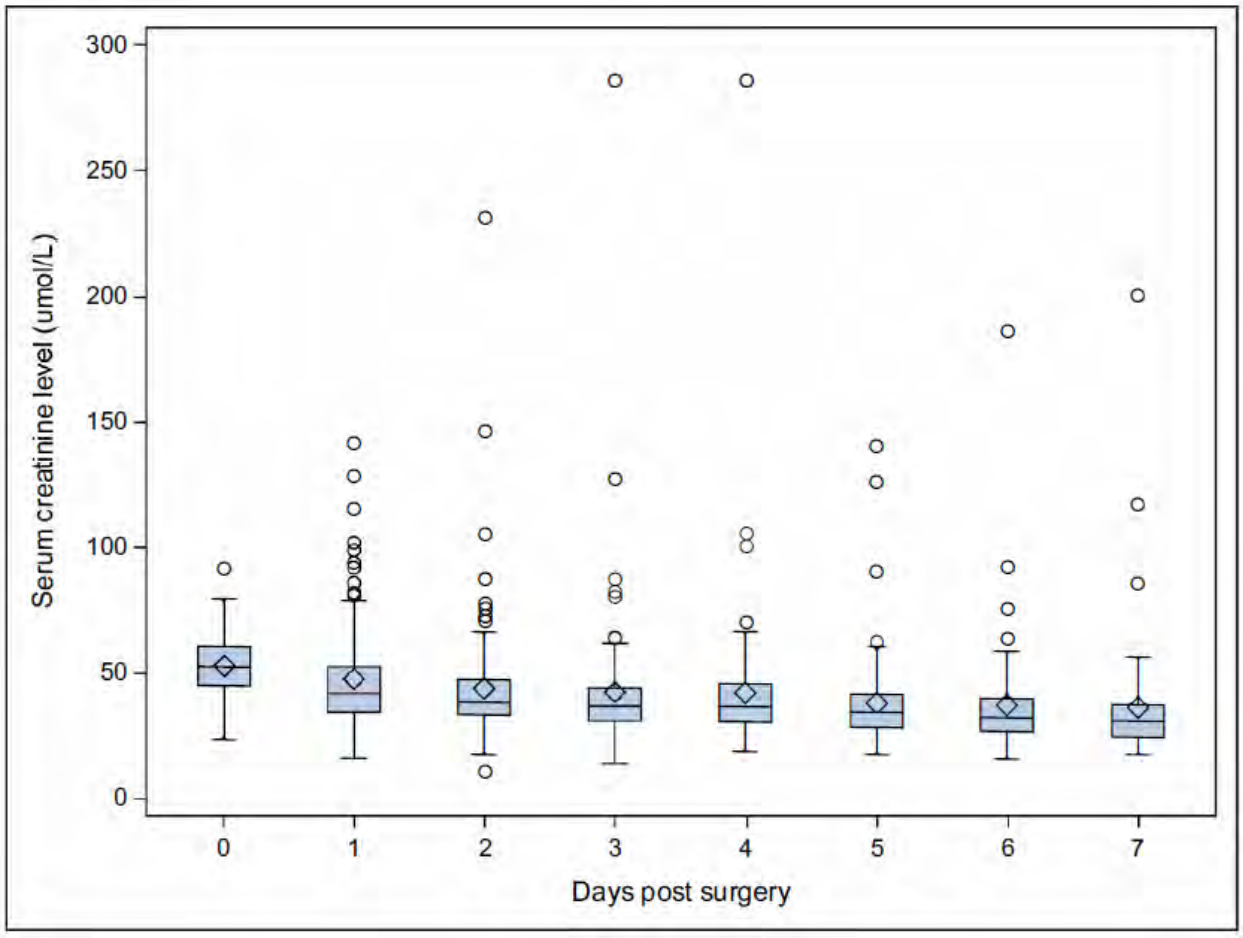
Serum creatinine level (umol/L)
300
250
200
150
100
50
0
0
1
2
3
4
5
6
7
Days post surgery

Reactive Oxygen Species Modulator 1 (ROMO1) Plays an Obligate Role in Cardiomyocyte Hypertrophy

Matthew D. Martens, Claudia D. Holody, Heidi Silver, Mostafa Khairy, Daniella Morales, Mourad Ferdaoussi, Nikole Byrne, Helene Lemieux, Gavin Oudit, Robert A. Screaton, Jason R.B. Dyck.

BACKGROUND

Mitochondrial spare respiratory capacity (SRC) allows cardiomyocytes to produce more energy during periods of increased stress or workload and is therefore a key regulator in the development of cardiac hypertrophy. In non- cardiomyocytes, the mitochondrial protein, reactive oxygen species modulator 1 (ROMO1), has been found to govern SRC by controlling electron transport chain (ETC) activity. However, very little is known about ROMO1 in the heart. Based on this, we sought to understand the role of ROMO1 in the cardiomyocyte and determine if it is involved in the development of cardiac hypertrophy.

METHODS/RESULTS

Using short interfering RNA to silence ROMO1 in human cardiomyocytes, we determined loss of ROMO1 significantly reduces SRC but does not alter basal respiration or mitochondrial morphology. Next, we treated cardiomyocytes with 100µM isoproterenol for 24 hours to induce hypertrophy. Through live-cell imaging we observed that the loss of ROMO1 completely prevents isoproterenol-induced cardiomyocyte growth.

Mechanistically, epifluorecsent imaging of a redox-sensitive, mitochondrial superoxide-specific dye, MitoSOX, demonstrated that ROMO1 is required for isoproterenol-induced reactive oxygen species (ROS) generation. While ROS generation is a deleterious side-effect of increased mitochondrial respiration, ROS can also act as a potent secondary messenger, activating several transcription factors in the cell. To this end, luciferase reporter assays demonstrated that ROMO1-induced mitochondrial ROS generation is required for isoproterenol-induced nuclear factor kappa B (NF-kB) activation, a well-established pro-hypertrophic transcription factor in the heart. To test the effects of the loss of cardiomyocyte ROMO1 in vivo we developed an inducible, cardiomyocyte- specific knockout (KO) mouse. At baseline, KO mice demonstrated no overt cardiac phenotype. However, unlike their wild-type counterparts KO mice failed to develop cardiac hypertrophy (i.e. left ventricular and septal wall growth) in response to a 2 week infusion of angiotensin-II to elevate blood pressure an stimulate cardiac hypertrophy. Finally, hearts from both mice and humans in overt heart failure (i.e. ejection fraction less than 40%) demonstrate a more than 50%reduction in ROMO1 protein expression, suggesting that a loss of SRC and a subsequent blunting of cardiac hypertrophy may contribute to the worsening of heart failure.

CONCLUSIONS

Our data suggest that ROMO1 is necessary for the maintenance of SRC and cardiomyocyte hypertrophic growth through a ROS and NF-kB dependent mechanism. Our data further suggests that a loss of ROMO1 impairs the ability of cardiomyocytes to adapt to increased workload and may contribute to the development of heart failure.

Timeliness of Reperfusion in ST-segment Elevation Myocardial Infarction and Outcomes in Kerala, India: Results of the TRUST Outcomes registry

Anoop Mathew MD, DM, **Muhammad Moolla MD,** Panniyammakal Jeemon PhD, Eapen Punnoose MD, DM, Ashraf SM MD, DM, Sunil Pisharody MD, DM, Sunitha Viswanathan MD, DM, Jayakumar TG MD, DM, Jabir Abdullakutty MD, DM, Jubil P Mathew MD, DM, Thomas John MD, DM, Vino

BACKGROUND
Transatlantic guidelines endorse timely reperfusion in ST-elevation myocardial infarction (STEMI) with quality metrics. Compliance in low- and middle-income countries (LMICs) is largely unknown.

METHODS/RESULTS
We prospectively evaluated 2,928 STEMI patients in Kerala, India, across 16 PCI-capable hospitals who received reperfusion with either primary percutaneous coronary intervention (PPCI) or fibrinolysis. Primary endpoint was a major adverse cardiovascular event (MACE) composite of death, non-fatal myocardial infarction, stroke or readmission for heart failure at 1-year.

In our cohort, 545 (18.6%) patients received timely primary PCI (PPCI), 80 (2.7%) received timely fibrinolysis, 1757 (60.0%) received delayed PPCI, and 546 (18.6%) received delayed fibrinolysis. 21.3% of the reperfused cohort had timely reperfusion with either PPPCI or fibrinolysis. Timely reperfusion had lower MACE than delayed PCI or fibrinolysis (timely reperfusion: 11.7%, delayed PPCI: 14.1%, delayed fibrinolysis: 24.7%, p=0.01). Mortality was lowest in timely reperfusion (timely reperfusion: 6.4%, delayed PPCI: 8.2%, delayed fibrinolysis 19.6%, p=0.01). Delayed fibrinolysis and PPCI were associated with increased risk of MACE (delayed fibrinolysis: HR 1.78, 95% CI 1.28-2.48; delayed PPCI: HR 1.34, 95% CI 1.01-1.79) and mortality (delayed fibrinolysis: HR 2.72, 95% CI 1.74-4.24; delayed PPCI: HR 1.67, 95% CI 1.07-2.46). Total ischemic time > 3 hours, delayed first medical contact (FMC)-to-device time and delayed FMC-to-needle time were independent predictors of MACE at 1-year.

CONCLUSIONS
Among STEMI patients in Kerala, India, one in five eligible patients recieved timely reperfusion. Longer total ischemic times and delayed FMC-to-reperfusion were associated with 1-year MACE. Quality efforts in improving timely reperfusion is critical to enhancing STEMI care and outcomes in LMICs.

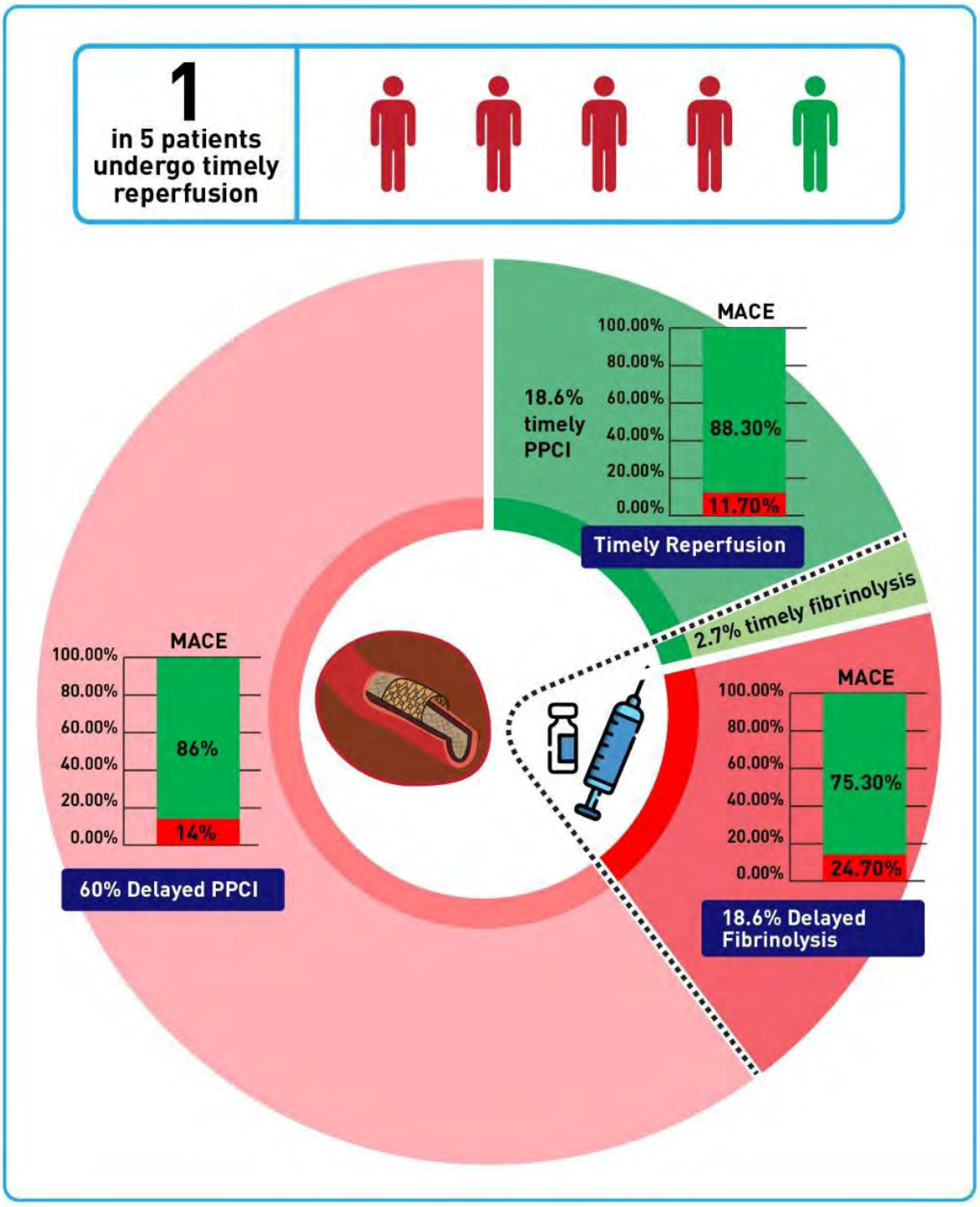

Figure 3. illustrative representation of the timeliness of reperfusion and its relationship to MACE.
MACE: major adverse cardiovascular events, PPCI: primary percutaneous coronary intervention

Table 4. Time intervals predicting major adverse cardiovascular events and mortality in ST-segment Elevation Myocardial Infarction

Variable	MACE: HR (95%CI), p value	All-cause mortality: HR(95%CI), p value
Delayed PPCI, Vs timely reperfusion	1.34 (1.01-1.79), p=0.045	1.62 (1.07-2.46), p=0.021
Delayed thrombolysis, Vs timely reperfusion	1.78 (1.28-2.48), p=0.001	2.72 (1.74-4.24), p<0.001
Total ischemic time 3-6 hours, Vs TIT<3 hours	1.34 (1.00-1.78), p=0.048	1.37 (0.97-1.92), p=0.068
Total ischemic time >6 hours, Vs TIT<3 hours	1.51 (1.09-2.08), p=0.011	1.25 (0.84-1.87), p=0.257
Door of PCI capable hospital to balloon <1 hrs Vs >=1 hr	0.84 (0.63-1.11), p=0.234	0.75 (0.52-1.08), p=0.12
Transfer-in with DIDO>=30mins Vs DIDO<30 mins	1.02 (0.76-1.35), p=0.903	0.99 (0.70-1.40), p=0.97
Procedure time >=30 mins Vs. Procedure time <30 mins	1.17 (0.78-1.74), p=0.440	1.00 (0.58-1.72), p=0.98
Transport time >=1 hrs Vs. Transport time <1 hr	0.84 (0.63-1.12), p=0.245	0.90 (0.64-1.29), p=0.58

PPCI: Primary percutaneous coronary intervention; delayed PPCI defined as first medical contact to balloon time ≥60 minutes for direct presenting patients and ≥120 minutes for transferred in patients.

Supervised ECG features outperform knowledge-based and unsupervised features in individualized survival prediction:

Yousef Nademi, MSc, PhD; Sunil Kalmady Vasu, PhD; Weijie Sun, MSc, Padma Kaul PhD; Russell Greiner, PhD

BACKGROUND
Electrocardiograms (ECGs) are a valuable and easily collected measurement of heart health. Many studies have used ECGs in combination with age and sex for various supervised tasks including mortality, suggesting ECGs contain the information needed for mortality prediction. Most ECG analysis and ECG-based prediction models use hand-crafted (knowledge-based) features, such as QRS duration and PR interval. This study explores the ways to obtain high-level features from ECG traces, through various approaches including supervised with clinical diagnoses, unsupervised approaches, or knowledge-based ECG features.

METHODS/RESULTS
We used a large ECG dataset from 244,077 patients with over 1.6 million 12-lead ECGs admitted to hospitals in Alberta, Canada between February 2007 and April 2020, where each is labeled with certain specified abnormalities. Using the ECG features obtained from discussed approaches along with age and sex, models were trained to estimate patient-specific individual survival distributions (ISD) to predict time to death. Using Neural- MTLR (N-MTLR) model to estimate ISD, supervised deep learning features showed the highest performance, having a C-index (0.80) followed by unsupervised ECG features (0.72) and knowledge-based ECG features (0.72).

CONCLUSIONS
The results showed that supervised learning approaches produced ECG features that can estimate patient- specific ISD curves better than ECG features obtained from unsupervised and knowledge-based methods. Supervised ECG features required less training sample size (as low as 500) to learn ISD models that performed better than models that only used age and sex. On the other hand, unsupervised and knowledge-based ECG features required over 5000 training samples to produce ISD models that performed better than age and sex alone. The study's findings may assist researchers in selecting the most appropriate approach for extracting high- level features from ECG signals to estimate patient-specific ISD curves.

Generative Data by beta-Variational Autoencoders Help Build Stronger Classifiers: ECG Use Case

Yousef Nademi, MSc, PhD; Sunil V Kalmady, PhD; Weijie Sun, MSc, Nariman Sepehrvand, MD, PhD; Amir Salimi, MSc, Padma Kaul, PhD, Russell Greiner, PhD

BACKGROUND
Electrocardiograms (ECGs) are a valuable and easily collected measurement of heart health, reflecting its morphology (R peak, QRS duration,..) and rhythm
(sequence of multiple heartbeats). Current open-source ECG datasets such as China Physiological Signal Challenge 2018 (CPSC 2018) were used to develop various deep-learned models for ECG diagnosis. However, the diagnostic performance of these models is not high for all labels. Adding more training synthetic ECG instances of the labels might help the learning algorithm produce more accurate models, particularly for the labels associated with those additional instances. However, this has not been investigated using the generative model of Beta Variational AutoEncoder (beta-VAE).

METHODS/RESULTS
Here, we learned a beta-VAE model of the rhythm of 12-lead ECG signals using a large dataset of 244,077 patients admitted to hospitals in Alberta, Canada between February 2007 and April 2020, where each instance is labeled with certain specified abnormalities – including ST-segment elevation (STE). As beta-VAE is a generative model, it can be used to generate synthetic signals that resemble the input ECG signals ideally by retaining the relevant characteristics of the input signals. We used this trained model to generate new instances with specific abnormalities, which we call Alberta VAE-generated ECGs. We then use the generated instances, in addition to the original labeled instances, to to produce discriminative ECG signals. we evaluate different data augmentation methods including Alberta VAE-generated ECGs, and oversampling of ECGs of CPSC 2018 dataset for the task of muti-label classification of ECG abnormalities of CPSC 2018. The results show that the addition of a synthetic ST-segment elevation (STE) label into training data, increased the F1 performance of this label by 4% compared with no data augmentation.

CONCLUSIONS
We found that a learner trained on this extended dataset performed better than one trained on only the original data or oversampling data on the targeted ST-segment elevation (STE) label. More studies are required to evaluate the beneficial effect of beta-VAE generated ECG data on other datasets.

Sex- and Enantiospecific Differences in the Formation Rate of Hydroxyeicosatetraenoic Acids in Rat Heart, Kidney, and Lung

Samar H. Gerges, Ahmad H. Alammari, Mahmoud A El-Ghiaty, Fadumo A. Isse, Ayman O.S. El-Kadi.

BACKGROUND

Hydroxyeicosatetraenoic acids (HETEs) are hydroxylated arachidonic acid (AA) metabolites that are classified into midchain, subterminal, and terminal HETEs. Hydroxylation of AA carbons results in the formation of R and S enantiomers for each HETE, except for 20-HETE. HETEs are now widely recognized to have important physiological and pathological functions including cardiovascular, renal, and pulmonary functions, modulation of vascular tone and ion transport, as well as inflammatory effects. Several studies have demonstrated sex-specific differences in AA metabolism in different organs. In addition, several reports have shown enantiospecific differences in the biological or pathophysiological effects of different enantiomers of the same HETE.

METHODS/RESULTS

Microsomes from the heart, kidney, and lung of adult male and female Sprague Dawley rats were isolated and incubated with AA. Thereafter, enantiomers of all HETEs were analyzed by liquid chromatography-tandem mass spectrometry. We found significant sex- and enantiospecific differences in the formation levels of different HETEs in all organs. Several midchain HETEs showed significantly higher formation rates in male organs. 20-HETE formation rate was significantly higher in male heart microsomes, while it showed no significant sex difference in the lungs and kidney. Only 19(S)-HETE was found in the heart and lungs, but both R and S enantiomers were produced in the kidney.

CONCLUSIONS

We demonstrated significant sex- and enantiospecific differences in HETE formation levels in microsomes isolated from heart, kidney, and lungs of adult male and female rats. This provides interesting insights into their physiological and pathophysiological roles and their possible implications in different diseases.

Predicting Preterm Birth: An Analysis of Prescription Medication Usage during Pregnancy

Animesh Kumar Paul, Sunil Vasu Kalmady, Padma Kaul, Russell Greiner

BACKGROUND

The use of prescription medications during pregnancy presents a special concern to both clinicians and patients due to uncertainty about their impact on maternal and child outcomes. Unfortunately, it is not always possible to avoid the use of pharmacological treatments as a result of pre-existing maternal chronic illnesses, or acute conditions that develop during pregnancy. Recent population studies from various countries have found that 60% to 90% of pregnant women take at least one prescription medication during their entire pregnancy, and between 50% to 70% take these in the first trimester of pregnancy.

METHODS/RESULTS

We have been studying the Alberta Pregnancy Birth Cohort using the administrative-health databases, which included drug claims, physician claims, and birth details for helping clinicians avoid drugs that can lead a pregnancy to preterm birth. For our preliminary descriptive analysis, we only consider singleton births between 2009 to 2018. As a part of the data filtering, we removed births of women who were not residents of Alberta for at least one-year prior to and during the entire time period of the pregnancy and for which gestational age and birth weight are missing. We computed the preterm and term distribution among women who did (versus did not) receive a particular drug of interest. We represented drugs by their first three levels of anatomical therapeutic chemical (ATC) codes. We calculated the maternal age and trimester distribution for pregnancies of women who received the drug of interest, basing the trimester distribution when women took that drug for the first time. Finally, we extracted the top 10 diagnoses that prompted the women to interact with their physicians in the one year before being prescribed that drug. We have these results, for 82 ATC categories that are selected from the pharmaceutical information network dataset, and incorporated into a web dashboard for helping clinicians; see https://alberta-pregnancy-preterm-info-a2sljre4oq-uc.a.run.app/.

CONCLUSIONS

It is crucial to have an a priori idea of the expected treatment outcomes for a given patient. As the first step towards this goal, we have built a tool to provide clinicians with relevant statistics from large observational cohort studies. In the future, we are planning to explore the use of data harmonization procedures to collate similar data, in real-time, from other provinces and to build a dashboard to visualize such big data, to help obtain relevant insights that we anticipate will improve the overall individualized predictions with respect to perinatal outcomes.

4/30/23, 10:28 PM Alberta_Preterm_Distribution - Streamlit

Preterm Distribution (PregnancyLevel)

Considerations:

1. Observational Data from 2009 to 2018
2. Only Singleton Birth.
3. Still Births are not included.
4. ATC Codes: Only consider first three levels.
5. Term and Post-term births are considered as Normal Birth
6. Trimesters: 1st Trimester (01-12 Weeks), 2nd Trimester (13-25 weeks), and Third Trimester (26 to 40 weeks)

Drug Group

BETA BLOCKING AGENTS

Show

For BETA BLOCKING AGENTS

Preterm Distribution

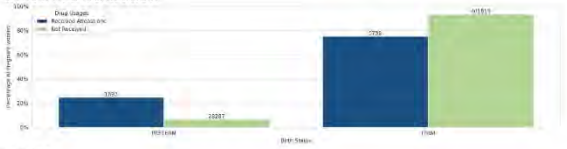

localhost:8502 1/4

4/30/23, 10:28 PM Alberta_Preterm_Distribution - Streamlit

Age Distribution

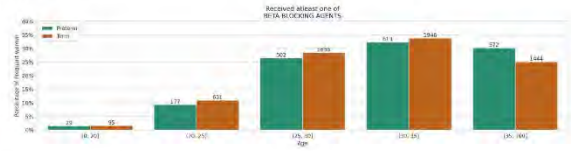

Trimester Distribution

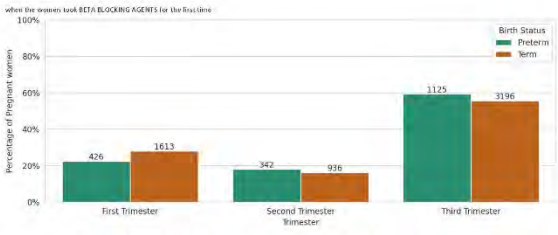

Diagnosis codes (1 year history prior to prescription)

localhost:8502 2/4

4/30/23, 10:28 PM Alberta_Preterm_Distribution - Streamlit

Development of novel vasopressor therapy during neonatal resuscitation

Marwa Ramsie, Po-Yin Cheung, Tze-Fun Lee, Megan O'Reilly, Georg M. Schmölzer

BACKGROUND
At birth, 0.1% of term infants and up to 15% of preterm infants receive cardiopulmonary resuscitation (CPR) including chest compressions and the vasopressor epinephrine (adrenaline). Despite receiving CPR, approximately one million of these newborns will die annually. Even with successful resuscitation, newborns receiving CPR in the delivery room have a high incidence of mortality
(41%) and severe short and long-term neurologic sequalae. Epinephrine
(adrenaline) is currently the only vasopressor recommended during neonatal resuscitation by the International Liaison Committee on Resuscitation. The inability to predict which newborns are at risk of requiring resuscitative efforts at birth has prevented the collection of large, high-quality human data as to its efficacy for this indication. Vasopressin may be an alternative to epinephrine as pediatric and adult studies suggested that is more effective if cardiac arrest was due to asystole, which is the main cause of cardia arrest in newborn infants. This study aimed to determine the optimal dosage of vasopressin for neonatal resuscitation using a neonatal piglet model. We hypothesized that vasopressin compared to epinephrine will decrease time to return of spontaneous circulation (ROSC).

METHODS/RESULTS
Piglets (n=8 per group) 1-3 days of age were anesthetized, intubated via a tracheostomy, and ventilated. After a stabilization period of 60 minutes, piglets were randomized to receive one of the following vasopressin (0.2U/kg, 0.4U/kg, 0.8U/kg) or epinephrine (0.02mg/kg) doses intravenously. Measurements of rates of ROSC and time to ROSC, survival after ROSC, hemodynamic, and blood gas changes were collected.

Results
Baseline parameters were similar between all groups. Piglets who received vasopressin had a higher rate of achieving ROSC (6/8(75%) in 0.2U/kg and 0.4U/kg groups and 7/8(88%) with 0.8U/kg) than those given epinephrine (5/8(63%);
P=0.94). Median (IQR) time to ROSC was shorter in vasopressin-treated piglets than the epinephrine group at 172 (103-418) seconds, 157 (100-413) seconds, 122 (93-289) seconds, and 276 (117-480) seconds (P=0.59) for the 0.2U/kg, 0.4U/kg, 0.8U/kg vasopressin groups, and 0.02mg/kg epinephrine group, respectively. Higher rates of survival post-ROSC were observed in the vasopressin groups (5/6(83%), 5/5(100%), and 4/6(67%) with 0.2, 0.4, and 0.8U/kg vasopressin, respectively) compared to the epinephrine group (3/5(60%), P=0.61).

CONCLUSIONS
Vasopressin may be an alternative to epinephrine in neonatal resuscitation when cardiac arrest was due to asystole. Piglets administered vasopressin had higher rates and less time to ROSC, and were more likely to survive following ROSC. Human clinical trials using vasopressin in neonatal resuscitation are warranted.

Invasive and Noninvasive Measurements in the Diagnosis of Pulmonary Arterial Hypertension: A Quality Improvement Project

Alexandra Saunders, Kevin Bainey, Evangelos Michelakis

BACKGROUND

The diagnosis and treatment of pulmonary hypertension (PH), a disease with high morbidity and mortality, depends on the accuracy of two tests: transthoracic echocardiography (TTE) and right heart catheterization (RHC). Elevation of right ventricular systolic pressure estimation (RVSP) and decrease in RV function (estimated by tricuspid annular plane excursion; TAPSE) on TTE, leads to a PH workup and RHC. With RHC, obtaining accurate right-sided pressures and pulmonary arterial wedge pressures (PAWP) is vital, as different etiologies of PH are based on these results (eg. PH due to heart failure with preserved ejection fraction; HFpEF versus pulmonary arterial hypertension; PAH) and require vastly different therapies.

METHODS/RESULTS

Charts of 252 patients with both RHC and TTE were reviewed from 2016-2021. Each study was given a penalty score if measurements were not reported correctly based on guidelines of best practice (Table).

Mean penalty score was -1.28 for Mazankowski TTE compared to -2.4 for all other Edmonton echo labs. Overall, 50% of TTE reports did not report the poor quality of the TR jet when reporting RVSP and 20% did not report a TAPSE score.

The quality of the RHC PAWP traces was reviewed. In a subset of patients who also had measurements of left ventricular end-diastolic pressure (LVEDP; which, in the absence of mitral stenosis, should equal PAWP), agreement of the two values was measured as an additional index of PAWP quality.

RHC mean penalty score was -0.9. The LVEDP values were moderately correlated with the PAWP (Pearson correlation coefficient 0.51). The most common error was not accounting for respiratory variation. In 25 patients, reported assessment of PAWP would have led to misclassification of PH.

TTE RVSP was only moderately correlated with RHC systolic PA pressure (sPAP). This differed depending on time between RHC and TTE. Pearson correlation coefficients were 0.76 ($p<0.05$) when within 2 days and 0.60 ($p<0.05$) when >2 weeks. The mean deviation of TTE RVSP from RHC sPAP (gold standard) was 18 mmHg (+/- 1). In 11 patients, this difference would have missed PH if RHC had not been performed.

CONCLUSIONS

Several areas for improvement were identified for the echo and cath labs, which may be improved by educational programs for all health care professionals. In addition to patient care, this may also impact health care costs, since HFpEF is very common and the (more rare) PAH is extremely expensive, with the yearly costs of a PAH patient often exceeding $200,000.

Table 1. Penalty scored used in evaluation of transthoracic echocardiography (TTE) and right heart catheterization (RHC)

TTE Penalty Scoring	
Poor quality TR jet not reported	-3
RA pressure not estimated using IVC	-2
TAPSE not reported	-2
TR jet not the average of 3 different views	-1
RHC Penalty Scores	
PCWP > dPAP	-3
Respiratory variation done incorrectly	-3
No respiratory variation recorded	-1
PCWP not the average of three beats	-1
LVEDP different from PCWP	-1 per 5 mmHg

Figure 1. Comparison of echo estimated right ventricular systolic pressure (RVSP) vs cardiac catheterization measured systolic pulmonary artery pressure (sPAP). The echo studies that did not report poor tricuspid regurgitation (TR) jet quality when it was present are outlined in orange, and all other studies are in blue.

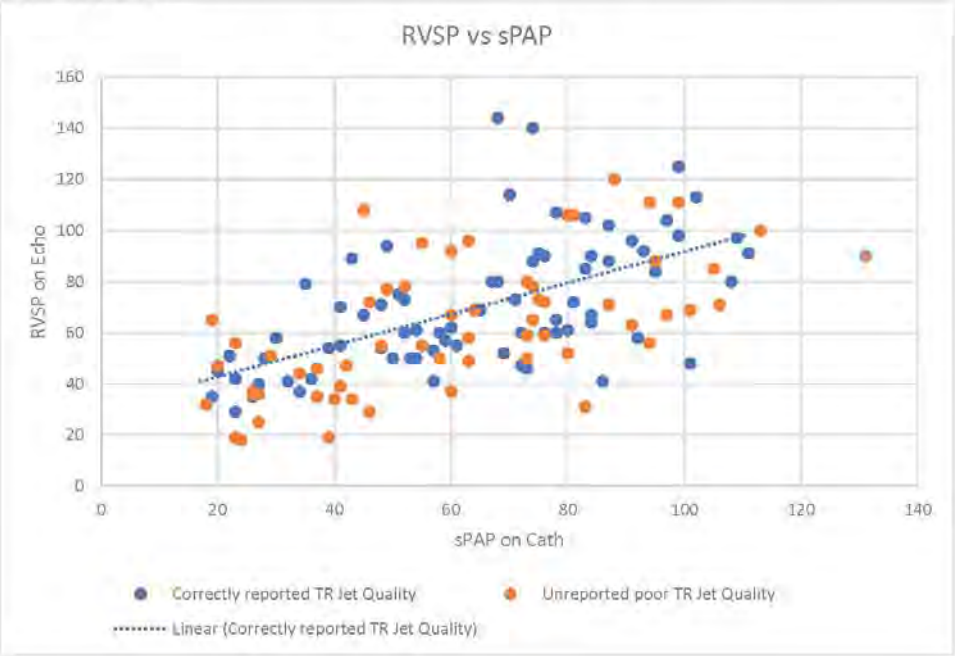

Determining the effect and mechanism of action of SARS-CoV-2 spike protein on von Willebrand factor expression and/or release from endothelial cells

Noorossadat Seyyedi, Parnian Alavi, Alexia Maheux, Samar Barazesh, Nadia Jahroudi

BACKGROUND

Von Willebrand factor (VWF) is a highly adhesive multimeric glycoprotein stored in the Weibel-Palade bodies (WPB) of endothelial cells and α-granules of megakaryocytes. VWF multimers released from endothelial cells through basal or regulated secretion may remain bound to the cell membrane or enter the circulation. VWF mediates platelet adhesion to endothelial/subendothelial surfaces, as well as platelet aggregate formation, thus maintaining hemostasis but also contributing to thrombogenicity. In addition to injury, various stimuli including bacterial and viral infections are associated with increased VWF levels. Coronavirus disease (COVID-19) is a viral infection caused by severe acute respiratory syndrome coronavirus 2 (SARS-CoV-2). Those severe and critically ill COVID-19 patients with significant thrombotic complications were shown to have highly elevated levels of VWF. Although the increase in VWF levels may result from a rise in the inflammatory response to SARS-CoV-2, we hypothesized that this virus may also directly induce VWF upregulation and/or release in endothelial cells. Since the receptor for SARS-CoV-2 spike protein, angiotensin-converting enzyme 2 (ACE2), is also present on endothelial cell surfaces; we hypothesized that the spike protein engagement of the ACE2 receptor may lead to VWF transcriptional upregulation and/or release from storage, and consequently contribute to increased platelet aggregate formation and thrombogenicity.

METHODS/RESULTS

Human umbilical vein endothelial cells (HUVECs), human brain microvascular endothelial cells (Brain MVECs), and human lung microvascular endothelial cells
(Lung MVECs) were treated with SARS-CoV-2 spike protein. Cells lysate and the culture media were collected at various time points after treatment. Exposure to SARS-CoV-2 spike protein resulted in a significant increase in released VWF in culture media of Lung MVECs and HUVECs, but not Brain MVECs within five minutes. Analyses of VWF mRNA levels revealed a significant increase specifically in Lung MVECs after 48-72 hours of treatment.
Immunofluorescence staining using an anti-ACE2 antibody confirmed the presence of this protein in all three endothelial cell types.

CONCLUSIONS

Our preliminary results demonstrated that SARS-CoV-2 spike protein directly induces VWF transcriptional upregulation and its release from endothelial cells, but it does so in a highly organ-specific manner. Elevated VWF secretion was detected in HUVECs and Lung MVECs, but VWF mRNA upregulation was observed only in Lung MVECs. Brain MVECs did not respond to spike protein exposure at either level.

Maternal Ketone Supplementation during Pregnancy Protects Against Iron Deficiency Induced Cardiac Dysfunction in the Offspring

Shubham Soni, Ronan Noble, Si Ning Liu, Claudia Holody, Jad-Julian Rachid, Alyssa Wiedemeyer, Matthew Martens, Mourad Ferdaoussi, Stephane Bourque, Jason R. B. Dyck

BACKGROUND

Iron deficiency (ID) is the most widespread nutritional disorder in the world and affects an estimated 39% of pregnant women globally. Maternal ID induces mitochondrial dysfunction, inflammation, and cardiac dysfunction in developing offspring. A noteworthy characteristic of ID neonates is an impaired ability to produce ketones.

Ketones, namely β-hydroxybutyrate (βOHB), are molecules produced by the liver from fatty acids that can be used as a source of energy. However, ketones also have signaling properties that inhibit inflammation. Thus, we hypothesized that gestational βOHB supplementation can reduce cardiac dysfunction in ID neonates by favorably acting on metabolic and/or inflammatory pathways.

METHODS/RESULTS

6-week-old female Sprague Dawley rats were fed an iron-restricted (3-10 mg/kg) or iron-replete (37 mg/kg) diet two weeks prior to and throughout gestation. Control dams were subcutaneously injected with saline and ID dams were given saline or 300mg/kg body weight βOHB throughout pregnancy (gestational day 1 to 21). After birth, all dams were fed an iron-replete diet. Cardiac function of the offspring was assessed by echocardiography on postnatal days 1, 4, and 14, and the hearts were assessed for markers of ketone metabolism and inflammation. Using this approach, we show that perinatal iron restriction reduced maternal hemoglobin in both ID and ketone-treated ID (KID) dams compared to controls. Similarly, ID and KID offspring also had lower hemoglobin, and both ID and KID offspring also had greater heart/body weights at all timepoints. Systolic function was impaired in the ID neonates, as evidenced by reduced ejection fraction (EF). Total oxygen delivery was also reduced in these ID neonates. However, KID neonates were protected from this reduction in EF, exhibiting EFs similar to that of control neonates. Similarly, KID neonates also had improved total oxygen delivery. Furthermore, while markers of cardiac inflammation and stress (e.g., Il-1b, Bnip3) were elevated in ID hearts at, the hearts of KID neonates were protected from these effects and had a lower expression of these markers.

CONCLUSIONS

Altogether, these data suggest that ketone supplementation to pregnant mothers can protect neonates against the cardiac dysfunction induced by iron deficiency. These data also shows that ketone supplementation in ID mothers is safe for the ID mother and offspring, and does not exacerbate ID-induced growth restriction. These findings reveal a potential novel therapeutic approach to mitigate the deleterious cardiac effects of perinatal ID and improve the health of anemic babies.

Cardiac Energy Metabolism is Disrupted in Heart Failure with Preserved Ejection Fraction (HFpEF)

Qiuyu Sun, Berna Güven, Cory S. Wagg, Amanda A. de Oliveira, Heidi Silver, Liyan Zhang, Ander Vergara, Brandon Chen, Ezra Ketema, Qutuba G. Karwi, Faqi Wang, Jason R.B. Dyck, Gavin Y. Oudit, Gary D. Lopaschuk

BACKGROUND
Heart failure with preserved ejection fraction (HFpEF) is a debilitating disease that is prevalent in our society. Patients with HFpEF are mostly older women with coexisting obesity, diabetes, and hypertension. Unfortunately, there is still no proven to be effective pharmacotherapy to date for treating HFpEF. As such, it is urgent to find new therapeutic targets and to understand the complex pathophysiology of HFpEF. While it is well-accepted that changes in myocardial energetics are involved in heart failure progression, it remains unknown whether alterations in cardiac energetics contribute to HFpEF severity. Therefore, the objectives of this study were to define the cardiac energy metabolic profile in aging female HFpEF mice and then attempt to lessen the severity of HFpEF by improving cardiac energetics.

METHODS/RESULTS
A '2-Hit' HFpEF protocol was used on 13-month-old female C57BL/6J mice by subjecting them to 10 weeks of 60% high fat diet (HFD) and 0.5g/L of Nω-nitro-L-arginine methyl ester (L-NAME) in the drinking water to induce obesity and hypertension. Control mice were fed with a regular chow diet. At the end of the study protocol, echocardiography, pressure volume (PV) loops, and glucose tolerance (GTT) test were performed. Hearts were excised out and perfused with radiolabeled energy substrates to directly measure rates of glucose oxidation, glycolysis, fatty acid oxidation, and ketone oxidation. A third intervention group of mice were treated with 40mg/ kg/day of the pyruvate dehydrogenase inhibitor
(PDKi) MMR-0053 while receiving the HFpEF protocol.

HFpEF mice exhibited increases in body weight, glucose intolerance, and elevated blood pressure. Echocardiography revealed that HFpEF mice developed diastolic dysfunction and concentric hypertrophy. In HFpEF mice hearts, glucose oxidation was significantly suppressed, whereas fatty acid oxidation was not decreased, but rather had a trend of increase. Total ATP production was reduced in HFpEF hearts compared to healthy control hearts. PDKi increased glucose oxidation rates in the HFpEF hearts. PDKi treated mice had improved systolic and diastolic function compared to vehicle treated mice. PDKi treatment also improved vascular function, ameliorated hypertension, and improved overall survival rates.

CONCLUSIONS
The heart becomes metabolically inflexible in HFpEF, as characterized by a prominent decrease in glucose oxidation with a simultaneous increase in fatty acid oxidation. Stimulation of cardiac glucose oxidation using a PDKi lessened the severity of HFpEF and exerted functional benefits. Therefore, targeting cardiac energy metabolism could be promising therapeutic targets for treating HFpEF.

ECG for high-throughput screening of multiple diseases: Proof-of-concept using multi-diagnosis deep learning from population-based datasets

Weijie Sun, Sunil V Kalmady, Amir Salimi, Nariman Sepehrvand, Eric Ly, Abram Hindle, Russell Greiner, Padma Kaul

BACKGROUND

In recent years, deep learning (DL) models have achieved remarkable success, approaching human-level performance in various applications. However, the majority of DL-based diagnostic predictions in patient Electrocardiograms (ECGs) have been restricted to a limited set of cardiac diseases. However, ECG abnormalities are also manifest in non-cardiovascular conditions, including mental, neurological, metabolic, and infectious disorders. In this study, we use a comprehensive population-based dataset to identify a broad spectrum of diseases that can be accurately diagnosed using a patient's first in-hospital ECG.

METHODS/RESULTS

We divided our ECG dataset from.Alberta, Canada into a development set (a random sample of 60% composed of 146,446 patients with 964,741 ECGs for training and internal validation) and an external holdout set (the remaining 40%with 97,631 patients and 640,527 ECGs), ensuring that ECGs from the same patient were not shared between the sets. We employed a population-based dataset encompassing various medical conditions and emergency department and in-hospital ECGsfor this task. Diagnoses were coded using the World Health Organization's International Classification of Diseases, 10th Revision (ICD-10), which served as the basis for diagnosis labels.
We then trained a deep learning model to evaluate the complete set of 1,414 ICD-10 codes based on the first ECG per episode. Our DL architecture was founded on the ResNet model, which input 12-lead ECG traces into a network comprising a convolutional layer, four residual blocks with two convolutions per block, and a dense layer, to which age and sex features were concatenated.
Our results showed that 210 ICD-10 codes, spanning 17 (ICD-10 code) categories, achieved an Area Under the Receiver Operating Characteristic (AUROC) greater than 80%.

CONCLUSIONS

In addition to the 61 ICD-10 codes from the cardiac-related ICD-10 category
(pertaining to diseases of the circulatory system), we identified 149 non-cardiac diseases that achieved an AUROC greater than 80%.
Our study investigates the predictability of multiple diseases across the ICD-wide diagnostic landscape using ECG data. Our deep learning models, trained and validated on population-scale datasets, exhibit excellent AUROC values (i.e., high sensitivity and specificity) for numerous diseases. However, their positive predictive value (PPV) may be limited, partially due to the low prevalence rates of certain diseases (89.8% of diseases had a prevalence of less than 1%). Consequently, model predictions for such diseases may be more appropriate for 'rule-out' screening rather than 'rule-in' diagnostics.

Machine-learning for the electrocardiogram-based prediction of short-term and long-term mortality at the time of discharge in a population-level cohort of patients with access to universal healthcare

Weijie Sun, Sunil V Kalmady, Nariman Sepehrvand, Amir Salimi, Yousef Nademi, Kevin Bainey, Justin A. Ezekowitz, Russell Greiner, Abram Hindle, Finlay A. McAlister, Roopinder K. Sandhu, Padma Kaul

BACKGROUND

The electrocardiogram (ECG) serves as a widely accessible diagnostic instrument, routinely employed in nearly all patient encounters within acute care settings. This tool offers valuable diagnostic and prognostic insights, with discharge ECGs potentially facilitating risk stratification and informing post-discharge management. It is unclear how the use of discharge ECG in addition to the information such as comorbidities that are at clinicians' disposal at discharge can further improve prognostication in patients.

METHODS/RESULTS

In this study, we leveraged a large, population-based cohort of 1,308,136 ECGs from 496,303 healthcare episodes of 255,162 patients (2007–2020) in Alberta, Canada under universal health insurance who sought care at emergency departments (ED) or hospitals in Alberta, Canada. Our aim was to develop deep learning (DL) models utilizing discharge ECG tracings and extreme gradient boosting (XGB) models based on discharge ECG measurements for predicting short-term and long-term mortality at 30-day, 1-year, and 5 years from the time of discharge. We then compared the performance of these models against an established Charlson Comorbidity Index (CCI) with demonstrable prognostic efficacy.

We divided the overall ECG dataset into a random split of 60% for the model development (for training and fine- tuning), and the remaining 40% as the holdout set for validation. The models for 30-day, 1-year, and 5-year mortality were trained on 145,026, 138,384, and 103,784 patients and evaluated on 81,767, 76,368, and 54,852 patients, respectively. In our holdout cohort, 8.7%, 19.7%, and 42.7%patients died by 30-days, 1-year, and 5- years, respectively. DL models with ECG traces, age, sex performed better (84.71%, 79.66%, 81.96%) than the XGB models of ECG measurements, age, sex (78.47%, 74.42%, 78.32%) in predicting outcomes for all three timepoints and the clinical risk model based on CCI, age, sex (81.38%, 80.95%, 82.34%) in predicting 30-day outcome. Moreover, addition of CCI information improved the performance of ECG models at all three time- points by 1.88%, 4.44%, 2.3% in DL and by 3.69%, 6.5%, 3.82% in XGB.

CONCLUSIONS

In this study, we developed mixed-input AI-augmented ECG-based prediction models to output a calibrated probability of mortality at 30-day, 1 year, and 5 years from discharge using discharge ECGs. Our observations show that although ECG-based models are more predictive than CCI-based clinical models particularly for short- term mortality, incorporating CCI improves the performance of ECG-based models at all three time- points.

Therefore, combining both ECG and CCI information can provide superior prognostic prediction and may be a more effective approach for planning care after a patient's discharge from the hospital.

Tumor-Secreted Nucleosides Promote RbFox1 Degradation and Signalling Pathways Relevant to Dedifferentiation in Cardiomyocytes; A Two-Hit Hypothesis with Implications for Cardiotoxicity

Saymon Tejay, Maria-Areli Lorenzana-Carillo, Joseph Nanoa, Yongsheng Liu, Alois Haromy, Ian Paterson, Edith Pituskin, John Ussher, Evangelos Michelakis, Gopinath Sutendra

BACKGROUND
It is well-documented that tumor cells can secrete numerous signalling factors that affect distant normal tissues. For example, tumor-secreted inflammatory factors can initiate muscle or fat tissue breakdown into protein or fatty acids, respectively, that can be used to feed the growing tumor, but consequently can severely decrease the weight of cancer patients. What remains incompletely understood is if tumor-secreted factors (TSFs) can initiate a signalling cascade in the heart, rendering cardiomyocytes (the contractile cells of the heart) susceptible to cell death when treated with anti-cancer drugs.

METHODS/RESULTS
We utilized clinically relevant xenotransplant cancer mouse models to study the effect of secretions on the myocardium. We utilized serum and breast cancer samples from patients that did and did not develop cardiotoxicity. We isolated primary cardiomyocytes to elucidate our proposed signalling cascade. We generated transgenic cardiomyocyte specific RbFox1 KO mice and assessed heart function with echocardiography after anthracycline treatment.

We show that tumor secreted nucleosides (i.e. inosine), which are precursors for generating DNA in the cell, were significantly increased in the serum of mice with lung cancer and breast cancer patients that developed cardiotoxicity. Mechanistically, we found that tumor secreted inosine activates the A2A receptor on cardiomyocytes initiating a signaling cascade leading to degradation of the RNA splicing factor RbFox1. RbFox1 loss induces the formation of the mitochondrial permeability transition pore and release of cytochrome C (a precursor for cell death), while also promoting cardiomyocyte dedifferentiation and a more receptive chromatin for anti-cancer intercalating agents (which induce the pro apoptotic transcription factor p53). In keeping, RbFox1 deficient mice develop significant cardiotoxicity when treated with low dose intercalating agents, including the commonly used doxorubicin.

CONCLUSIONS
This work provides both a potential biomarker (i.e. inosine) and mechanism for susceptibility to our most cardiotoxic anti-cancer drugs including doxorubicin and cisplatin.

Negative Pressure Ventilation Ex-situ Lung Perfusion Successfully Preserves Porcine Lungs And Rejected Human Lungs For 36-hours

Abeline R. Watkins, Keir A. Forgie, Alynne Ribano, Katie Du, Darren H. Freed, Jayan Nagendran

BACKGROUND
Continuous Ex-Situ Lung Perfusion (ESLP) beyond 24-hours is required to optimize the extended criteria donor pool through cell- and gene-based therapies. Preclinically, continuous ESLP for 24-hours is the longest duration achieved in large animal models and rejected human lungs. Here, we present the results of our
36-hour Negative Pressure Ventilation (NPV)-ESLP protocol applied to porcine and rejected human lungs.

METHODS/RESULTS
Five sets of donor lungs from domestic pigs (45-55kg) underwent 36-hours of normothermic negative pressure ventilation (NPV)-ESLP. Two sets of human lungs rejected for clinical transplant were donated to research and preserved on NPV-ESLP for
36-hours. Graft function was assessed via physiologic parameters, edema formation, and cytokine profiles.

Porcine and human lung function was stable during 36-hours of NPV-ESLP with mean PF ratios throughout preservation of 473 ± 11.79 and 554.7 ± 13.26, respectively (mean ± SEM). In porcine lungs, the average compliance (Cdyn) during ESLP was 33.96 ± 2.18, mean pulmonary artery pressure (PAP) 13.03 ± 0.53, and pulmonary vascular resistance (PVR) 481.20 ± 21.86. In human lungs, the average Cdyn was 82.68 ± 3.54, mean PAP 6.00 ± 0.33, and mean PVR 184.00 ±9.71. Average percentage weight-gain/hour after 36-hours of ESLP was 1.64 ± 0.73 in the porcine group and 3.24 ± 0.19 in the rejected human lungs.

CONCLUSIONS
Normothermic NPV-ESLP can preserve porcine lungs and rejected human lungs for 36-hours with acceptable physiologic function. The significant difference in weight-gain between porcine and human lungs is likely due to the rejected status of the human lungs with significant dysfunction in the donor prior to preservation. Continuous 36-hour NPV-ESLP could support gene- and cell-based therapies that improve endothelial protection and mitigate fluid accumulation.

The Impact of Early-Stage Breast Cancer on Cardiac Structure and Function

Kai Yi Wu, Amy Kirkham, James A. White, Mark J. Haykowsky, Jason Dyck, Justin A. Ezekowitz, Gavin Oudit, Joseph Kurian, Richard Thompson, Edith Pituskin, Ian Paterson

BACKGROUND
Previous studies suggest that cancer alone is associated with subtle changes in cardiac structure and function, even before cancer therapy. However, these studies are limited by retrospective designs and a lack of adequate controls. Therefore, we extensively characterized cardiac phenotype in patients with newly diagnosed early- stage breast cancer (ESBC) compared to age and sex-matched controls.

METHODS/RESULTS
163 females with stage 0-3 breast cancer were recruited prior to receiving cancer treatment. Those with previous cancer treatment, hypertension, diabetes, or cardiac disease were excluded. 55 age and sex-matched healthy controls were included. Cardiac magnetic resonance (CMR) at 1.5T was used to image cardiac chamber size, mass and function and myocardial tissue characterization through T1 mapping. Serum high-sensitivity troponin and BNP were also measured. Independent-sample t-test was used to compare demographic, imaging metrics and biomarkers between healthy controls and patients with ESBC.

There were no significant differences in age, body mass index, and blood pressure between groups except for a higher resting heart rate in the ESBC cohort compared to healthy controls (76.6±11.7 bpm vs. 66.6±10.6 bpm, $p<0.01$). On CMR, LVEF (62.4±5.3% vs. 61.9±4.0%, $p=0.43$) was similar between groups, but global longitudinal strain (GLS) was reduced in the ESBC cohort (-20.5±2.4% vs. -22.4±2.0%, $p<0.01$). Left ventricular mass index (50.0±7.2 g/m2 vs. 47.0±5.9 g/m2, $p<0.01$) and concentricity (LV mass/LV end-diastolic volume) (0.73±0.13 vs. 0.69±0.08, $p<0.01$) were increased in the ESBC group compared to controls with similar myocardial tissue characterization on native T1 mapping. No difference in serum biomarkers was observed between the groups. Cancer stage and receptor status were not associated with CMR measures of cardiac function and structure on regression analyses.

CONCLUSIONS
Patients with new ESBC are characterized by relatively elevated resting heart rate, LV hypertrophy and reduced GLS. These findings may provide a rationale for prophylactic therapies, such as beta-blockers, to prevent cancer-related cardiac dysfunction and heart failure.

Does Cardiac Imaging Surveillance Strategy Influence Outcomes in Patients with Early Breast Cancer?

Kai Yi Wu, Sarah Parent, Lingyu Xu, Maryam Yaqoob, W. Allan Black, Andrea Shysh, John R. Mackey, Karen King, Harald Becher, Edith Pituskin, D. Ian Paterson.

BACKGROUND
Many patients with breast cancer receive therapies with the potential to cause cardiotoxicity. Echocardiography and multiple-gated acquisition (MUGA) scans are the most used modalities to assess cardiac function during treatment in high-risk patients; however, the optimal imaging strategy and the impact on outcome are unknown.

METHODS/RESULTS
Consecutive patients with stage 0-3 breast cancer undergoing pre-treatment echocardiography or MUGA were identified from a tertiary care cancer center from 2010-2019. Demographics, medical history, imaging data and clinical events were collected from hospital charts and administrative databases. Cancer therapy-related cardiac dysfunction (CTRCD) was defined as a drop in left ventricular ejection fraction of ≥10% to a value <50%. The primary outcome is a composite of all-cause death or heart failure event. Clinical and imaging predictors of outcome were evaluated on univariable and multivariable analyses.

1028 patients underwent pre-treatment MUGA and 1032 underwent echocardiography. The groups were well matched for most clinical characteristics except patients undergoing MUGA were younger, had more stage 3 breast cancer and more HER2 over-expressing and triple-negative cases. A follow-up cardiac imaging scan was obtained in 47.8% of patients with MUGA and 44.1% with echocardiography. During a median follow-up of 2448 (1489, 3160) days, there were 194 deaths and 49 heart failure events with no difference in events between the MUGA and echocardiography groups. Imaging predictors of the composite outcome included CTRCD, HR 3.0 (1.4, 6.3), p = 0.004, and no follow-up imaging, HR 0.5 (0.3, 0.8), p=0.005.

CONCLUSIONS
The selection of pretreatment echocardiography or MUGA did not influence the risk of death or heart failure in patients with early breast cancer. Many patients did not have any follow-up cardiac imaging and did not suffer worse outcomes. Heart failure event rates were low and the value of long-term cardiac imaging surveillance should be further evaluated.

Table 1. Prediction of All-Cause Death or New or Worsening Heart Failure- 2060 subjects (221 events)					
		Univariable analysis		Multivariable analysis	
		HR(95% CI)	p-value	HR(95% CI)	p-value
Age		1.01(1.00, 1.03)	0.088		
Body mass index		1.01(1.00, 1.03)	0.088		
Medical History					
Diabetes		1.3(0.9, 2.0)	0.202		
Hypertension		1.3(1.0, 1.7)	0.102		
Dyslipidemia		1.1(0.8, 1.7)	0.552		
Coronary artery disease		2.5(1.2, 5.3)	0.018		
Prior heart failure		5.2(2.5, 11.1)	<0.001	2.7(1.2, 6.0)	**0.012**
Chronic kidney disease		2.8(1.2, 6.2)	0.014	2.9(1.3, 6.7)	**0.01**
Chronic obstructive pulmonary disease		2.3(1.4, 3.9)	0.002	1.9(1.1, 3.2)	**0.024**
Smoking		1.0(0.9, 1.2)	0.581		
Beta blocker		1.3(0.8, 2.2)	0.331		
ACE-inhibitor		1.1(0.7, 1.7)	0.561		
Angiotensin receptor blocker		1.4(1.0, 2.1)	0.079		
Aldosterone antagonist		6.1(2.0, 19.1)	0.002	5.9(1.8, 19.1)	**0.003**
Statin		1.1(0.7, 1.6)	0.659		
Breast Cancer Characteristics					
Cancer stage	0 or 1	Reference			
	2	1.3(0.8, 2.2)	0.32	1.2(0.7, 2.1)	0.444
	3	3.4(2.0, 5.8)	<0.001	3.2(1.9, 5.6)	**<0.001**
Receptor status	Hormone positive, HER2 negative	Reference			
	HER2 positive	0.8(0.6, 1.2)	0.293	1.6(0.8, 3.0)	0.184
	Triple negative	2.8(2.0, 3.9)	<0.001	2.8(2.0, 3.9)	**<0.001**
Cancer Therapy					
Use of anthracycline therapy		1.1(0.8, 1.4)	0.463		
Anthracycline dose		1.0(1.0, 1.0)	0.883		
Number of trastuzumab cycles		0.97(0.95, 0.99)	0.002	0.9(0.9, 1.0)	**0.002**
Left chest irradiation		1.0(0.7, 1.3)	0.812		
Cardiac Imaging					

Baseline imaging (Echo vs. MUGA)		0.9(0.7, 1.1)	0.297		
Baseline LVEF, per 1% increase		1.02(1.00, 1.04)	0.124		
Occurrence of CTRCD		3.0(1.5, 6.0)	0.002	3.0(1.4, 6.3)	**0.004**
Follow-up cardiac imaging	All MUGA	Reference			
	All Echo	0.8(0.5, 1.4)	0.443	0.8(0.5, 1.3)	0.361
	Mixed modality	1.5(1.0, 2.4)	0.076	1.0(0.6, 1.6)	0.971
	None	1.0(0.7, 1.5)	0.956	0.5(0.3, 0.8)	**0.005**
HFA-ICOS risk	Low	Reference			
	Moderate	1.2(0.9, 1.6)	0.169		
	High	2.0(1.2, 3.4)	0.005		
	Very high	3.8(2.1, 6.7)	<0.001		

Figure 1. Plot of unadjusted Kaplan-Meier event-free survival for patients with breast cancer assigned to pretreatment multiple-gated acquisition (MUGA) scan (Blue) or echocardiography (Red). The composite event included death or new heart failure.

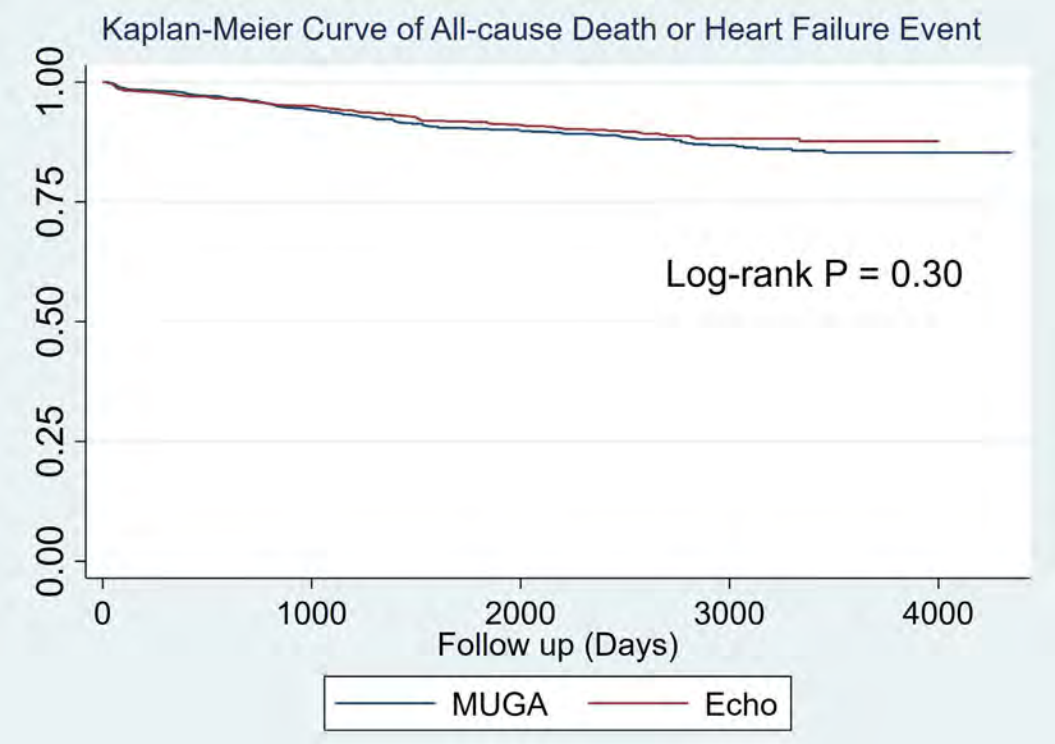

Sex Differences in Post-Operative Cardiovascular Outcomes Following Non-Cardiac Surgery

Kai Yi Wu, Xiaoming Wang, Pishoy Gouda, Erik Youngson, Michelle Graham

BACKGROUND
It is uncertain whether sex is an independent risk factor for poor postoperative outcomes. We examined the sex differences in short- and long-term postoperative mortality, readmission, and cardiac morbidity in patients undergoing non-cardiac surgery in Alberta, Canada.

METHODS/RESULTS
Using a linked administrative database, we identified 552 224 patients undergoing non-cardiac surgery between 2008 and 2019. Adjusted odds ratios (95% CIs) for mortality, hospital readmission, heart failure (HF) hospitalization, and acute coronary syndrome (ACS) hospitalization, at 30-days, 6-months, and 1-year.
Multivariable logistic regressions were adjusted for sex, age, surgery type, the components of the Charlson Comorbidity Index, and the Revised Cardiac Risk Index.

Males demonstrate a higher risk of mortality and hospital readmission at 30-days, 6-months, and 1-year. While males demonstrated higher odds of HF and ACS post-operatively in univariate models, this did not persist in the multivariate model.

CONCLUSIONS
In patients undergoing non-cardiac surgery, males have a higher risk of all-cause mortality and readmission at 30- days, 6-months, and 1-year after adjustment for baseline risk factor differences. No sex differences were observed for postoperative cardiac complications.

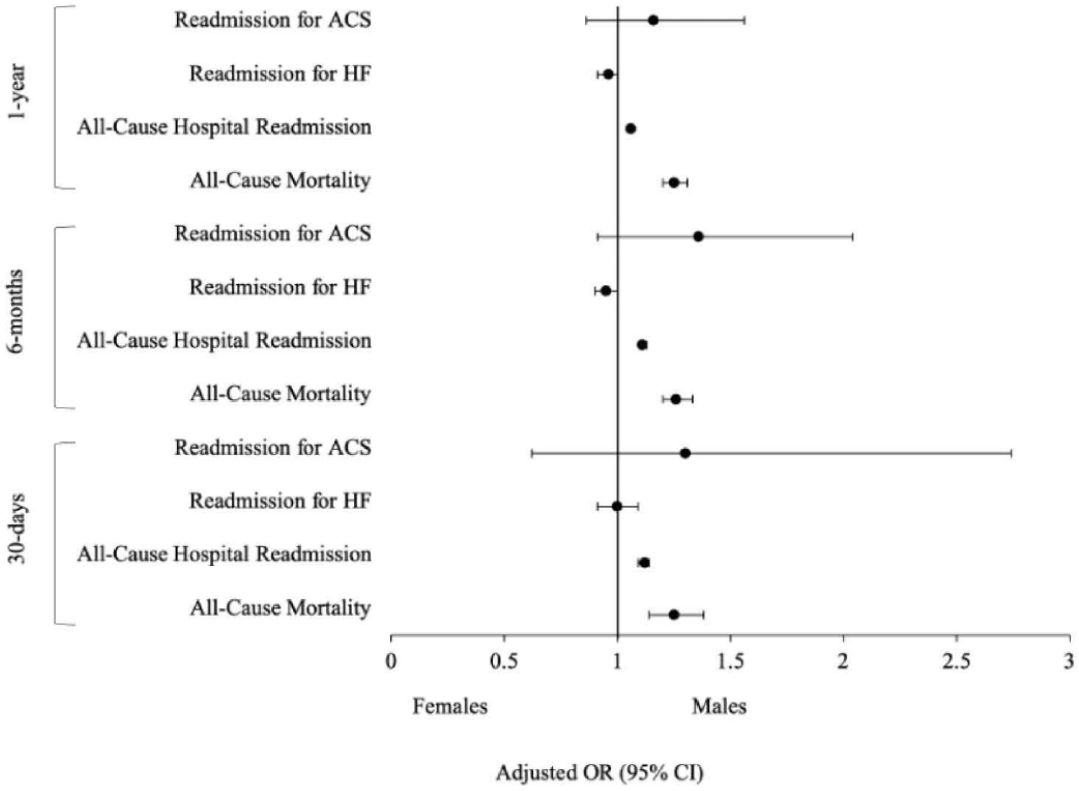
1-year
Readmission for ACS
Readmission for HF
All-Cause Hospital Readmission
All-Cause Mortality
6-months
Readmission for ACS
Readmission for HF
All-Cause Hospital Readmission
All-Cause Mortality
30-days
Readmission for ACS
Readmission for HF
All-Cause Hospital Readmission
All-Cause Mortality
0
0.5
1
1.5
2
2.5
3
Females
Males
Adjusted OR (95% CI)

Early Atherosclerotic CVD and Impaired Cardiac Function in High-Risk Young Women with and without Polycystic Ovary Syndrome

X Wu, M Wilke, M Ghosh, P Raggi, H Becher, D Vine

BACKGROUND

Polycystic ovary syndrome (PCOS) is a most common reproductive-endocrine disorder that affects up to 15% of women. Previously, we identified women with PCOS have exacerbated lipid profile compared to BMI-matched counterparts. It has been established that women with PCOS have higher incidence of atherosclerotic cardiovascular disease (ACVD); however, results from a few studies examining cardiac function in PCOS women were inconsistent. The objective of this study was to examine ACVD and the cardiac function in obese women with and without PCOS.

METHODS/RESULTS

Methods: A case-control study was conducted. Ultrasound-speckled echocardiography was used to measure carotid intimal-medial thickness (cIMT) and presence of carotid plaque. In addition, cardiac function indices such as wall thickness, left ventricle ejection fraction (LVEF), early diastolic inflow velocity (E peak rate), late diastolic inflow velocity (A peak rate) were also examined by echocardiography.

Results: cIMT were similar between PCOS and non-PCOS controls; however, carotid plaque was 19% higher in PCOS group compared to non-PCOS controls. All cardiac function indices were comparable between PCOS and non-PCOS controls. PCOS showed significantly increased LV mass index and A peak rate, as well as lower E/A ratio compared to healthy-weight controls, but it did not reach statistical significance between non-PCOS controls and healthy-weight controls. This indicates that obese women have a trend of impaired diastolic function, and it is exaggerated in PCOS women.

CONCLUSIONS

Our results showed that women with PCOS have increased risk of atherosclerosis and impaired diastolic function which may be an early sign of CVD.

Figure 1. Carotid Intima-Media Thickness, Carotid Plaque, and Plaque Height in PCOS, non-PCOS, and Healthy-weight Controls.

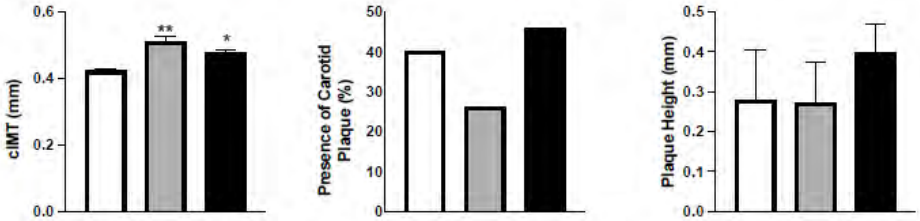

* indicates a statistical significance when comparing to healthy-weight control group. ** indicates a statistical significance when comparing to the other two groups. cIMT, carotid intima-media thickness. ASE, American Society of Echocardiography.

Table 1. Blood Pressure and Cardiac function in PCOS, Non-PCOS Control and Healthy-Weight Control groups.

	Healthy-Weight Control n=10	**Non-PCOS Control n=19**	**PCOS n=48**
SBP (mmHg)	108.3±2.58	129.4±3.13*	128.3±1.65*
DBP (mmHg)	66.80±2.28	81.84±3.22*	78.43±1.59*
Heart Rate (bpm)	74.30±3.43	75.11±2.36	77.81±2.19
LV Mass Index (g/cm^2)	50.33±2.83	62.14±2.31	64.78±1.99*
LV End Diastolic (cm)	4.29±0.15	4.83±0.13*	4.77±0.06*
LV End Systolic (cm)	2.65±0.11	3.12±0.11*	3.08±0.07*
LVPW Thickness (cm)	0.69±0.04	0.86±0.02*	0.84±0.02*
IVS Thickness (cm)	0.70±0.03	0.84±0.03*	0.84±0.02*
Left Atrial Dimension (cm)	25.32±1.14	31.35±1.41*	28.27±1.10
RWT (cm)	0.33±0.02	0.36±0.01	0.35±0.008
Fractional Shortening (%)	38.48±2.79	35.44±1.52	35.55±1.09
LVEF (%)	64.20±0.47	62.21±0.75	61.69±0.49
LV GLS (%)	22.61±0.49	21.52±0.31	21.73±0.18
E Peak Rate, m/s	0.85±0.03	0.83±0.04	0.82±0.02
A Peak Rate, m/s	0.47±0.02	0.58±0.03	0.65±0.02*
Em Peak Rate, m/s	0.13±0.008	0.13±0.009	0.12±0.006
Mitral E/A Ratio	1.85±0.14	1.44±0.09*	1.26±0.05*
IV Relaxation Time, ms	64.44±2.94	79.47±3.10*	77.45±2.18*
IV Contraction Time, ms	64.44±1.76	68.42±3.69	67.23±1.87

Sex-differences in 5 year Survival with Percutaneous Coronary Intervention Compared to Coronary Artery Bypass Graft surgery in patients with Diabetes and Multivessel Disease

Xiang Xiao, Anamaria Savu, Douglas C. Dover, Robert C. Welsh, Kevin R. Bainey, Padma Kaul

BACKGROUND
Coronary artery bypass graft (CABG) surgery is preferred over percutaneous coronary intervention (PCI) in patients with diabetes (DM) and multivessel disease (MVD). However, differences in survival are equivocal and outcomes according to sex remain unknown.

METHODS/RESULTS
Patients with DM and MVD undergoing either PCI (with drug-eluting stents) or CABG within 90-days of cardiac catheterization between 01/05/2009-03/29/2019 in Alberta, Canada were included.Patients were required to be free of prior revascularization or other cardiac interventions. The outcomes of interest were all-cause death and the composite of all-cause death or myocardia infraction (MI) at 5-years. Rates and survival probabilities to 5- years were estimated by type of revascularization and sex. Cox proportional hazards model was used to examine sex difference outcomes stratified by revascularization.Among 4803 patients, 2941 underwent PCI (805 females [27%]; 2136 males [73%]) and 1862 underwent CABG (391 females [21%] and 1471 males [79%]). Regardless of type of revascularization females were older, had higher body mass index and comorbidity burden, were less likely to smoke and more likely to present with non ST-elevation MI. Females versus males had higher rates of death (PCI: F 4.2, M 3.0 per 100 person-year, p=0.0013; CABG: F 4.8, M: 3.7 per 100 person-year, p=0.0035) and death or MI (PCI: F 6.2, M 4.7 per 100 person-year, p=0.0026; CABG: F 5.9, M: 4.7 per 100 person-year, p=0.0044) at 5 years. However, regardless of revascularization, there was no difference in survival by sex after adjusting other covariates (PCI: Adjusted HR 1.15, 95% CI 0.90-1.46; CABG: Adjusted HR 1.26, 95%CI 0.93-1.70). Similar findings were observed for death or MI (PCI: Adjusted HR 1.14, 95% CI 0.94-1.40; CABG: Adjusted HR 1.23, 95% CI 0.94-1.61).

CONCLUSIONS
In a large real-world analysis of diabetics with MVD selected for revascularization, female sex was associated with a higher risk of death and death/MI at 5 years compared to male sex. However, the higher risk associated with both revascularization strategies among women compared to men was explained by differences in demographic and clinical characteristics. Our results could be considered when contemplating a revascularization strategy based on sex and clinical outcome.

Table 1. Adjusted association of sex and death and death/MI outcomes by revascularization status.

	Total patients, N	Number of events at 5 years, n (%)	Total Follow-up time, year	Rate per 100 person-year	Survival probability at 5 years	Unadjusted HR (95% CI) p-value	Adjusted HR (95% CI) p-value*
Outcome=Death							
PCI	2941	307 (10.4)	9675.71	3.2	0.857		
Female	805	135 (16.8)	3252.26	4.2	0.820	1.46	1.15
Male	2136	268 (12.6)	8931.95	3.0	0.871	(1.16, 1.85) 0.001	(0.90, 1.46) 0.26
CABG	1862	227 (12.2)	6338.18	3.6	0.837		
Female	391	80 (20.5)	1675.26	4.8	0.781	1.53	1.26
Male	1471	241 (16.4)	6512.97	3.7	0.852	(1.15, 2.05) 0.004	(0.93, 1.70) 0.13
Outcome=Death/MI							
PCI	2941	473 (16.1)	9250.36	5.1	0.783		
Female	805	187 (23.2)	3023.17	6.2	0.748	1.34	1.14
Male	2136	401 (18.8)	8456.80	4.7	0.796	(1.11, 1.63) 0.003	(0.94, 1.40) 0.19
CABG	1862	292 (15.7)	6163.15	4.7	0.793		
Female	391	96 (24.6)	1616.25	5.9	0.734	1.45	1.23
Male	1471	297 (20.2)	6304.22	4.7	0.809	(1.12, 1.88) 0.005	(0.94, 1.61) 0.12

n/N: number; HR: hazard ratio of female vs male; CI: confidence interval; PCI: primary coronary intervention using drug eluting stent; CABG: coronary artery bypass graft surgery; *Model included age, sex, extent of disease, treatment indication, smoking, hypertension, heart failure, chronic obstructive pulmonary disease, cerebrovascular disease, peripheral vascular disease, cancer, ulcer, rheumatic disease, liver disease and renal disease.

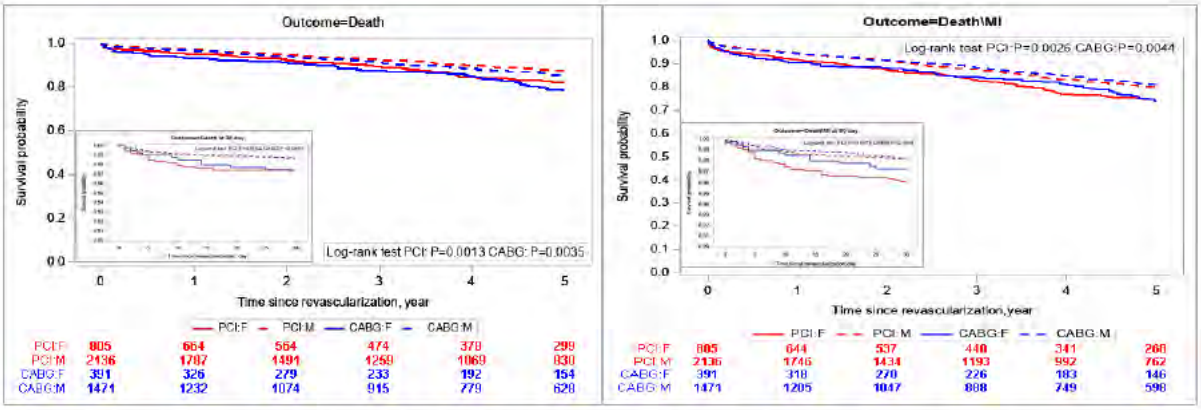

Figure 1. Sex difference in death and death/MI among males and females by type of revascularization strategy

5 year Survival with Percutaneous Coronary Intervention Compared to Coronary Artery Bypass Graft surgery in patients with Diabetes and Multivessel Disease

Xiang Xiao, Anamaria Savu, Douglas C. Dover, Robert C. Welsh, Padma Kaul, Kevin R. Bainey

BACKGROUND
Coronary artery bypass graft (CABG) surgery is preferred over percutaneous coronary intervention (PCI) in patients with diabetes (DM) and multivessel disease (MVD). However, it is unclear whether CABG confers a survival advantage.

METHODS/RESULTS
Patients with DM and MVD undergoing either PCI (with drug-eluting stents) or CABG within 90-days of cardiac catheterization for myocardial infarction (MI) or angina between 01/05/2009-03/29/2019 in Alberta, Canada were included. Patients were required to be free of prior coronary revascularization or other cardiac interventions. We examined all-cause death and composite of all-cause death or myocardial infraction (MI) at 5- years post revascularization via linkage with vital statistics death registry and hospitalization data. Inverse probability of treatment weighting (IPTW) was used to balance baseline characteristics between PCI and CABG groups and then compared the survival difference with Cox proportional hazards model.Among 4803 patients, 2941 (61.2%) had PCI and 1862 (38.8%) had CABG. PCI recipients were more likely to be female, younger, to have higher body mass index, present with ST-elevation MI, and have lesser extent of MVD compared to CABG patients. Mortality rate at 5-years was not significantly different between the two groups (PCI: 3.2 vs CABG 3.6 events per 100 person-year, log-rank test: p=0.16). Adjusting for patient characteristics did not change the association
(adjusted HR of PCI vs CABG: 0.96, 95% CI 0.73, 1.24). Similarly, for the outcome of death or MI at 5-years, rates (PCI: 5.1 vs CABG 4.7 events per 100 person-year, log-rank test: p=0.35) and adjusted hazards (adjusted HR of PCI vs CABG: 1.16, 95% CI 0.92, 1.45) did not differ between PCI and CABG recipients.

CONCLUSIONS
Our study showed no significant difference in all-cause death or death/MI between revascularization strategies, providing guidance on selection for patients with DM and MVD

Table 1. Associations between type of revascularization and two outcomes: death and death/MI

	Total patients, N	Number of events at 5 years, n (%)	Rate to 5 year per 100 person-year	Survival probability at 5 years	Unadjusted HR (95% CI) *p-value*	Adjusted HR via IPTW (95% CI) *p-value*
Outcome = Death						
					0.88	0.96
Overall	4803	534 (11.1)	3.3	0.849	(0.74, 1.05)	(0.73, 1.24)
					0.16	0.74
CABG	1862	227 (12.2)	3.6	0.837	NA	NA
PCI	2941	307 (10.4)	3.2	0.857	NA	NA
Outcome = Death/MI						
					1.07	1.16
Overall	4803	765 (15.9)	5.0	0.787	(0.93, 1.24)	(0.92, 1.45)
					0.35	0.20
CABG	1862	292 (15.7)	4.7	0.793	NA	NA
PCI	2941	473 (16.1)	5.1	0.783	NA	NA

n/N: number; HR: hazard ratio of PCI vs CABG; CI: confidence interval; PCI: primary coronary intervention using drug eluting stent; CABG: coronary artery bypass graft surgery; * The probability of receiving PCI or CABG was estimated for each patient from a logistic model that included the following variables: age (continuous and linear), sex (male/female), extent of disease (two vessel/three vessel/left main), treatment indication (SA, UA, NSTEMI, STEMI), smoking (never/past/current), hypertension, heart failure, chronic obstructive pulmonary disease, cerebrovascular disease, peripheral vascular disease, cancer, ulcer, rheumatic disease, liver disease and renal disease. Robust variance estimation was applied to IPTW models for both outcomes.

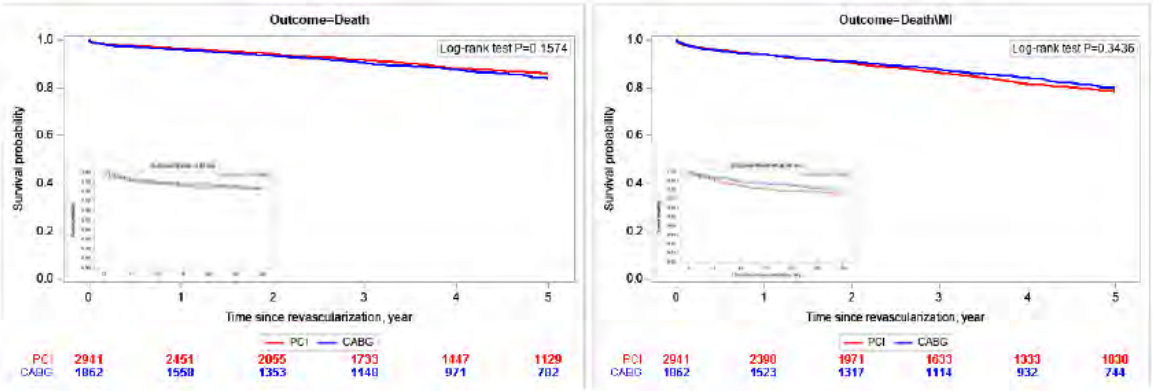

Figure 1. Survival (left panel) and survival free of MI (right panel) in PCI and CABG

Age-Specific Response to LPS-induced Endotoxemia and Cardioprotective Effects of sEH Inhibition in Female Mice.

Ala Yousef, Deanna Sosnowski, John M Seubert1

BACKGROUND
Purpose: Elderly individuals are more susceptible to external stressors due to their declining biological systems. LPS-induced endotoxemia triggers a multiorgan inflammatory response that can lead to cardiac dysfunction and possibly death. The metabolism of PUFA by CYP450 enzymes results in the production of numerous lipid mediators, which can be further metabolized by the enzyme soluble epoxide hydrolase (sEH). sEH hydrolyzes epoxy fatty acids into diol metabolites that potentially attenuate their beneficial effects. Previous research has demonstrated genetic deletion of sEH is cardioprotective and limits LPS-induced inflammation in young male mice. However, the cardioprotective effect of sEH deletion/inhibition in young and aged female mice has not been investigated.

METHODS/RESULTS
Methods: Young (2-5mo) and aged (18-25mo) female C57BL/6 wild type (WT) and sEH null (sEH KO) mice were administered an intraperitoneal saline (control) or LPS (10 mg/kg). Echocardiography was used to assess heart function and overall health status was monitored at baseline and 24 hours after injections. Cardiac protein expression of SIRT1 was determined using immunoblotting while IL-6, MCP-1, and GDF15 gene expressions were determined using qPCR. Plasma GDF15 concentration was assessed by ELISA. Results: Young female mice demonstrated tolerability without significant changes in overall health status and cardiac function. However, sEH deletion improved overall survival, attenuated systolic and diastolic cardiac injury, and significantly reduced cardiac inflammatory genes in aged mice. In addition, plasma GDF15 concentrations were significantly lower in aged sEH KO mice.

CONCLUSIONS
Conclusion: These data highlight age-dependent differences in female response to acute LPS exposure. Targeting sEH in elderly female patients may be an effective strategy for attenuating endotoxemia-induced cardiac dysfunction. Further experiments are needed to determine the underlying mechanism and to determine if sEH inhibition can be translated effectively in clinical settings.

The clinical impact of HFpEF on Interstitial Lung Diseases: clinical characteristics, comorbidities and outcomes.

Umberto Zanini, Giovanni Ferrara, Rhea Varughese, Meena Kalluri, Jason Weatherald.

BACKGROUND
Cardiovascular diseases such as coronary artery disease, pulmonary hypertension, and heart failure (HF) are among the most frequent comorbidities associated with interstitial lung disease (ILD). The overall prevalence of HF is estimated to be 1-2%in adults, rising to ≥10% among people older than 70. About 50% of patients with heart failure have preserved ejection fraction (HFpEF). Because many patients with ILD are elderly, HFpEF may affect many ILD patients. The prevalence, clinical features, and outcomes of patients with ILD and HFpEF are still unclear.

METHODS/RESULTS
This study is a retrospective cohort analysis of ILD patients who had an echocardiogram from Jan 2013 to Dec 2022 at the University of Alberta Hospital at their baseline visit. HFpEF was defined as a H2FPEF score >5 which reflects >95%probability of HFpEF. Clinical features and survival were compared between patients with and without HFpEF.
Out of 130 ILD patients, 12 had HFpEF (9.23%). Patients with HFpEF were older (75.58±6.89 vs 65.30±14.69, $p<0.05$) and had higher body mass index (34.18±6.27 vs 29.16±6.64 kg/m2, $p<0.05$). Left atrial volume index was significantly greater in HFpEF patients (38.63±12.64 vs 24.13±8.47 mL/m2, $p<0.001$). There was no difference in baseline KB-ILD questionnaire and mMRC. Both groups had similar 6- minute walk distance (346.71±108.44 vs 389.95±134.08, $p=0.28$). Survival in patients with HFpEF was not different than patients without HFpEF ($p=0.57$).

CONCLUSIONS
In conclusion, the prevalence of HFpEF among ILD patients is similar to that of the general population (10%). Symptoms, clinical features, and survival were similar for patients with HFpEF and without. Left atrial enlargement may be an additional clue to the presence of HFpEF.